HYDRONAUTICS, incorporated
research in hydrodynamics

Research, consulting, and advanced engineering in the fields of NAVAL and INDUSTRIAL HYDRODYNAMICS. Offices and Laboratory in the Washington, D. C., area: Pindell School Road, Howard County, Laurel, Md.

153

DISCLAIMER NOTICE

THIS DOCUMENT IS THE BEST QUALITY AVAILABLE.

COPY FURNISHED CONTAINED A SIGNIFICANT NUMBER OF PAGES WHICH DO NOT REPRODUCE LEGIBLY.

HYDRONAUTICS, Incorporated

TECHNICAL REPORT 823-1

A STUDY OF THE STEADY FLOW OF A RIGID-PLASTIC CLAY BENEATH A DRIVEN RIGID WHEEL

By

G. Dagan and M. P. Tulin

August 1968

Prepared For

Cornell Aeronautical Laboratory, Inc.
Buffalo, New York 14221
Under Contract DAHC 04-67-C-0005
U. S. Army Research Office,
Durham, North Carolina

Sponsored By

Advanced Research Projects Agency
Project AGILE
Department of Defense
ARPA Order No. 841, dated 7 May 1966

HYDRONAUTICS, Incorporated

FORWARD

The research reported herein was performed by HYDRONAUTICS, Incorporated for Cornell Aeronautical Laboratory, Inc. (CAL), and supports the Soil Mechanics Task of the Off-Road Mobility Research (ORMR) program sponsored by OSD/ARPA for which CAL is the prime contractor and the U. S. Army Research Office - Durham is the contracting agency.

The reported study is part of a broad research program designed to acquire off-road mobility knowledge; develop analysis, prediction and decision methodologies; and organize knowledge and methods to facilitate use by military planners, vehicle designers and field personnel concerned with off-road mobility. Under these broad objectives, soil mechanics research is directed at developing techniques for analyzing off-road mobility problems related to soft-soil conditions. The present study is concerned with steady state two-dimensional flow generated by a driven rigid cylindrical wheel moving in soft saturated clay, assumed to behave like a rigid plastic material. The study was performed during the period April 1968 - September 1968. Funds for this study were allocated to HYDRONAUTICS, Incorporated by CAL under ARPA Order No. 841 dated 7 May 1966 with amendment Nos. 1-4. Dr. Patrick Miller was the CAL ORMR Soil Mechanics Task Leader; Mr. G. E. Bartlett was ORMR Program Manager at CAL; and Mr. A. N. Tedesco was ARPA Technical monitor.

TABLE OF CONTENTS

LIST OF FIGURES

NOTATION

Dotted symbols have dimensions. Undotted variables are dimensionless: length by dividing with r', velocities by U_o', stresses by k' and forces by k'r'.

g	Gravity acceleration
$G = \frac{g\rho'}{k'}$	Dimensionless gravity plastic number
h'	Thickness of the plastic zone at the bottom of the wheel ($h = h'/\pi'$)
$H = \frac{\rho' U_o'^2}{k'}$	Dimensionless inertial plastic number; also horizontal force acting on the wheel ($H = H'/r'k'$)
J_o	Bessel function of zero order
k'	Yield stress (max. shear stress)
ℓ, L	Auxiliary lengths defined in Figures 17 and 19
M'	Torque on the wheel ($M = M'/k'r'^2$)
n	Direction normal to streamlines
p'	Isotropic pressure ($p = p'/k'$)
r'	Wheel radius
r	Radial coordinate
R'	Resistance ($R = R'/k'r'$)
s	Direction along streamlines
S	Slippage coefficient $\left(S = \frac{V_w' - U_o'}{V_w'}\right)$
u', v'	Velocity components in cartesian coordinates ($u = u'/U_o'$, $v = v'/U_o'$)
u_b	Velocity in the plastic zone at the bottom of the wheel

U_o'	Translational velocity of the wheel
V'	Velocity modulus ($V = V'/U_o'$)
$V_w' = \omega' r'$	Peripheral rotational velocity of the wheel ($V_w = V_w'/U_o'$)
v_α, v_β	Velocity components in characteristic directions
v_r, v_θ	Velocity components in radial coordinates
W'	Vertical force acting on the wheel ($W = W'/k'r'$)
x', y'	Cartesian coordinates ($x = x'/r'$, $y = y'/r'$)
x_α, x_β	Curvilinear characteristic coordinates
z'	Sinkage ($z = z'/r'$)
α, β	Characteristic directions
γ'	Shearing strain
$\delta V, \delta\tau$	Velocity and shear stress jumps
$\epsilon_{xx}, \epsilon_{yy}, \gamma_{xy}$	Rates of strain
η	Auxiliary angle defined in Figure 19
θ	Angle between streamline and x direction (in particular polar coordinate along the wheel)
λ	Slope of characteristic directions
ρ'	Soil density
σ'	Normal stress ($\sigma = \sigma'/k'$)
σ_x, σ_y	Cartesian components of the normal stress tensor
σ_w	Normal stress acting on the wheel
σ_1, σ_2	Principal normal stresses
τ'	Shear stress ($\tau = \tau'/k'$)

τ_w	Constant shear stress along the wheel
ϕ	Angle between α characteristic and x axis
ϕ_w	ϕ along the wheel
ω'	Rotational speed of the wheel

ABSTRACT

The steady two-dimensional flow beneath a driven rigid cylindrical wheel moving in a soft saturated clay is solved by assuming that the soil behaves like a rigid-plastic material. The general equations of plastic flow are discussed, with emphasis on the inertial effects which generally are not negligible. A plastic flow pattern is suggested and the quasi-static equations of flow are integrated in two regions of the plastic zone. An approximate solution provides the magnitude of the recovery angle, the vertical and horizontal forces and the torque acting on the wheel as function of wheel radius, sinkage and shear stress along the wheel (assumed constant on the bow portion). A minimum slippage necessary to maintain the shear stress on the wheel is found. The theoretical results are compared with some existing measurements and the agreement is generally satisfactory.

1. INTRODUCTION

The capability of a vehicle to navigate in a soft soil depends on the magnitude of the forces developed at the wheel (or track) and soil interface. The prediction of these forces as functions of the wheel geometry, soil characteristics and wheel speed is necessary in order to design vehicles or to estimate the mobility of a given vehicle under different conditions.

Unfortunately, at this stage of development of the art (see Section 2) there is no reliable theory which can produce design formulae. Moreover, even the fundamentals are not well understood and similitude criteria which allow extrapolation of model tests to prototype are not clearly formulated.

The purpose of this study is to solve in a basic way the problem of soil flow beneath a wheel under some simplifying assumptions. While existing approaches use empirical results obtained from static tests of plates on the soil surface and apply them to the moving wheel, in the present study the whole region of soil flow beneath the wheel is considered. The solution of the problem follows the lines of the classical applied mechanics: the soil behavior is represented by material constitutive equations, the stresses and velocity fields are interrelated through the equations of motion and the particular solution for the wheel is obtained by integration with the appropriate boundary conditions.

Unfortunately, the difficulties encountered in such a type of solution are formidable. The most important of them is the lack of a good mathematical representation of the soil behavior in form of constitutive equations, i.e., relationships between stresses and deformations. But even if some simplified constitutive equations are adopted, the exact integration of the equations of motion in the wheel case seems impossible at this stage.

For the above reasons, in this preliminary study the problem has been simplified by adopting the following assumptions: (i) the soil behaves like a rigid-plastic incompressible material, (ii) the wheel is two-dimensional and rigid, (iii) the motion is steady and (iv) the soil surface is plane and unperturbed far from the wheel. Assumption (i) limits the applicability of the results to soft clays with a high water content, although even in this case the plastic-rigid model is a foregoing simplification. It may describe roughly the behavior of a saturated undrained clay with a dispersed structure (Reference 14, p. 369), (Reference 7, p. 188).

Considering the highly empirical character of existing theories it is felt that the present work, in spite of the above simplifications, constitutes an important step forward in the understanding of soil-vehicle interaction. This is only a first step, and the results obtained so far encourage the continuation of the study along the same lines, with steady improvement and extension of results to more complex conditions, like: representation of soil as a work-hardening material and incorporation of friction, consideration of three-dimensional wheels and of unsteady motions, influence of wheel or track shape, etc.

2. BRIEF LITERATURE REVIEW

The purpose of this section is not to give a comprehensive review of the publications in the field of vehicle-soil interaction, but a critical discussion of the most important contributions, relevant to this study.

A. Theoretical Works on Soil Wheel-Interaction

The most known and applied theories of wheel-soil interaction are those of Bekker and Uffelmann.

Bekker's theory (2), (3) is based on the following assumptions on development of stresses on the soil-wheel interface: (i) The normal stress at a point is related to the wheel sinkage at the same point. The relationship, known as Bernstein equation, is obtained empirically by pressing plates in the soil and representing the dependence of force on sinkage. (ii) The horizontal resisting force to the wheel motion is a result of the work done in compacting the soil and creating the rut. There is no soil recovery beyond the wheel bottom. (iii) The shear stress along the wheel is computed by using the relationship between shear stress and deformation obtained empirically by pulling a flat plate on the soil surface.

The soil layer adjacent to the wheel has an angular deformation which is computed by assuming that on the wheel side the speed is equal to the wheel rotational speed and on the soil side equal to the translational speed. This permits the determination of the shear stress as function of slippage and position.

By using seven soil constants in the representation of the empirical curves and some additional computational simplifications Bekker was able to calculate the forces acting on the wheel by using the above assumptions.

The inconsistency of Bekker's theory when compared with experimental results have been largely discussed in literature (see, for instance, (19), (20)) and will not be repeated here.

From a basic point of view, Bekker's theory is an attempt to apply results of measurements of forces on flat plates in static conditions to moving wheels. There is no a priori reason that such an attempt should be successful since the soil-flow beneath a flat-plate is different from that beneath a wheel. If we adopt the plastic-rigid model and observe the plastic flow pattern beneath a footing (7), (8) and that beneath a rolling surface (1), (8) we will find that they are different. Moreover, the normal stress at a certain point is depending on the whole flow-field and not on the vertical displacement of that particular point. There is no theoretical ground for the assumption of pressure-sinkage relationship along the wheel.

The rolling resistance of a wheel cannot be attributed to the soil compaction, excepting possible agricultural soils with high content of air-filled pores. A soft clay with a high water content is practically incompressible and in a two-dimensional case there is no ultimate rut. There is definite evidence of soil recovery at the rear with normal stresses contributing to draw-bar pull (18), (22).

The distribution of shear stresses along the wheel is different from that assumed by Bekker because a soil particle moving along the wheel has velocity gradients depending again on the whole flow-field and it starts to be sheared before it reaches the wheel surface.

Concluding these remarks on Bekker's theory it may be said that in spite of the progress marked by this theory in the quantitative representation of the soil-wheel interaction, it has not clarified the mechanism of soil flow beneath the wheel.

Uffelmann (18) has assumed that the normal stress on a wheel is constant and equal to that under a static rough footing in a plastic incompressible clay and he suggested the computation of the wheel-resistance on this basis. Again, because of the different plastic flow patterns in the two cases, the pressures are generally different. The normal stress is constant on a footing, but varies along a wheel.

Reece and Wong (13) have refined Bekker's theory by empirically relating the position of the point of maximum normal stress on the wheel to slippage. Consequently the well-known fact that the tangential stress influence the distribution of normal stresses is reflected by the formulae (fact ignored by both Bekker and Uffelmann theories). Again, this generalization is based on some empirical data and not on the analysis of the flow-field.

In conclusion, there is no comprehensive theory of soil-flow beneath a wheel. All existing approaches are empirical and consider the soil-wheel interaction as a surface effect. They ignore the stress and velocity distribution in the soil body. No consideration has been given to inertial or strain-rate effects.

B. Experimental Work

The experimental works on soil-wheel interactions are dominated by the same trend as the theoretical works: only forces acting on wheels or stress distribution have been measured.

Experiments in which the flow-pattern of the soil has been observed are reported in (21), (22), most of them being carried out with sand. Because of the small dimensions of the experimental soil bin and the low speed of the wheel, the quantitative value of the results is questionable. Moreover, no stress measurements - to be correlated with the kinematics - have been carried out. Qualitatively, however, these experiments confirm beyond any doubt that the dynamics of wheel motion is determined by the soil flow beneath the wheel and not just by a surface effect at the interface.

The stress distribution along wheels and the resulting forces have been measured by different authors, but there is no general agreement between measurements. For instance Uffelmann (18) has found that the maximum normal stress acts at the bottom of the wheel, while in (15) and (13) it has been found somewhere forward near the bow. Any analysis is hampered by the fact that

results are dependent on the type of soil and its preparation. Since generally there is no detailed description of the mechanical behavior of the soil used by different experimenters it is difficult to compare different results on a common basis.

The comprehensive measurement of forces on towed and driven wheels by Cullen, Cullingford and Mayfield (5) gives some qualitative trends as the decrease in flotation with slippage at constant sinkage.

Some experiments are compared with the results of the present work in Section 9.

In conclusion, there is an urgent need for careful experiments in which both soil velocity distributions and stress distributions along the wheel should be measured. These experiments have to be carried out under thorough control of the soil behavior and respecting the inertial similitude requirements.

C. Theoretical Works on Rigid-Plastic Flow

Although the present study relies on the rigid-plastic theory, it is beyond our purpose to review the publications consulted for this study. The most referred work is Hill's book (8) and to a lesser extent Prager's (10), (11) and Thomas (17) books. The results of some papers of special interest (1), (9), are recalled in some detail in the context of the following sections.

3. THE STATEMENT OF THE PROBLEM AND THE GENERAL EQUATIONS OF RIGID-PLASTIC FLOW

A. The Statement of the Problem

Under the assumptions enumerated in Section 1, the soil-wheel problem may be stated in the following terms (Figure 1):

A standing rigid cylinder of radius r' rotates with constant speed ω' and has a given constant sinkage z'. The soil approaches the wheel with a constant speed at infinity U_o' and unperturbed free-surface elevation. Find the free-surface shape, the soil velocity and stress fields in the whole semi-infinite domain and particularly along the wheel. The normal and shear stresses along the wheel (σ' and τ') result in a vertical force W', a horizontal force H' and a torque M'.

The equations of rigid plastic flow, on which the solution is based in this study, are discussed in the following paragraphs. The boundary conditions are analyzed in Section 5. The approximate solution is given in Sections 6 and 7.

In applications the sinkage z' is not given, but the vertical load W'. From a mathematical point of view, however, it is much more convenient to start with a given sinkage. Once the problem is solved, a correlation between sinkage and flotation is found and z' may be determined for a given W'.

B. The Physical Behavior of a Rigid-Plastic Material

The ideal rigid-plastic model, adopted here for representing the clay behavior, is based on the following assumptions (8), (17):

- The plastic deformations are much larger than the elastic ones (which may be neglected). The elastic state is therefore approximated by a rigid state (Young modulus tends to infinity). The only possible rigid motions are translation and rigid rotation.

- In the plastic state the maximum shearing stress at any point is constant and equal to the yield stress k'. In the rigid state $\tau' < k'$.

- The material in plastic state flows, the direction of maximum shear stress and the direction of maximum shearing strain-rate being parallel (i.e. the stress and strain-rate tensors have parallel principal axes). There is no one to one correspondence between the stress and the strain-rate, which means that in a plastic flow the maximum shear stress is constant but the shearing strain rate may vary. The deformation work is totally irreversible in a thermodynamic sense.

- The material is incompressible and a hydrostatic pressure does not influence the plastic flow. Only the deviatoric stress plays a role in creating plastic flow. The material is homogeneous and isotropic.

The above assumptions lead to the simplest rigid-plastic model. They may be modified in order to take into account elastic effects, anisotropy, friction and work-hardening. Although this study is restricted to the application of the ideal rigid-plastic model, it is worthwhile to discuss briefly the work-hardening model, which is useful for future work on wheel-soil interaction.

While an ideal non-hardening material yields under constant yield stress, otherwise being rigid, the yield stress of work-hardening material is dependent on the history of strain and increases with the total shearing strain (or with the work of deformation). The stress-strain curve of a non-hardening ideal rigid-plastic material is a straight line (Figure 2), while in a work-hardening material it is curved. The physical microscopical mechanisms which underlie work-hardening of metals (8) and of soils are probably different, but the macroscopical description is satisfactory in both cases. Due to mathematical difficulties the work-hardening theory has apparently not yet been used in soil mechanics. An ideal rigid-plastic material (meaning also non-hardening here) may be regarded as a limit of a work-hardening material with a very high rate of hardening (Figure 2). This interpretation will be useful in the discussion of Section 4C.

C. The Equations of Two-Dimensional Steady Flow (Cartesian Coordinates)

Although the equations of plastic flow may be found in text-books (3), it is worthwhile to discuss them here briefly.

The kinematics of flow is described with the aid of the velocity components u', v', and the stress field by σ_x', σ_y' τ_{xy}' (Figure 3).

The equations of motion, valid for any type of material are

$$\frac{\partial \sigma_x'}{\partial x'} + \frac{\partial \tau_{xy}'}{\partial y'} = \rho' \left(u' \frac{\partial u'}{\partial x'} + v' \frac{\partial u'}{\partial y'} \right) \qquad [3.1]$$

$$\frac{\partial \tau_{xy}'}{\partial x'} + \frac{\partial \sigma_y'}{\partial y'} = \rho' \left(u' \frac{\partial v'}{\partial x'} + v' \frac{\partial v'}{\partial y'} \right) + \rho' g \qquad [3.2]$$

The positive signs of the different quantities being those of Figure 3.

The assumption of incompressibility yields the continuity equation

$$\frac{\partial u'}{\partial x'} + \frac{\partial v'}{\partial y'} = 0 \qquad [3.3]$$

The assumption of constancy of yield stress in the plastic zone is reflected by Von-Mises criterion (8)

$$(\sigma_x' - \sigma_y')^2 + 4 \tau_{xy}'^2 = 4k'^2 \qquad [3.4]$$

and finally, the parallelism of principal directions of stress and strain-rate tensors is mathematically described by Saint-Venant relationships

$$\frac{\frac{\partial u'}{\partial x'}}{\sigma_x' - \sigma_y'} = \frac{\frac{\partial v'}{\partial y'}}{\sigma_y' - \sigma_x'} = \frac{\frac{\partial u'}{\partial y'} + \frac{\partial v'}{\partial x'}}{4 \tau_{xy}'} \qquad [3.5]$$

which by the continuity equation become

$$\frac{\sigma_x' - \sigma_y'}{2\,\tau'_{xy}} = \frac{\dfrac{\partial u'}{\partial x'} - \dfrac{\partial v'}{\partial y'}}{\dfrac{\partial u'}{\partial y'} + \dfrac{\partial v'}{\partial x'}} \qquad [3.6]$$

The five differential Equations [3.1], [3.2], [3.3], [3.4] and [3.6] are in principle sufficient in order to determinate the unknown functions σ_x', σ_y', τ'_{xy}, u' and v'.

The five equations may be reduced in a particularly convenient way to a system of four equations by introducing Von Mises variables $p' = -(\sigma_x' + \sigma_y')/2$ (the isotropic pressure) and ϕ-the angle between the direction of maximum shearing stress and the x' axis. The two orthogonal directions of maximum shearing stress α and β (Figure 4) are selected such that the maximum algebraic normal stress acts in the first or third quadrant (Figure 4).

The new variables p', ϕ replace σ_x', σ_y' and τ'_{xy} through the relationships

$$\begin{aligned} \sigma_x' &= -p' - k' \sin 2\phi \\ \sigma_y' &= -p' + k' \sin 2\phi \\ \tau'_{xy} &= k' \cos 2\phi \end{aligned} \qquad [3.7]$$

which satisfy Von Mises criterion [3.4].

Using dimensionless variables (defined in "Notation") the equations of plastic flow become

$$\frac{\partial p}{\partial x} + 2 \cos 2\phi \frac{\partial \phi}{\partial x} + 2 \sin 2\phi \frac{\partial \phi}{\partial y} = - H \left(u \frac{\partial u}{\partial x} + v \frac{\partial u}{\partial y} \right) \qquad [3.8]$$

$$\frac{\partial p}{\partial y} + 2 \sin 2\phi \frac{\partial \phi}{\partial x} - 2 \cos 2\phi \frac{\partial \phi}{\partial y} = - H \left(u \frac{\partial v}{\partial x} + v \frac{\partial v}{\partial y} \right) - G \qquad [3.9]$$

$$\cos 2\phi \left(\frac{\partial u}{\partial x} - \frac{\partial v}{\partial y} \right) + \sin 2\phi \left(\frac{\partial u}{\partial y} + \frac{\partial v}{\partial x} \right) = 0 \qquad [3.10]$$

$$\frac{\partial u}{\partial x} + \frac{\partial v}{\partial y} = 0 \qquad [3.11]$$

The plastic-inertial dimensionless number $H = \frac{\rho' U_o'^2}{k'}$ (somehow similar to Reynolds number in a viscous flow) is particularly significant for the soil-wheel interaction.

D. The Characteristic Directions and the Inertial Terms

In plasticity theory the inertial and gravitational terms are neglected (equivalent to assuming H = 0.G = 0). In this case Equations [3.8] - [3.11] form an uncoupled quasi-linear system of first order: the derivatives of p and ϕ appear in the two first equations, while those of u and v in the last equations. Each of the two systems is totally hyperbolic and has two characteristic directions (8). Accidentally, the characteristic directions for p,ϕ and u,v coincide and are the α and β directions.

The equations are rewritten in curvilinear characteristic coordinates x_α, x_β by using the variables transformation (8)

$$\frac{\partial}{\partial x} = \cos \phi \frac{\partial}{\partial x_\alpha} - \sin \phi \frac{\partial}{\partial x_\beta}$$

$$\frac{\partial}{\partial y} = \sin \phi \frac{\partial}{\partial x_\alpha} + \cos \phi \frac{\partial}{\partial x_\beta} \qquad [3.12]$$

$$v_\alpha = u \cos \phi + v \sin \phi$$

$$v_\beta = - u \sin \phi + v \cos \phi$$

the velocity being now referred to the new coordinates.

After some algebraic manipulations the system [3.8] - [3.11] becomes (with H = G = 0)

$$\left.\begin{aligned} \frac{\partial p}{\partial x_\alpha} + 2 \frac{\partial \phi}{\partial x_\alpha} = 0 \\ \frac{\partial p}{\partial x_\beta} - 2 \frac{\partial \phi}{\partial x_\beta} = 0 \end{aligned}\right\} \qquad [3.13]$$

$$\left.\begin{aligned} \frac{\partial v_\alpha}{\partial x_\alpha} - v_\beta \frac{\partial \phi}{\partial x_\beta} = 0 \\ \frac{\partial v_\beta}{\partial x_\beta} + v_\alpha \frac{\partial \phi}{\partial x_\beta} = 0 \end{aligned}\right\} \qquad [3.14]$$

Equations [3.14] are known as Geiringer equations. The lines α = const and β = const are known as sliplines and they determine an orthogonal network.

Equations [3.13] and [3.14], known as the equations of quasi-static plasticity, have the well-known properties of hyperbolic systems: The Cauchy problem for p, ϕ, v_α, v_β has a unique solution if the data are given on a noncharacteristic curve; the solution at a point depends only on the data on the portion cut by the two-characteristics through the given point; velocity tangential discontinuities are possible along a characteristic; the velocity derivatives or p and ϕ derivatives may be discontinuous along charac eristics. p and ϕ may be discontinuous along a line of stress-discontinuity which cannot be a characteristic. All the above properties are discussed in detail by Hill (8), and will be used extensively in Sections 5 and 6.

The neglection of the inertial terms in plasticity theory when applied to metal technology is entirely justified since $H \ll 1$ there (because of the very high value of k'). The same is true for foundation engineering where only cases of limit equilibrium are considered. In the case of wheel-soil interaction, however, H may be of the order O(1). For instance, for a soil with k' = 3 psi, $\rho'g$ = 120 pcf, H becomes equal to unity for a translational speed U_o' = 7.5 mph. The inertial terms, therefore, may be important in mobility problems. This aspect has been ignored in both plasticity theory and mobility studies. Most of the laboratory tests have been carried out with values of H much smaller than in field conditions.

An attempt to discuss the full equations of plastic flow is presented by Spencer (16). Spencer analyzes the system [3.12] as a quasi-linear system for p, ϕ, u, v and determines the characteristic directions by the well-known method (see (4), p. 171-173).

The characteristic determinant of the system [3.8] - [3.11] considered by Spencer has the form

$$\begin{vmatrix} 1 & \cos 2\phi - \lambda \sin 2\phi & H(u - \lambda v) & 0 \\ -\lambda & \sin 2\phi + \lambda \cos 2\phi & 0 & H(u - \lambda v) \\ 0 & 0 & \cos 2\phi - \lambda \sin 2\phi & \sin 2\phi + \lambda \cos 2\phi \\ 0 & 0 & 1 & -\lambda \end{vmatrix} = 0$$

conclusion is open to criticism for the following reason: Like in the quasi-statical case, Equations [3.10] and [3.11] form a decoupled system for u and v which is hyperbolic and has the characteristic directions of [3.15]. No matter what the form of the right hand sides of Eqations [3.8] and [3.9], the determinant will vanish for these two characteristic values of λ, which can be easily seen from the inspection of the last two lines of the determinant. No conclusion regarding the influence of the right hand side of Equations [3.8] and [3.9] can be drawn from its vanishing. A better insight into the problem may be obtained by writing the system [3.8] - [3.11] in characteristic coordinates i.e., by the aid of Equations [3.12]. The result is (16)

$$\left.\begin{aligned} \frac{\partial p}{\partial x_\alpha} + 2\,\frac{\partial \phi}{\partial x_\alpha} &= -\,H\,v_\beta\left(\frac{\partial v_\alpha}{\partial x_\beta} - v_\beta\,\frac{\partial \phi}{\partial x_\beta}\right) + G\sin\phi \\ \frac{\partial p}{\partial x_\beta} - 2\,\frac{\partial \phi}{\partial x_\beta} &= -\,H\,v_\alpha\left(\frac{\partial v_\beta}{\partial x_\alpha} + v_\alpha\,\frac{\partial \phi}{\partial x_\alpha}\right) + G\cos\phi \end{aligned}\right\} \qquad [3.16]$$

$$\left.\begin{aligned} \frac{\partial v_\alpha}{\partial x_\alpha} - v_\beta\,\frac{\partial \phi}{\partial x_\alpha} &= 0 \\ \frac{\partial v_\beta}{\partial x_\beta} + v_\alpha\,\frac{\partial \phi}{\partial x_\beta} &= 0 \end{aligned}\right\} \qquad [3.17]$$

Obviously the Geiringer Equations [3.17] are the same as [3.14]. Equations [3.16], however, do not satisfy the requirement of fully hyperbolicity ((4), p. 173) which states that all the quantities should be differentiated along the same characteristic. The presence of the cross-derivatives in the right-hand sides of Equations [3.16] shows that the usual properties of a hyperbolic system are not met here.

It is beyond the purpose of this study to investigate the nature of the system [3.16] and [3.17] which in fact is the basis of a new chapter of applied mechanics which can be called dynamic plasticity. At this stage, assuming that for the soil-wheel interaction $H < 1$, a perturbation expansion, similar to that suggested by Spencer (16), will be adopted. In such an expansion, in which H is a small parameter, the leading term satisfies the hyperbolic quasi-static equations [3.13] and [3.14]. The wheel-problem will be studied (Sections 5,6) in this first quasi-static approximation at this stage. In Section 4 the influence of the inertial terms on singular points and lines will be discussed and the quasi-static solution will be built in the light of the results. In this sense the influence of the inertial terms will be reflected in the proposed solution, which is different from the type of solutions adopted in rolling and extrusion theories (8), (1).

It is worthwhile to mention here that in a hypothetical case of very high H (for instance, for a vehicle which is not wheel-propelled) a perturbation expansion of Equations [3.16],

[3.17] starts with the equations of inviscid flow (Euler equations) as the leading term. The soil behaves in this case as an inviscid fluid, rather than a plastic solid. The Euler equations have an elliptic character. The problem for intermediate H is therefore somewhere between these two extremes.

In an analysis of the equations of flow, written in the form of a second order system for p, u, v by the elimination of $\emptyset$ from [3.8] - [3.11], Thomas (17) has found the same characteristic directions [3.15], but he did not discuss at all the nature of Equations [3.16], [3.17]. Assuming continuous velocities and pressures, Thomas showed that discontinuities in the second derivatives of the velocities can occur only along the characteristics. The only applications discussed by Thomas are of unsteady flows with no inertial convective terms.

E. The Equations Along Streamlines

The equations of plastic flow have been written so far in cartesian and characteristic coordinates. It is worthwhile to rewrite them in coordinates attached to the streamlines.

With θ the angle between the streamline and x axis, s and n coordinates along and normal to the streamline (Figure 3), the following relationships hold

$$\frac{\partial}{\partial x} = \frac{\partial}{\partial s}\cos\theta - \frac{\partial}{\partial n}\sin\theta$$

$$\frac{\partial}{\partial y} = \frac{\partial}{\partial s}\sin\theta + \frac{\partial}{\partial n}\cos\theta \qquad [3.18]$$

$$u = V\cos\theta$$

$$v = V\sin\theta$$

The substitution of Equation [3.18] into Equations [3.8] - [3.11] gives

$$\frac{\partial p}{\partial s} + 2 \cos 2(\phi-\theta) \frac{\partial \phi}{\partial s} + 2 \sin 2(\phi-\theta) \frac{\partial \phi}{\partial n} = - H \frac{\partial V^2}{\partial s} - G \sin \theta$$

$$\frac{\partial p}{\partial n} + 2 \sin 2(\phi-\theta) \frac{\partial \phi}{\partial s} - 2 \cos 2(\phi-\theta) \frac{\partial \phi}{\partial n} = - HV^2 \frac{\partial \theta}{\partial s} - G \cos \theta$$

$$\cos 2(\phi-\theta) \frac{\partial V}{\partial s} + \sin 2(\phi-\theta) \frac{\partial V}{\partial n} + V \sin 2(\phi-\theta) \frac{\partial \theta}{\partial s} -$$

$$- V \cos 2(\phi-\theta) \frac{\partial \theta}{\partial n} = 0$$

$$\frac{\partial V}{\partial s} + V \frac{\partial \theta}{\partial n} = 0 \qquad [3.19]$$

The Equations [3.19] are used in Section 4 for some applications.

F. The Condition of Positive Work

The Saint-Venant condition [3.6] expresses the parallelism between the principal directions of stress and strain-rate tensors, but does not specify the signs of the two, which permits for two alternatives. Only one of them, which satisfies the requirement of positive dissipation work is a valid representation of a plastic flow.

The power of dissipation is given by

$$E = \epsilon_{xx}\sigma_x + 2 \tau_{xy}\gamma_{xy} + \epsilon_{yy}\sigma_y > 0 \qquad [3.20]$$

In terms of u,v and $\emptyset$.E is expressed as

$$E = \sin 2\emptyset \left(\frac{\partial v}{\partial y} - \frac{\partial u}{\partial x} \right) + \cos 2\emptyset \left(\frac{\partial u}{\partial y} + \frac{\partial v}{\partial x} \right) > 0 \qquad [3.21]$$

In characteristic coordinates, Equation [3.21] transforms with the aid of Equations [3.12] into

$$E = \frac{1}{v_\alpha v_\beta} \left(v_\alpha \frac{\partial V^2}{\partial x_\alpha} + v_\beta \frac{\partial V^2}{\partial x_\beta} \right) > 0 \qquad [3.22]$$

Equation [3.22] has been found by Prager (10) from graphical considerations. Since the operator $v_\alpha \frac{\partial}{\partial x_\alpha} + v_\beta \frac{\partial}{\partial x_\beta}$ represents differentiation along streamlines $(\frac{\partial}{\partial s})$, E may be finally expressed as

$$E = \frac{V}{v_\alpha v_\beta} \frac{\partial V^2}{\partial s} > 0 \ . \qquad [3.23]$$

4. SOME APPLICATIONS OF THE GENERAL EQUATIONS OF PLASTIC-RIGID FLOW

As stated in Section 3, the general study of the equations of plastic-rigid flow [3.8] - [3.11] or [3.16], [3.17] is beyond the scope of this report. A discussion of the application of the equations to some particular lines and singular points is presented here because of its importance for the wheel problem.

A. The Free-Surface

The soil free-surface in the rigid zone of uniform flow is horizontal. In the vicinity of the wheel, in the plastic region, the free-surface curves. Three boundary conditions have to be satisfied on a free-surface

$$\left.\begin{aligned} \sigma_n &= 0 \\ \tau_n &= 0 \end{aligned}\right\} \qquad [4.1]$$

$$V_n = 0 \qquad [4.2]$$

i.e., the free-surface is stress-free and it is a streamline (in a steady flow).

From Equations [3.7] we immediately find that Equations [4.1] are equivalent to (Figure 5)

$$\begin{aligned} \phi - \theta &= \pm \frac{\pi}{4} \\ p &= \pm 1 \end{aligned} \qquad [4.3]$$

i.e., the α lines intersect the free-surface at 45 degrees. The plus sign in Equations [4.3] corresponds to a state of compression, the maximum compressive stress being $\sigma = -2$. For $\phi - \theta = -\pi/4$ the normal stresses are tensile with a maximum value of $\sigma = 2$, i.e. twice the yield stress (Figure 5).

Considering first the state of compression, it is easy to ascertain that (Figure 5a)

$$v_\alpha = V \cos \frac{\pi}{4}$$
$$v_\beta = -V \sin \frac{\pi}{4} \qquad [4.4]$$

Hence, from the condition of positive work [3.23] it is found that

$$\frac{\partial V^2}{\partial s} < 0 \qquad [4.5]$$

which means that the speed along a free-surface has to decrease in the direction of flow.

The equations of flow [3.19] become in the case of a free-surface ($\phi - \theta = \pi/4, p = 1$)

$$2 \frac{\partial \phi}{\partial n} = - \frac{H}{2} \frac{\partial V^2}{\partial s} - G \sin \theta$$

$$\frac{\partial p}{\partial n} + 2 \frac{\partial \Phi}{\partial s} = - HV^2 \frac{\partial \theta}{\theta s} - G \cos \theta \qquad [4.6]$$

$$\frac{\partial V}{\partial n} + V \frac{\partial \theta}{\partial s} = 0$$

$$\frac{\partial V}{\partial s} + V \frac{\partial \theta}{\partial n} = 0$$

The second equation of [4.6] shows that for a convex free-surface the pressure decreases along the normal, inside the flow region, i.e., tensile stresses are induced beneath the free-surface. The last equation of [4.6] shows that $\partial\theta/\partial n > 0$, i.e., the streamlines diverge in the flow direction.

In the case of tension ($\phi - \theta = -\pi/4$, $p = 1$) the speed has to increase along the free-surface.

B. A Boundary With a Rigid Body

In plasticity theory (8) two conditions are imposed on a boundary with a rigid body: the normal speed is zero (streamline) and a stress condition. Three types of stress conditions are assumed: on a "rough" surface $\tau = 1$, on a "smooth" lubricated surface $\tau = 0$ and on a frictional surface τ is proportional to σ (Coulombian friction). There is no restriction on the tangential velocity which is generally different from that of the rigid body (Figure 6). The sign of the shearing stress on the rigid body depends, however, on the relative flow along the body: τ acts in the direction of relative flow.

Assuming for the time being (see Section 5) that the stress boundary condition is $\tau = \tau_w$, i.e., the shearing-stress is given ($0 \leq \tau_w \leq 1$), let us first consider the Equations [3.7]. For a given τ_w the angle between the α line and the body is given by (Figure 6)

$$\tau_w = \cos 2(\phi - \theta) \qquad [4.7]$$

Since τ_w acts in the direction of relative flow, the angle between the α line and the boundary is smaller than $\pi/4$ with respect to the relative flow direction. Three cases of a locally slipping and skidding boundary are represented in Figure 6.

The velocity components on the characteristic directions are

$$\begin{aligned} v_\alpha &= V \cos (\phi - \theta) \\ v_\beta &= -V \sin (\phi - \theta) \end{aligned} \qquad [4.8]$$

The condition of positive work [3.23] applied along the boundary gives

$$\frac{1}{\cos (\phi - \theta) \sin (\phi - \theta)} \frac{\partial V^2}{\partial s} > 0 . \qquad [4.9]$$

Hence, for an accelerating flow along the boundary in the direction of relative flow Equation [4.9] gives

$$\sin (\phi - \theta) > 0 , \qquad [4.10]$$

since $\cos (\phi - \theta) > 0$ for $|\phi - \theta| \leq \frac{\pi}{4}$. Consequently, in the case of an accelerating flow $\phi > \theta$ (Figure 6a), while for a retarded flow $\phi < \theta$ (Figure 6b).

A limit case is particularly important since it permits the exact integration of the equations of flow, namely $\tau_w = 1$ (a rough boundary) i.e., $\phi - \theta = 0$.

In this case the boundary is a characteristic line and Equations [3.19] become

$$\frac{\partial p}{\partial s} + 2\frac{\partial \theta}{\partial s} = -\frac{H}{2}\frac{\partial V^2}{\partial s} - G \sin\theta$$

$$\frac{\partial p}{\partial n} - 2\frac{\partial \phi}{\partial n} = -H V^2 \frac{\partial \theta}{\partial s} - G\cos\theta \qquad [4.11]$$

$$\frac{\partial V}{\partial s} - V\frac{\partial \theta}{\partial n} = 0$$

$$\frac{\partial V}{\partial s} + V\frac{\partial \theta}{\partial s} = 0$$

From the last two equations we find $\frac{\partial V}{\partial s} = 0$, $V = \text{const.}$ Hence, the speed is constant along a streamline which is a characteristic.

The first equation of [4.11] yields

$$p + 2\theta + Gy = \text{const.} \qquad [4.12]$$

Equation [4.12] shows how the pressure variation depends on the curvature of the boundary. In the case of a wheel p decreases along the boundary, since $\partial\theta/\partial s > 0$ (assuming that the gravity effect is negligible.).

In the case in which a streamline is an envelope of characteristics the velocity may vary along it. This property has been used in Prandtl solution (8) of flow between two rigid plates and Alexander (1) solution of rolling. This possibility is used in this work too (see Section 6).

C. A Line of Separation Between Regions of Rigid and Plastic Flows

A body moving in a rigid-plastic material generates a region of plastic nonuniform flow in its vicinity. Since at infinity the flow is uniform and in a rigid state, there is a transition between the two regions. In all problems of metal technology similar to the soil-wheel problem (extrusion, rolling, wedge indentation (1), (8), and solved with the aid of the quasi-state equations), it is assumed that this transition is realized through a line of tangential velocity discontinuity.

Such a line is regarded as a limit of a narrow zone of plastic flow in which the tangential velocity varies rapidly (Figure 7), (8). In this layer the direction of maximum shearing strain-rate is parallel to the layer axis. It is, therefore, assumed that the discontinuity line is a characteristic line.

Along such a line the tangential velocity jump is constant. This is simply found from Geiringer's Equations [3.17] (Figure 7b). Assuming that the discontinuity line is an α line, from continuity normal to the line

$$v_\beta' = -U_o' \sin \phi \qquad [4.13]$$

The first of Equations [3.17] gives

$$\frac{\partial v_\alpha'}{\partial x_\alpha'} = -U_o' \sin \phi \frac{\partial \phi}{\partial x_\alpha'} \quad \text{or} \qquad [4.14]$$

$$v_\alpha' - U_o' \cos \phi = \text{const} \qquad [4.15]$$

Since the component of the rigid uniform flow along the line is $U_o' \cos \phi$, Equation [4.15] states that the tangential jump is constant.

In a rigid-plastic material the shear stress in the plastic narrow zone is constant and equal to the yield-stress, $\tau' = k'$. Since there is no variation in the shear stress across a thin layer when inertial effects are neglected, the shear stress at the boundary between the plastic layer and the rigid zone is $\tau' = k'$ and decreases inside the rigid zone.

In a work-hardening material in which inertial effects are neglected the discontinuity layer has to diffuse and to have a finite thickness, since the shearing stress at the limit of the rigid zone must be smaller than the ultimate yield-stress. If the zone of work-hardening in the stress-strain diagram (Figure 2b) is narrow, the transition layer may be thin and the discontinuity line is still a valid approximation.

When inertial effects are taken into account the first question to be asked is if a line of velocity discontinuity is possible. Applying the momentum equation to such a discontinuity

line (Figure 7c) it is found that a shear-stress discontinuity exists across the line

$$\delta\tau' = \tau'_{plastic} - \tau'_{rigid} = \rho' U_o' \sin \phi \, \delta V \qquad [4.16]$$

or in dimensionless variables

$$\delta\tau = H \sin \phi \, \delta V \, . \qquad [4.17]$$

If $\delta\tau$ is much smaller than unity ($\delta\tau' \ll k'$) or $\phi = 0$ (no cross-flow), inertial jump may be neglected and the conclusions obtained from quasi-static considerations are valid. But in the case of soil-wheel interaction H may be of order unity and the inertial jump cannot be neglected. The important conclusion is that (assuming that in the transition layer the characteristics are directed along the layer), the inertial effect causes the thickening of the layer in an ideal rigid-plastic material, since otherwise the plastic flow will start with $\tau'_{max} < k'$. Hence, a velocity discontinuity is not acceptable in an ideal rigid-plastic material.

If work-hardening is taken into consideration, then a narrow transition zone becomes possible again when inertial effects are considered, since plastic flow may start with $\tau'_{max} < k'$. At any rate, since $\tau_e' > 0$ (Figure 2b) the inertial jump is limited by the value

$$\delta\tau = H \, \delta V \sin \phi < 1 \, . \qquad [4.18]$$

In a similar context the direction of the velocity discontinuity has to be such that

$$\delta\tau = H\delta V \sin \phi \geq 0 \qquad [4.19]$$

i.e., the maximum shearing stress in the rigid zone is smaller than the yield stress.

At this stage it will be assumed that in the case of soil-wheel interaction the rigid and plastic zones may be separated by a line of velocity discontinuity, provided that Equations [4.18] and [4.19] are satisfied. It is however, fair to say that this point needs further theoretical and experimental investigation in the framework of dynamic plasticity.

The velocity jump is constant and given by Equation [4.15], since inertial terms do not affect the Geiringer equations.

D. The Centered Fan

A bundle of intersecting characteristics of the same family determine a centered fan (Figure 8a). The vertex of the fan is a singular point. This singularity plays an important role in quasi-static plasticity and it is used in the solution of extrusion, rolling and sheet-drawing problems (1), (8). In all these solutions a velocity discontinuity is admitted at the vertex. It will be subsequently shown that in a plastic flow with inertial effects such a discontinuity is not possible.

Assuming, for sake of definiteness, that the straight characteristics are α lines, we may replace the α, β coordinates by polar coordinates (Figure 8)

$$\frac{\partial}{\partial x_\alpha} = \frac{\partial}{\partial r} \quad ; \quad \frac{\partial}{\partial x_\beta} = \frac{1}{r}\frac{\partial}{\partial \theta} \quad ; \quad v_\alpha = v_r \quad ; \quad v_\beta = v_\theta \qquad [4.19]$$

while, by definition

$$\frac{\partial \phi}{\partial x_\alpha} = 0 \qquad \frac{\partial \phi}{\partial x_\beta} = \frac{1}{r} \qquad [4.20]$$

Substituting the above relationships in Equations [3.16] - [3.17] we obtain

$$\frac{\partial p}{\partial r} = - H \frac{v_\theta}{r}\left(\frac{\partial v_r}{\partial \theta} - v_\theta\right) - G \sin\theta \qquad [4.21]$$

$$\frac{\partial p}{\partial \theta} - 2 = - H v_r \frac{\partial v_\theta}{\partial r} - G \cos\theta \qquad [4.22]$$

$$\frac{\partial v_r}{\partial r} = 0 \qquad \frac{\partial v_\theta}{\partial \theta} + v_r = 0 \qquad [4.23]$$

Equation [4.21] implies that generally p becomes infinite at the vertex. This inadmissible effect may be avoided in three cases: (i) $v_\theta = 0$ which by Equation [4.23] gives $v_r = 0$, i.e., rest;

(ii) $\frac{\partial v_r}{\partial \theta} - v_\theta = 0$ which together with Equation [4.23] provides for v_r and v_θ the solutions

$$v_r = C_1 \sin\theta + C_2 \cos\theta \qquad [4.24]$$
$$v_\theta = C_1 \cos\theta - C_2 \sin\theta$$

In a cartesian system the velocity distribution [4.24] is equivalent to

$$u = v_r \cos\theta - v_\theta \sin\theta = C_2$$
$$v = v_r \sin\theta + v_\theta \cos\theta = C_1 \qquad [4.25]$$

representing a <u>uniform</u> flow.

The pressure distribution is, according to Equations [4.21] and [4.22]

$$p = 2\theta - Gy \qquad [4.26]$$

which is obviously identical with that obtained in a quasi-static case;

(iii) $$v_\theta = v_\theta(r) \qquad \lim_{r \to 0} \frac{v_\theta}{r} = 0 \qquad [4.27]$$

Equations [4.23] and [4.26] shows that $v_r = 0$ and this is, therefore, a rotational flow around the vertex. The pressure distribution in the centered fan is given by

$$p = 2\theta - Gy + H \int \frac{v_\theta^2}{r} dr \qquad [4.28]$$

Case (iii) offers the possibility of matching plastic flows around concave corners (Figure 8b). In the case of a convex corner, in quasi-static solutions it is generally assumed that the flow passes from the uniform regime to the plastic flow (Figure 8c) through a line of velocity discontinuity AD followed by a centered fan with discontinuous ADC velocity at the vertex A (1), (8), (10). In a flow with inertial terms taken into account, the only possible type of flow behind the discontinuity line is a uniform flow (Figure 8d). This important difference has to be kept in mind when solving the soil-wheel problem.

E. A Line of Stress Discontinuity

The shear (τ) and normal stresses (σ_n) have to be continuous across a line. The normal stress parallel to the line (σ_t) may be discontinuous (Figure 9). Hill ((8), p. 157) has analyzed this type of discontinuity along a line separating two plastic zones.

His conclusions are: (i) such a line cannot be a characteristic; (ii) the characteristics of the same family from the two sides intersect the line at a same angle λ (Figure 9) ; (iii) the pressure jump is given by $|p_1 - p_2| = 2 \sin \lambda$, and (iv) the

velocity is continuous across the stress discontinuity line. The last property shows that such a line is acceptable in a plastic flow when inertial effects are taken into account and all above conclusions remain valid.

5. APPLICATION TO THE WHEEL PROBLEM

A. General

A rigid cylindrical wheel (roller) rotating and moving with constant speeds is considered here. The study is limited here to a driven slipping wheel which by definition has peripheric rotational speed larger than the soil speed at any point of the soil-wheel interface. Consequently the shearing stress along the wheel is positive everywhere on the interface.

Assuming that the soil, a soft undrained clay, behaves like a rigid-plastic material,one has to solve mathematically the problem by integrating the equations of plastic flow [3.8] - [3.11] with the appropriate boundary conditions.

Due to the difficulties caused by the inertial terms a perturbation expansion technique is used in order to simplify the equations (16). The influence of the inertial terms on some particular lines (Section 4) will be, however, taken into account.

B. The Perturbation Expansion

Spencer (16) has suggested a perturbation expansion of the equations of flow [3.16], [3.17] in which H is considered a small parameter. Assuming that all the variables may be expanded in a power series as

$$
\begin{aligned}
p &= p_o + H\, p_1 + H^2 p_2 + \ldots \\
\phi &= \phi_o + H\, \phi_1 + H^2 \phi_2 + \ldots \\
v_\alpha &= v_{\alpha_o} + H\, v_{\alpha_1} + H^2 v_{\alpha_2} + \ldots \\
v_\beta &= v_{\beta_o} + H\, v_{\beta_1} + H^2 v_{\beta_2} + \ldots
\end{aligned}
\qquad [5.1]
$$

and substituting in Equations [3.16], a set of separate systems of equations is obtained for each order of approximation. Here only the zero order terms are considered. They are satisfying the quasi-static equations [3.13] and [3.14], assuming that G (gravity effects) is also small.

Since only the zero-order approximation will be subsequently considered, the zero sub-index is omitted.

A legitimate question is that of the validity of the expansion in cases in which H is not small. A rigorous investigation of this problem is suggested for a later stage (Section 11). Intuitively, it seems that for moderate value of H ($H < 1$) the inertial effects are mainly concentrated in the discontinuity lines rather than in the plastic region. It is, therefore, hoped that taking certain precautions in the zero-order approximation, the zero-order solution is an acceptable approximation for the soil-wheel interaction at moderate speeds.

C. General Properties of Quasi-Static Solutions

The solution of the soil-wheel problem in the quasi-static approximation is still very difficult, as may be ascertained from the examination of similar solutions in metal technology.

In fact, almost all solutions obtained so far in plasticity theories are approximate, or "incomplete." A complete solution of a plasticity problem requires the determination of p, $\emptyset$, u, v satisfying the equations of flow [3.13] - [3.14] in the plastic region and the boundary conditions, and the determination of σ_x, σ_y and τ_{xy} in the rigid zone satisfying the elasticity equations and matching the stresses at the rigid-plastic interface. The equations are elliptic in the elastic zone and hyperbolic in the plastic zone. The location of the line of separation between the two zones is unknown and the same is true for the free-surface, if it occurs. Since the complete solution is very difficult the usual approach in plasticity is to look for approximate incomplete solutions which give lower and upper bounds of the exact solutions (8), (11).

A lower bound is found by assuming a plastic pattern which satisfies only the stress boundary conditions, while kinematical boundary conditions are neglected. In other words, if a stress distribution in both the assumed plastic and rigid zones which equilibrates the external forces is found, then the exact solution will allow for larger external forces.

The upper bound is found by assuming a plastic flow pattern which satisfies the velocity boundary conditions. The forces become in this case an upper bound to allowable external forces. The solution is found generally by assuming a priori a certain qualitative distribution of discontinuity lines, centered fans and slip-line field and trying to adjust them in order to satisfy the equations of flow and the boundary conditions.

In the soil-wheel problem the boundary conditions, for a given sinkage, are expressed in kinematical terms mainly (see Section 5E). It is, therefore, natural to seek an incomplete upper bound solution. Such a solution may be eventually proved to be an exact one if the stress field may be continued in the rigid zone. Otherwise, the validity of the solution has ultimately to be checked by comparison with experiments (see Section 9).

It is worthwhile to mention here that in view of the different simplifying assumptions it seems somehow futile to refine the computations beyond a certain limit. An approximate solution which reflects the main features of the problem and shows the characteristic trends should be satisfactory in the soil-wheel case.

D. Qualitative Analysis of the Problem

The solution of the soil-wheel problem has to be found now by assuming a slipline field which has to satisfy equations of plastic flow and boundary conditions. This is facilitated by a qualitative analysis of the problem.

First, it is reasonable to assume that, similarly to all known solutions in plasticity literature, the plastic region is of finite extent and attached to the body (experiments tend to confirm it, at least at low speeds). Moreover, in quasi-static conditions, there is no reason to assume a forward influence of the driven wheel. This is the case at least in the solutions of rolling, extrusion and sheet-drawing processes. If slight upstream influences are observed in experiments (22), it may be well due to work-hardening effects (see Section 9E) not taken into account in a rigid-plastic model. At any rate in all tests of driven wheels in clays no sensible upstream disturbances of the free-surface have been reported (18), (5) which confirms the assumption of upstream rigid flow.

In the downstream region the free-surface has to leave the wheel smoothly and a plastic "wake" of finite dimension is created. This is different from rolling and extrusion processes in which it is assumed that the free-surface is horizontal immediately behind the body (1), (8), by locating a centered fan and a discontinuity line at the rear. Inertial effects do not allow for such a type of solution (see Section 6C) and experiments, even at low speeds, in both sand and clay confirm this conclusion (18), (21), (22).

Consequently, the free-surface has qualitatively the shape suggested in Figure 10.

The kinematics of flow may be also depicted from qualitative considerations. Since the flow is incompressible, from continuity requirements the streamlines have to look somehow

as in Figure 10a. The average speed in the plastic zone is maximum at the bottom of the wheel. The flow is converging from upstream to the bottom section and diverges downstream in order to match the uniform-rigid downstream flow. Obviously, in an incompressible material and a two-dimensional flow there is no rut and both free-surface and speed have to reach the unperturbed state downstream.

A qualitative picture of a suggested slipline field built in the light of the above observations is presented in Figure 10b. A detailed argumentation and examination is presented in Section 6.

At the bow A a line of discontinuity AB separating the rigid and plastic zone is suggested. This is an α line since shearing stresses acting on the rigid material have to have the same sign as those acting on the wheel. The speed along the wheel is increasing from A to C, so that the β lines have to intersect AC at the angles shown in Figure 10b (according to Section 4B). On the rear portion CR it is assumed that the flow is decelerated. Hence, the β sliplines have to intersect CR at the angles of Figure 10b. The transition between the two zones, of converging and diverging flow, is realized through a rigid core BCD which moves horizontally with the bottom soil speed. A somehow similar rigid region is assumed in rolling solutions (1). Although not necessarily rigorous, this separation of the two plastic regions ABCA and CBETRC by a zone of uniform flow is very convenient for computational purposes (Section 6). The zone RTER

is a curvilinear triangle created by the free-surface TR. The line ET separating plastic and rigid zones at the rear again has to be a characteristic line since at least the second derivatives of the velocity are discontinuous there (17). This is assumed again to be an α line, with the rigid zone sheared in the same direction as the soil beneath the wheel. From inertial considerations (Section 6C) there is no possible velocity jump on the line ER and the flow has to match smoothly the uniform downstream flow.

The region CDER is a transition region in which the flow diverges. Along DE the speed drops from its maximum value to the unperturbed speed. The only possible way to satisfy this requirement is to assume that DE is an envelope of α lines similar to that suggested by Prandtl in block compression ((8), p. 228) or by Alexander (1) in rolling. RE is assumed to be a line of stress discontinuity, so that the angle between the sliplines is discontinuous on it, while the velocity is continuous. The suggested slipline is examined in detail in Section 6.

E. Boundary Conditions

The boundary conditions on the different portions of the plastic flow domain ABDETRCA (Figure 10b) have been in part discussed in Section 4, but will be briefly recalled here. The problematic boundary condition - that of stress on the wheel - will be discussed in more detail later.

The separation line AB is assumed to be an α characteristic line with a velocity jump along it. The line DE is assumed to be a horizontal envelope of α lines with a varying velocity jump along it. The line ET is an α line with continuous velocity across, i.e., $u = 1$, $v = 0$ on this boundary. CB and CD are assumed to be β lines with continuous velocity across $u = u_b$, $v = 0$ (Figure 10a). The free-surface RT is stress-free and a streamline (Equations [4.1] and [4.2]. The location of all these lines is a priori unknown.

The only remaining boundary is the soil-wheel interface which is obviously a streamline. An additional stress condition is necessary in order to solve the problem. We have not been able to find experimental evidence on this condition in the literature for the case of a wheel-clay interface.

A perfectly rough wheel may be imagined as a rim with a series of spuds which cut the soil. The spuds have to be very small if the wheel is to be considered as a smooth continuous line and the quantity of entrained material has to be negligible. A perfectly smooth wheel may be imagined as a smooth lubricated surface with zero shear stress along it. A real rough wheel is probably somewhere between the two. In Uffelmann's experiments for instance, (18), the highest shear stress attained on the wheel was $\tau \cong 0.3$. In (5), rough and smooth wheels tested in the same kinematical conditions gave approximately the same resultant forces. We are inclined, therefore, to admit that the shear stress on rigid wheels is less than the yield stress and there are no perfectly rough wheels. In reality the problem

is more complex. Between the wheel and the soil body moving with different speeds a boundary layer of wet clay probably develops. This problem needs special consideration and analysis.

At this stage, and in the framework of the rigid-plastic model, it will be assumed that on the forward part of the wheel AC the shear stress τ is constant and given ($0 \leq \tau_w \leq 1$). Its magnitude has to be determined experimentally. It will be shown that there is no major difficulty in solving the problem when more complex relationships are used, like τ_w depending on the slippage along the wheel or on pressure; the effect of such relationships on the plastic flow is left for future investigation. At the rear portion CR it is assumed that the shear stress drops along the wheel from τ_w at C to $\tau = 0$ at R. This type of τ distribution seems to be confirmed by experiments with driven wheels (18).

In addition to velocity and stress conditions the line ACR is the only one whose location is known, having the equation $x^2 + y^2 = 1$. The determination of the slipline field in the xy physical plane starts always from this line. The angle of detachment θ_r is unknown and constitutes one of the important parameters of the problem.

6. THE SOLUTION OF THE QUASI-STATIC EQUATION FOR THE DRIVEN WHEEL

A. The Method of Solution

The wheel-soil problem belongs to the difficult category of problems in which both kinematical and stress boundary conditions are imposed on the different boundaries, which is different from the foundation engineering problems in which the problems are formulated in terms of forces solely. For this reason the four variables p, $\emptyset$, v_α, v_β are interrelated and the whole set of Equations [3.13] and [3.14] has to be used.

The method used here is the analytical method of Hill's book ((8), Chap. VI). The problem will be solved in an auxiliary characteristic plane rather than in the physical xy plane.

Selecting arbitrarily, but conveniently, two parameters α and β such that α is constant on β lines and β is constant on α lines, the variables p, $\emptyset$, v_α, v_β, x,y become functions of α,β and satisfy the following set of equations

$$\frac{\partial p}{\partial \alpha} + 2\frac{\partial \emptyset}{\partial \beta} = 0 \qquad [6.1]$$

$$\frac{\partial p}{\partial \beta} - 2\frac{\partial \emptyset}{\partial \beta} = 0 \qquad [6.2]$$

$$\frac{\partial v_\alpha}{\partial \alpha} - v_\beta \frac{\partial \emptyset}{\partial \alpha} = 0 \qquad [6.3]$$

$$\frac{\partial v_\beta}{\partial \beta} + v_\alpha \frac{\partial \phi}{\partial \beta} = 0 \qquad [6.4]$$

$$\frac{\partial y}{\partial \alpha} - \tan \phi \frac{\partial x}{\partial \alpha} = 0 \qquad [6.5]$$

$$\frac{\partial y}{\partial \beta} + \text{cotan } \phi \frac{\partial x}{\partial \beta} = 0 \qquad [6.6]$$

Equations [6.1] - [6.4] are obtained from Equations [3.13] - [3.14] by reducing by the factors $h_\alpha = dx_\alpha/d\alpha$, $h_\beta = dx_\beta/d\beta$. h_α and h_β are the metrics coefficients (or Lamme' coefficients) and they represent the scale factors between the characteristic and physical planes. A well-known property of hyperbolic systems is their invariance under a change in characteristic variables. Note that the full equations of flow [3.6] and [3.7] do not possess this property.

Equations [6.5] and [6.6] are simply a transcription of the characteristic directions (Equations [3.15].)

A convenient transformation of Equations [6.5] and [6.6] is achieved by using the new variables ((8), Chap. VI).

$$\bar{x} = x \cos \phi + y \sin \phi \qquad [6.7]$$
$$\bar{y} = - x \sin \phi + y \cos \phi$$

which give

$$\frac{\partial \bar{y}}{\partial \alpha} + \bar{x} \frac{\partial \phi}{\partial \alpha} = 0 \qquad [6.8]$$

$$\frac{\partial \bar{x}}{\partial \beta} - \bar{y} \frac{\partial \phi}{\partial \beta} = 0 \qquad [6.9]$$

B. An Incorrect Slipline Field

Before proceeding to the detailed solution of the flow problem it is worthwhile to discuss a slipline field suggested in the early stage of this work which proved later to be incorrect. This analysis is also valuable since in (22) it is claimed that the experiments show such a field.

In the preliminary stage of the work it was assumed that the plastic region is delimited by a closed α line (Figure 11). This was proved ultimately wrong for at least two reasons:

(i) At R the free-surface is intersected by the CR α line at 45 degrees (Figure 11). According to Section 4A the region TCRT is in a state of compression. Under these circumstances the detailed solution of flow in the triangle TCRT (the method is given in Section 6C) has shown that the free-surface is concave (Figure 11) and the speed is increasing from T to R and negative work is done in the entire TCRT region, which contradicts the basic condition of plastic work.

(ii) The velocity jump along ABCR is constant and a typical streamline has the shape depicted in Figure 11. It is easy to ascertain that along the rear portion BCR the inertial shear

stress jump along CR is such that the shear stress in the rigid zone is larger than the shear stress in the plastic zone, i.e., larger than the yield stress.

For these two reasons this initial slipline field, although esthetically appealing at first glance, has been abandoned in the favor of that of Figure 10b.

C. The Free-Surface Region RETR (Figures 9b and 11)

Let us consider in detail the free-surface curvilinear triangle TFRT in the physical plane (Figure 12a). A point P has the coordinates x,y and the characteristic coordinates α_P, β_P. The characteristic coordinates are selected as follows: the value of β on the α characteristic line P'P is $\beta = \phi_{P'}$, i.e. the value of ϕ at the intersection of the α line and the free-surface; the value of α on the β characteristic P"P is equal to $\phi_{P"}$, i.e. the value of ϕ at the intersection of the β line and the free-surface. As long as the free-surface RT is curved with no inflexion points a one-to-one correspondence exists between x,y and α,β.

At point T the free-surface has to be tangent to the horizontal unperturbed rigid free-surface. Otherwise a velocity jump δV will exist along FT (Figure 11). Such a velocity jump induces an inertial shear-stress jump along FT (see Section 4C) which increases the shear stress in the rigid zone beyond the yield-stress. Hence, the free-surface has to match smoothly the horizontal and $\alpha_T = \beta_T = \phi_T = \pi/4$.

At point R the free-surface must be tangent to the wheel. Again, an angle different of zero between the free-surface and the wheel means a discontinuity in velocity along RF. But a velocity jump cannot exist in the interior of a plastic zone since due to inertial shear stress jump the shear stress on one side of the line will be different from the yield-stress, which is absurd. Consequently $\alpha_R = \beta_R = \phi_R = \pi/4 + \theta_r$.

The representation of RFTR in the characteristic plane $\alpha\beta$ is very simple (Figure 12b). By the definition of α and β the free-surface is represented by the line $\alpha = \beta$, while the characteristics are parallel to the axes. Now p, ϕ, v_α, v_β, x, y as functions of α and β, for a given θ_r have to be determined.

(i) Solution of p, ϕ (dynamics of flow) -

The elimination of p from Equations [6.1] and [6.2] shows that ϕ satisfies the equation

$$\frac{\partial^2 \phi}{\partial \alpha \partial \beta} = 0 \qquad [6.10]$$

The general solution of Equation [6.10] is

$$\phi = f(\alpha) + h(\beta) \qquad [6.11]$$

where f and h are arbitrary functions. On the free-surface TR($\alpha = \beta$) $\phi = \alpha = \beta$ by definition, which gives

$$f(\beta) + h(\beta) = \beta$$

or $$h(\beta) = \beta - f(\beta)$$

and

$$\emptyset = f(\alpha) - f(\beta) + \beta \ . \qquad [6.12]$$

From Equations [6.1] and [6.2] it is easily found that

$$p = -2\left(\int \frac{\partial \emptyset}{\partial \alpha} \, d\alpha - \frac{\partial \emptyset}{\partial \beta} \, d\beta \right) \qquad [6.13]$$

The Equations [6.12] and [6.13] yield

$$p = -2[f(\alpha) + f(\beta) - \beta] + C \ . \qquad [6.14]$$

On the free-surface RT the isotropic pressure is constant and for the compression state (Equation [4.3] $p = 1$. Hence, for $\alpha = \beta$ Equation [6.14] gives

$$-4f(\alpha) + 2\alpha + C = 1 \ . \qquad [6.15]$$

From Equations [6.12], [6.14] and [6.15] the final expressions for p and $\emptyset$ are

$$\phi = \frac{\alpha + \beta}{2} \qquad [6.16]$$

$$p = -\alpha + \beta + 1 \qquad [6.17]$$

which completely solves the problem.

It is worthwhile to note that at point F (Figure 12) $\phi_F = \frac{\alpha_F + \beta_F}{2} = \frac{\pi}{4} + \frac{\theta_r}{2}$, i.e., the characteristic line TF bends with an angle $\frac{\theta_r}{2}$ and the characteristic FR with the same angle $\frac{\theta_r}{2}$. The pressure drops along TF and reaches a minimum value at F, $p_F = -\alpha_F + \beta_F + 1 = 1 - \theta_r$ which means that the soil is under slight tension in this region.

(ii) Solution of v_α, v_β (kinematics) -

From Equations [6.3], [6.4] and [6.16] it is found that v_α and v_β satisfy the following relationships

$$\frac{\partial v_\alpha}{\partial \alpha} - \frac{v_\beta}{2} = 0 \qquad [6.18]$$

$$\frac{\partial v_\beta}{\partial \beta} + \frac{v_\alpha}{2} = 0 ,$$

or, by elimination of v_α and v_β

$$\frac{\partial^2 v_\alpha}{\partial\alpha\partial\beta} + \frac{v_\alpha}{4} = 0$$

$$\frac{\partial^2 v_\beta}{\partial\alpha\partial\beta} + \frac{v_\beta}{4} = 0 \ , \qquad [6.19]$$

i.e., v_α and v_β satisfy the telegraph equation.

The kinematic boundary conditions are as following: On the characteristic FT (Figure 12) the velocity is continuous and equal to the rigid velocity u = 1. Hence, from Equation [3.12]

$$v_\alpha = \cos \phi = \cos \frac{\frac{\pi}{4} + \alpha}{2}$$

$$v_\beta = - \sin \phi = - \sin \frac{\frac{\pi}{4} + \alpha}{2} \qquad [6.20]$$

On the free-surface, according to Equation [4.4]

$$v_\alpha + v_\beta = 0 \ . \qquad [6.21]$$

v_α and v_β may be found from Equations [6.19], [6.20] and [6.21] by the following procedure. Let us introduce a new variable $v = v_\alpha + v_\beta$. v satisfies the following equations and boundary conditions in the characteristic plane (derived from Equations [6.19], [6.20] and [6.21]

$$\frac{\partial^2 v}{\partial_\alpha \partial_\beta} + \frac{v}{4} = 0 \qquad \text{(in TFRT)} \qquad [6.22]$$

$$v = \cos \frac{\frac{\pi}{4} + \alpha}{2} - \sin \frac{\frac{\pi}{4} + \alpha}{2} \qquad \text{(on TF)} \qquad [6.23]$$

$$v = 0 \qquad \text{(on TR)} \qquad [6.24]$$

The triangular domain TFRT in the α,β plane (Figure 12b) may be reflected across TR in TF'RT. From the symmetry of the telegraph equation and the condition [6.24] v may be determined in the whole rectangular domain TFRF'T by reflection. Since TF' is the reflection of FR, v takes on the value

$$v = -\left(\cos \frac{\frac{\pi}{4} + \beta}{2} - \sin \frac{\frac{\pi}{4} + \beta}{2} \right) \qquad \text{(on TF')} \qquad [6.25]$$

The solution of the telegraphic equation for a function given along two intersecting characteristics by the Riemann procedure is described by Hill ((8), p. 155). In the present case the solution is (Figure 12b)

$$v(P) = \int_T^{P_2} G \frac{\partial v}{\partial \alpha} \, d\alpha + \int_T^{P_1} G \frac{\partial v}{\partial \beta} \, d\beta \qquad [6.26]$$

where $G(\alpha,\beta;\ \alpha_P,\beta_P) = J_o\left[\sqrt{(\alpha_P - \alpha)(\beta_P - \beta)}\right]$ is the Green Function.

The substitution of the expressions of the Green function and the values of $\partial v/\partial\alpha$ and $\partial v/\partial\beta$ on the boundaries in Equation [6.26] gives finally

$$v(\alpha,\beta) = -\frac{1}{2}\int_{\pi/4}^{\alpha} J_o\left[\sqrt{(\alpha-\xi)(\beta-\frac{\pi}{4})}\right]\left(\sin\frac{\xi+\frac{\pi}{4}}{2} + \cos\frac{\xi+\frac{\pi}{4}}{2}\right)d\xi$$

$$+\frac{1}{2}\int_{\pi/4}^{\beta} J_o\left[\sqrt{(\alpha-\frac{\pi}{4})(\beta-\xi)}\right]\left(\sin\frac{\xi+\frac{\pi}{4}}{2} + \cos\frac{\xi+\frac{\pi}{4}}{2}\right)d\xi \qquad [6.27]$$

Equation [6.27] completely determines v. In order to find v_β, for instance, the second equation of [6.18] is written as

$$\frac{\partial v_\beta}{\partial\beta} - \frac{v_\beta}{2} = -\frac{v}{2} \qquad [6.28]$$

The integration of this ordinary differential equation along a β line from P_a to P (Figure 12) gives

$$v_\beta(\alpha,\beta) = -\sin\frac{\frac{\pi}{4}+\alpha}{2}\, e^{\frac{1}{2}(\beta-\frac{\pi}{4})} - e^{\beta/2}\int_{\pi/4}^{\beta} v(\alpha,\xi)\, e^{-\xi/2}\, d\xi\,, \qquad [6.29]$$

which determines v_β once v is known. Obviously v_α is found from $v_\alpha = v - v_\beta$.

The integrals in Equations [6.27] and [6.29] have been computed numerically (by Simpson rule) on HYDRONAUTICS' IBM 1130 computer.

The resulting values of v_α, v_β, $\emptyset$ and $V = \sqrt{v_\alpha^2 + v_\beta^2}$ are given in Appendix 1. The computations have been carried out to the maximum possible value of $\theta_r = \pi/4$ and the results may be used for any arbitrary θ_r in the range $0 < \theta_r < \pi/4$. Each group of results in Appendix 1 corresponds to a constant α in the range $\pi/4 < \alpha < \pi/2$ and a variable β in the range $\pi/4 \leq \beta < \alpha$. The velocity V on the free-surface has the value of the last line of each group, where $\alpha = \beta$. It is easy to ascertain that the velocity decreases along the free-surface, or increases from T ($V_T = 1$) to R ($V_R = 1.75$ for $\theta_r = \pi/4$). For moderate values of θ_r, as encountered in applications, V_R is smaller. The velocity distribution along TR will be used in Section 7A in order to determine the magnitude of the recovery angle θ_r.

The results of this section and of Appendix 1 are valid not only in the triangle RFTR, but in the whole region REFTR (Figure 10b). The plastic flow in RFER is just the continuation of the flow in RFTR across the characteristic RF.

(iii) The determination of x,y (geometry of flow) -

The mapping of the free-surface triangle TFRT from the characteristic plane to the physical plane may be done by using Equations [6.5], [6.6] or Equations [6.8], [6.9]. In order to solve the problems the location of the line RE (Figure 10b) has to be known. In principle this can be done by starting with the solution of the x,y equations from the wheel, but this is not done here.

The $x(\alpha,\beta)$ and $y(\alpha,\beta)$ of the line RE are enough in order to solve the problem since an additional boundary condition exists on the free-surface, namely the fact that $\phi - \theta = \pi/4$ (Equation [4.3]. Since $\tan\theta = dy/dx$, on the free-surface RT

$$\frac{dy}{dx} = \tan\left(\phi - \frac{\pi}{4}\right) = \tan\left(\frac{\alpha+\beta}{2} - \frac{\pi}{4}\right). \qquad [6.30]$$

This additional condition permits, in principle, the mapping of the whole region TERT from the α,β plane onto the x,y plane.

D. The Bow Region ABCA (Figures 10b and 13)

In this case the characteristic coordinates of a generic point P (Figure 13a) are selected as following: α is the angle $\phi_{P''}$ at the intersection between the β line PP" and the α base line AP"B and β is $\phi_{P'}$ at the intersection of the α line PP' and the β base line BP'C.

Some general relationships may be found before solving the problem in detail. At point A (the leading edge) the velocity inside the plastic zone has to be parallel to the wheel, since no velocity discontinuity is admitted inside the plastic zone from inertial considerations (see Section 4D). AB is a line of velocity jump. The jump δV may be found from continuity considerations at point A (Figure 13b).

From the velocity triangle, by projecting on the direction of δV and on the normal to it, the following is obtained:

$$V_a = \frac{\sin \theta_\ell}{\sin (\theta_\ell - \theta_a)} \qquad [6.31]$$

$$\delta V = V_a \cos (\theta_\ell - \theta_a) - \cos \theta_\ell = \frac{\sin \theta_a}{\sin(\theta_\ell - \theta_a)} \qquad [6.32]$$

The angle θ_a is related to the sinkage z by (Figure 12a)

$$z = 1 - \cos \theta_a \, . \qquad [6.33]$$

The angle θ_ℓ is determined by the shearing stress τ_w on the soil-wheel interface at A. θ_ℓ is the angle between the α line AB and horizontal, i.e., $\theta_\ell = \phi_{wA}$. The relationship between τ_w and ϕ_{wA} is, according to Equation [4.7]

$$\tau_w = \cos 2(\phi_w - \theta) = \cos 2(\theta_\ell - \theta_a) \qquad [6.34]$$

which determines θ_ℓ for given τ_w and θ_a. Obviously τ_w may vary in the range $0 \leq \tau_w \leq 1$, i.e., between perfectly smooth and perfectly rough conditions. For $\tau_w = 0$ at A, $\theta_\ell - \theta_a = \pi/4$ while for $\tau_w = 1$, $\theta_\ell - \theta_a = 0$ and the characteristic AB sticks to the wheel.

According to our present concept on soil-wheel interface (see Section 5E) τ_w is assumed constant on AC.

The line BC is a characteristic β line between the plastic zone ABCA and the assumed rigid core BCDB (Figure 10b). The velocity in the rigid core is horizontal and constant $u = u_b$, $v = 0$. There is no velocity jump along BC since at C, inside the plastic zone, the velocity along the wheel is also horizontal. Hence, the slipline AB has a horizontal tangent at B ($\phi_B = 0$). Since δV, the velocity jump along AB is constant (Section 4C), we have

$$u_b = 1 + \delta V = 1 + \frac{\sin \theta_a}{\sin(\theta_\ell - \theta_a)} , \qquad [6.35]$$

which gives u_b in terms of known quantities. From continuity considerations

$$z + h = u_b h \qquad [6.36]$$

or

$$h = \frac{z}{u_b - 1} = \frac{(1 - \cos \theta_a) \sin (\theta_\ell - \theta_a)}{\sin \theta_a} \qquad [6.37]$$

which gives the thickness of the plastic zone at bottom.

Finally, for the slipping wheel considered here the wheel peripheral velocity $V_w' = \omega' r'$ has to be larger than the soil velocity at the interface AC (Section 5E). Since the maximum soil velocity occurs at bottom where $u = u_b$, the following inequality holds

$$V_w \geq u_b ,$$

or in terms of slippage coefficient $S = \frac{V_w - 1}{V_w}$

$$\frac{1}{1 - S} \geq u_b \quad , \quad S \geq \frac{u_b - 1}{u_b} \; . \qquad [6.38]$$

Using the value of u_b of Equation [6.35]

$$S \geq S_m = \frac{\sin \theta_a}{\sin(\theta_\ell - \theta_a) + \sin \theta_a} \qquad [6.39]$$

This is the minimum slippage necessary in order to ensure a positive τ_w along the wheel. The real slippage may be larger than S_m and rigid-plastic considerations solely permit τ_w to remain unchanged. A more detailed study, experimental or theoretical, may reveal a relationship between S_m and τ_w.

If we assume that the real slippage coefficient S is equal to S_m, then a relationship between τ_w and S_m (for given z) is established through Equation [6.39]. For $\tau_w = 1$, $S_m = 1$, as expected.

Now, a detailed solution of the plastic flow is presented along the lines of Section 6D. The domain ABCA is represented in the characteristic α,β plane in Figure 13C. The representation follows straightforward from the definition of α and β. The wheel-soil interface AC is represented by an unknown curvilinear line in the characteristic plane.

(i) The determination of p, ϕ (dynamics)

Again, ϕ has the general expression [6.11]. But, from the definition of α and β, we have $\phi = \alpha$ on AB ($\beta = 0$) and $\phi = \beta$ on BC ($\alpha = 0$). This gives immediately

$$\phi = \alpha + \beta \qquad [6.40]$$

The isotropic pressure p is related to ϕ through Equation [6.13]. Hence,

$$p = -2(\alpha - \beta) + \text{const} \qquad [6.41]$$

Let p_C be the pressure at C. Then, [6.41] becomes

$$p = p_C - 2(\alpha - \beta - \phi_{wc}) \qquad [6.42]$$

where $\phi_{wc} = \phi_w - \theta = -\frac{1}{2}\cos^{-1}\tau_w$.

The pressure increases along the wheel from p_C to p_A, p_A being given by

$$p_A = p_C + 2(\theta_\ell + \phi_{wc}) \ . \qquad [6.43]$$

The normal stress acting on the wheel is (Equation [3.7])

$$\sigma_w = -p + \sin 2(\phi_w - \theta) \ . \qquad [6.44]$$

Since $\tau_w = \cos 2(\phi_w - \theta)$ is assumed constant, $\phi_w - \theta$ is constant and σ_w is simply equal to the isotropic pressure plus a constant. For a perfectly smooth wheel ($\tau_w = 0$), $\phi_w - \theta = -\pi/4$ and $\sigma_w = -p - 1$; for a rough wheel ($\tau_w = 1$), $\phi_w - \theta = 0$ and $\sigma_w = -p$.

(ii) The determination of v_α, v_β (kinematics) -

Similarly to Equations [6.18] and [6.19] we have this time for v_α and v_β

$$\frac{\partial v_\alpha}{\partial \alpha} - v_\beta = 0 \qquad \frac{\partial v_\beta}{\partial \beta} + v_\alpha = 0 \qquad [6.45]$$

$$\frac{\partial^2 v_\alpha}{\partial \alpha \partial \beta} + v_\alpha = 0 \qquad \frac{\partial^2 v_\beta}{\partial \alpha \partial \beta} + v_\beta = 0 \; . \qquad [6.46]$$

The boundary conditions for the telegraph Equations [6.46] are as follows:

- On AB v_α and v_β satisfy the conditions along a line of separation between a plastic and a rigid zone (Section 4C)

$$v_\alpha = 1 + \delta V \cos \phi$$
$$v_\beta = - \sin \phi \qquad [6.47]$$

or by Equation [6.40]

$$v_\alpha = 1 + \delta V \cos \alpha$$

$$v_\beta = - \sin \alpha \quad . \qquad (\text{on } \beta = 0;\ -\theta_\ell < \alpha < 0) \qquad [6.48]$$

- On the line BC there is no velocity jump, hence

$$v_\alpha = u_b \cos \phi = u_b \cos \beta$$

$$v_\beta = -u_b \sin \phi = -u_b \sin \beta \quad . \qquad (\text{on } \alpha = 0;\ -\phi_{wc} < \beta < 0) \qquad [6.49]$$

These conditions completely determine the values of v_α and v_β at any point in the characteristic rectangle ABCB'A of Figure 13c).

Following the same Riemann method as in Section 6D, v_α and v_β at a point $P(\alpha,\beta)$ are given by

$$v_\alpha(P) = \int_B^{P''} G \frac{\partial v_\alpha}{\partial \alpha} \, d\alpha - \int_{P'}^{B} G \frac{\partial v_\alpha}{\partial \beta} \, d\beta + G(P,B)\, v_\alpha(B)$$

$$v_\beta(P) = \int_B^{P''} G \frac{\partial v_\beta}{\partial \alpha} \, d\alpha - \int_{P'}^{B} G \frac{\partial v_\alpha}{\partial \beta} \, d\beta + G(P,B)\, v_\beta(B) \qquad [6.50]$$

where G, the Green Function, is

$$G(\alpha_P,\beta_P;\alpha,\beta) = J_o\left[2\sqrt{(\alpha_P-\alpha)(\beta_P-\beta)}\right] . \qquad [6.51]$$

Using the values of v_α, v_β on the boundaries (Equations [6.48] and [6.49] and the definition of G (Equation [6.51]), Equations [6.50] become

$$v_\alpha(\alpha,\beta) = -\int_o^\alpha J_o\left[2\sqrt{\beta(\alpha-\xi)}\right]\sin\xi d\xi - u_b\int_o^\beta J_o\left[2\sqrt{\alpha(\beta-\xi)}\right]\sin\xi d\xi$$

$$+ u_b J_o(2\sqrt{\alpha\beta}) \qquad [6.52]$$

$$v_\beta(\alpha,\beta) = -\int_o^\alpha J_o\left[2\sqrt{(\alpha-\xi)\beta}\right]\cos\xi d\xi - u_b\int_o^\beta J_o\left[2\sqrt{\alpha(\beta-\xi)}\right]\cos\xi d\xi \qquad [6.53]$$

For the illustration of the method we have selected an example with the following data

$$\theta_a = 30^\circ \rightarrow z = 0.134$$

$$\phi_w - \theta = \phi_{wc} = -35^\circ \rightarrow \tau_w = 0.34 , \theta_\ell = 65^\circ \qquad [6.54]$$

v_α and v_β have been determined by numerical integration and their values for different α and β in the rectangle $-\theta_\ell < \alpha < 0$, $\phi_{wc} < \beta < 0$ are given in Appendix 2.

The location of the line AC is found now by using the condition that AC is a streamline and a line of constant $\tau = \tau_w$. According to Equation [4.8], v_α and v_β satisfy the condition

$$\frac{v_\beta}{v_\alpha} = - \tan (\phi_w - \theta) \qquad [6.55]$$

or, in our example ($\phi_w - \theta = -35^\circ$)

$$\frac{v_\beta}{v_\alpha} = \tan 35^\circ = 0.7 \ . \qquad [6.56]$$

In the numerical results v_β/v_α has been given for each point (Appendix 2) and it was a simple matter to pick from the results the location of the points which satisfy Equation [6.56]. In Figure 14 the characteristic plane, including AC, is represented according to the data of Appendix 2.

Once AC is known the same Appendix 2 provides the speed $V = \sqrt{v_\alpha^2 + v_\beta^2}$ along the wheel. In Figure 15 the velocity variation along the wheel and along corresponding points (i.e., on same α lines) along the separation line AB is given graphically. In Figure 17 the velocity distribution along a few characteristics is also given.

The velocity along the wheel increases from its value at the leading edge A ($V = 1.57$) to its value at the bottom B ($V = 1.88$) and the requirement of positive work is satisfied.

The velocity along the slipline AB is somehow higher than the value on AC. A rough check has shown that the positive work condition (Equation [3.22]) is satisfied everywhere in the plastic zone. The small difference between V on AC and AB for the same β slipline shows that the distribution is almost uniform on the β lines, but changes in α direction (Figure 17).

(iii) The solution of x,y (geometry) -

Equations [6.8] and [6.9] have been used in order to map the characteristic region of Figure 15 onto the physical plane.

Along the wheel AC x and y are known, namely,

$$x = \sin\theta \qquad y = -\cos\theta \tag{6.57}$$

According to Equations [6.7] $\bar{x}$ and $\bar{y}$ are given by

$$\begin{aligned} \bar{x} &= \sin\theta\cos\phi_w - \cos\theta\sin\phi_w = -\sin(\phi_w - \theta) \\ \bar{y} &= -\sin\theta\sin\phi_w - \cos\theta\cos\phi_w = -\cos(\phi_w - \theta), \end{aligned} \tag{6.58}$$

But, from the assumption of constant τ_w we have

$$\phi_w - \theta = \phi_{wc} = -\frac{1}{2}\cos^{-1}\tau_w \tag{6.59}$$

Hence, from Equation [6.54]

$$\bar{x} = \sin 35^\circ \qquad \bar{y} = -\cos 35^\circ \qquad \text{(On AC)}$$

With these values of $\bar{x}$ and $\bar{y}$ along AC, the Equations [6.8] and [6.9] have been integrated numerically, by finite differences. The results, in terms of the mapping of α,β region ABCA on x,y plane, are given in Appendix 3. The slipline field has been plotted graphically in Figure 16. The sliplines are orthogonal, as required by the theory. They intersect the wheel at the constant angle corresponding to $\tau_w = 0.34$ ($\phi_w - \theta = -35^\circ$).

Hence, for the selected example, the plastic flow in the bow region has been completely solved. The stress distribution has been determined (Equations [6.40] and [6.42] excepting the constant p_c which has to be found from the matching of bow and rear plastic regions.

There is no problem, in principle, to find graphically the streamlines in the bow region, but the work involved is quite tedious. A simpler problem is to depict the velocity distribution along characteristics, based on the data of Appendices 2 and 3. Such a representation, for the discussed example, is given in Figure 17. Figure 17 shows that v_α is almost uniformly distributed along the β characteristics, while v_β has approximately a linear variation. This observation may help in constructing the kinematical field approximately without solving the problem in detail. It may be also useful in future work in which inertial terms inside the plastic zone or work-hardening effects would be taken into account.

E. The Plastic Zone CDERC and the Rigid Core CBDC (Figures 10b and 18)

The solution of the plastic flow in CDERC has to start with the horizontal envelope of α lines DE. There is no systematical study of such lines in literature.

Again, the representation of the plastic domain in the characteristic plane has to start with a selection of the characteristic variables α,β. The zone CDERC is represented in detail in Figure 18a.

Let α,β in the subregion DQED be the following (Figure 18a): α_P is the distance between D and P" on the base line DF ($\alpha_P = s_{P"}$) and β_P is $s_{P'}$. A one-to-one correspondence is thus established between points in DQED and the α,β plane. The image of DE in α,β plane is obviously the line $\alpha = \beta$ (Figure 18b).

Since $\phi = 0$ on this line it is easy to ascertain that ϕ has the expression

$$\phi = \alpha - \beta \qquad [6.60]$$

in the domain DQED.

The Equations [6.3], [6.4], [6.8] and [6.9] become now

$$\frac{\partial v_\alpha}{\partial \alpha} - v_\beta = 0$$

$$\frac{\partial v_\beta}{\partial \beta} - v_\alpha = 0 \qquad [6.61]$$

$$\frac{\partial \bar{y}}{\partial \alpha} + \bar{x} = 0$$

$$\frac{\partial \bar{x}}{\partial \beta} + \bar{y} = 0 \ .$$

All the functions v_α, v_β, $\bar{x}$ and $\bar{y}$ satisfy telegraphic equations of the type

$$\frac{\partial^2 f}{\partial \alpha \partial \beta} - f = 0 \qquad [6.62]$$

which admits as Green function

$$G(\alpha,\beta;\alpha_P,\beta_P) = I_o \left[2\sqrt{(\alpha_P - \alpha)(\beta_P - \beta)} \right] . \qquad [6.63]$$

Hence, all the dependent functions may be found, in principle, by Riemann's method.

The plastic domain CDQR (Figure 18a) may be represented on the same α,β plane by selecting as α variable the $\emptyset$ angle on the base line CD. With $\emptyset = \alpha - \beta$ the region CDQRC is mapped on the lower part of the α,β plane (Figure 18b).

Both images of CR (the wheel) and of RQE (the stress discontinuity line) in the α,β plane are unknown, including the detachment angle θ_r.

The functions v_α, v_β, x,y and the location of CR and RE in the characteristic plane have now to be found by using Equations [6.61] and the boundary conditions. The latter are the following: (i) On CD the velocity is known ($u = u_b$, $v = 0$). (ii) On DE one of the velocity components is known, $v = v_\beta = 0$. x and y are also known, $x = s$, $y = 0$. Hence, since $\emptyset = s$, one has $x = \alpha^2 + \beta^2 = \alpha\sqrt{2}$, $y = 0$. (iii) On RE the velocity components v_α, v_β have to match continuously the velocity in the free-surface region RETR which have been found previously. Moreover, since RE is a line of stress-discontinuity, it bisects the angle between the sliplines on its two sides (Figure 18a). This is an additional condition of matching between the two plastic zones. (iv) The wheel CR is a streamline and x,y are interrelated by the Equation $x^2 + y^2 = 1$.

Unfortunately the analytical solution of the problem by Riemann's method is very difficult since the boundary conditions, unlike the bow and free-surface regions, do not permit to march with the solution from one boundary. The analytical approach leads to integral equations for the dependent functions which have to be solved by matching the solution with the flow in the free-surface region.

A finite difference solution is also difficult because of the unknown location of CR and RE. For this reason a detailed solution of the plastic flow in the region CDERD has been abandoned at this stage. An approximate solution is presented in Section 7.

Finally, the geometry of the rigid core CBDC is determined from the solution of the flow in the bow region from one side (CB) and from the solution of the flow in CREDR from the other side (CD).

The stresses on CR are found from the solution in CREDC starting from the free-surface where p = 1. The pressure on the left hand side of the rigid core at C has to be found from the equilibrium of the rigid core. When p_c is known, the stress distribution in the bow region is totally determined.

7. THE APPROXIMATE DETERMINATION OF THE DETACHMENT ANGLE θ_r AND OF STRESS DISTRIBUTION ALONG THE WHEEL

The detailed solution of the problem of plastic-flow beneath a wheel, discussed and exemplified in section 6 requires a large amount of computations. Since the solution is an approximate one because of the different simplifying assumptions underlying the mathematical representation, it is highly desirable to find a simple, approximate method of determining the forces on the wheel. Such a method is presented in this section.

A. The detachment (or recovery) angle θ_r

θ_r may be found approximately from the continuity requirements between the β line CD and the line RE (Figures 10b and 19).

Since there is no soil flow across CR (the wheel) and DE, the flux through CD and RE have to be equal, i.e.

$$h u_b = \int_E^R V \cos\eta \, ds \qquad [7.1]$$

Since the mapping of RE on the physical plane is not known, the relationship [7.1] in its exact form is of little help. An approximate evaluation of the integral may be obtained as follows.

First, Equation [7.1] is equivalent to

$$u_b h = \int_E^R V \cos\eta \, ds = \int_o^{h_R} V \frac{\cos\eta}{\cos\xi} \, dy \qquad [7.2]$$

η being the angle between the normal to RE and the velocity vector and ξ the angle between the normal and x axis (Fig. 19).

At R it is reasonable to assume that the stress jump is negligible and RE is tangent to the characteristic RF. η at R is known since the characteristic RF intersects the free surface at $\pi/4$. Hence $\xi_R = \pi/4 + \theta_r$, while $\eta_R = \theta_r$. From the other hand V at R is the speed along the free surface and it has been found by solving the kinematic problem in RTFR (Section 6c). For each given θ_r, V_R may be found in Appendix 1 (in the last line of each group of results) taking into account that $\phi = \pi/4 + \theta_r$ at R. Hence the integrand of [7.2] has a well determinated value at R, for a given θ_r.

At E again V = u = 1 is known and there also $\eta = \xi$ since the velocity vector is horizontal. The value of $V(\cos\eta/\cos\xi)$ being known at the two extremities, a reasonable approximation of the integral [7.2] is obtained by assuming a linear variation of the integrand with y. Hence, Equation [7.2] becomes

$$u_b h \approx \frac{1}{2} \left[1 + \frac{V_R \cos\theta_r}{\cos(\pi/4 + \theta_r)} \right] h_R \qquad [7.3]$$

A few values of V_R as a function of θ_r, from Appendix 1, are given in the following table

θ_r	Φ_R	V_R
5.1°	50.1°	1.08
11.2°	56.25°	1.20
20.2°	65.20°	1.35
27°	72°	1.76
31.5°	76.5°	1.54

The quantity h_R is simply related to h (Fig. 19) by

$$h_R = h + 1 - \cos \theta_r \qquad [7.4]$$

Equations [6.35] and [6.37] relate $u_b h$ to θ_a and $\theta_\ell - \theta_a = -\Phi_{wc}$. Hence, in Equation [7.3] all quantities are functions of θ_r, θ_a, and Φ_{wc} and it permits the determination of θ_r (recovery angle) for given θ_a (sinkage) and Φ_{wc} (shear stress at bow). Equation [7.3] has been solved by trial and error. In Figure 20 the dependence of θ_r on the shear stress on the wheel is given for three sinkages z = 0.036, z = 0.134 and z = 0.293 corresponding to $\theta_a = 15^\circ$, $\theta_a = 30^\circ$ and $\theta_a = 45^\circ$ respectively. The minimum slippage as function of z and τ_w is given in Figure 23.

The examination of Figure 20 shows that θ_r increases with sinkage and with τ_w. For small sinkages, as encountered in application, and $\tau_w \approx 0.5$, θ_r is of order $\theta_a/2$.

B. The Stresses Along RC (Figure 10b)

As stated in Section 5e the shear stress is assumed constant $\tau = \tau_w$ along the bow region AC, and dropping linearly along RC from $\tau = \tau_w$ to $\tau = 0$

$$\tau = \tau_w \, (1 - \theta/\theta_r) \text{ (on RC, } 0 < \theta < \theta_r) \qquad [7.5]$$

The isotropic pressure at C, on the right side of CD (Figures 12b and 18a) is found from the integration of Equations [6.1] and [6.2] along the sliplines RN and NC as

$$P_{Cr} = 1 + 2 \left[\left(\frac{\pi}{4} + \theta_r \right) - \Phi_N \right] - 2 \, (\Phi_N - \Phi_{wc}) \qquad [7.6]$$

the terms in brackets being the variation of Φ between R-N and N-C respectively. The value of Φ_N is unknown, but its range of variation is $0 < \Phi_N < \Phi_{wc}$, corresponding to N → D or to N → C, respectively. Assuming the average value $\Phi_N = \Phi_{wc}/2$ we obtain from Equation [7.6]

$$P_{Cr} = 1 + \pi/2 + 2\theta_r \qquad [7.7]$$

The normal stress on the wheel at C, on the right side of CD, is [Equation 3.7]

$$\sigma_{Cr} = - p_{Cr} + \sin 2\Phi_{wc} = -(1 + \frac{\pi}{2} + 2\theta_r) + \sin 2\Phi_{wc} \qquad [7.8]$$

where Φ_{wc} is related to τ_w by $\Phi_{wc} = - 1/2 \cos^{-1}\tau_w$.

The type of variation of σ_w from $\sigma_w = 0$ at R to $\sigma_w = \sigma_{Cr}$ at C is not known. From the assumed slipline distribution it is reasonable to assume a linear variation

$$\sigma_w = \sigma_{Cr}\left(1 - \frac{\theta}{\theta_r}\right) = - \left(1 + \frac{\pi}{2} + 2\theta_r - \sin 2\Phi_{wc}\right)\left(1 - \frac{\theta}{\theta_r}\right)$$

$$(\text{on CR, } 0 < \theta < \theta_r) \qquad [7.9]$$

Equations [7.5] and [7.9] gave the approximate distribution of shear and normal stresses along the rear portion of the wheel CR as a function of θ, θ_r, and τ_w (or equivalently Φ_{wc}).

C. <u>The Equilibrium of the Rigid Core CBDC (Figure 10b)</u>

In the rigid (elastic) core the maximum shearing stress has to be lesser than the yield stress anywhere. The shape of the two lines CB and CD is only partially known. CB is known from the solution of the bow region (Figure 16) while CD has to be found from the solution of the rear region. Figure 16 shows that an acceptable approximation is to replace the lines CD and CB by two arcs of circles (Figure 21). The two arcs are completely determined by the known angles at C(Φ_{wc}) and at B and D

($\pi/2$) and by the height h. The isotropic pressure distribution is also determined from the β characteristic relationship [6.2] as (Figure 19)

$$\begin{aligned} p &= p_{Cr} + 2\phi_{wc} - 2\eta \quad \text{(on CB)} \\ p &= p_{C\ell} - 2\phi_{wc} + 2\eta \quad \text{(on CD)} \end{aligned} \qquad [7.10]$$

The shearing stress distribution along the three sliplines CB, BD and DC is also known and given in Figure 21.

All the stresses of Figure 21 are known excepting $p_{C\ell}$, the pressure at C on the left side of CB. The equilibrium of the forces acting on the rigid case in horizontal direction will provide the value of $p_{C\ell}$.

The horizontal force from the pressures on CD is

$$H_{CD} = \int_0^h (p_{Cr} + 2\phi_{wc} - 2\eta)dy = \frac{h}{\sin \phi_{wc}} \int_0^{\phi_{wc}} (p_{Cr} + 2\phi_{wc} - 2\eta)\cos\eta d\eta$$

$$= h\left(p_{Cr} - 2\frac{\cos \phi_{wc}}{\sin \phi_{wc}} + \frac{2}{\sin \phi_{wc}}\right) \qquad [7.10]$$

The same type of computation gives for the pressure resultant on CB

$$H_{CB} = h\left(p_{C\ell} + 2\frac{\cos \phi_{wc}}{\sin \phi_{wc}} - \frac{2}{\sin \phi_{wc}}\right) \qquad [7.11]$$

The resultant of the shearing stresses is

$$H_s = 4\ell = 4h \frac{1 - \cos \Phi_{wc}}{\sin \Phi_{wc}} \qquad [7.12]$$

The equilibrium requires

$$H_{CD} + H_s - H_{CB} = 0 \qquad [7.13]$$

Introducing the expressions [7.10], [7.11] and [7.12] into [7.13] and after some algebraic manipulations, it is found that

$$p_{C\ell} = p_{Cr} = p_C \qquad [7.14]$$

i.e. the pressure at C is transmitted unchanged though the rigid core. This shows that the rigid core is effectively not in a plastic state, in which case p would increase. Hence from Equations [7.7] and [7.14]

$$p_{(} = 1 + \frac{\pi}{2} + 2\theta_r \qquad [7.15]$$

D. The Stresses Along CA (Figures 10b and 13a)

A method of determining the stress distribution by the exact integration of the quasi-static equations has been presented in Section 6d. The inspection of Figure 14, which shows the image of the line AC in the characteristic plane, reveals that the curve may be approximately replaced by a straight segment between

A and C. The equation of this straightline is (Figure 13c)

$$\alpha + \frac{\theta_\ell}{\Phi_{wc}} \beta + \theta_\ell = 0 \qquad [7.16]$$

From the other hand Φ, p and θ are related to α,β by Equations [6.40], [6.42] and [6.58]. From these equations and [7.16] we find that along CA

$$\Phi = \left(1 - \frac{\Phi_{wc}}{\theta_\ell}\right) \alpha - \Phi_{wc}$$

$$p = p_C - 2 \left(1 + \frac{\Phi_{wc}}{\theta_\ell}\right) \alpha \qquad [7.17]$$

$$\theta = \left(1 - \frac{\Phi_{wc}}{\theta_\ell}\right) \alpha$$

Replacing p_C by its value of Equation [7.15], p is expressed as function of θ along the wheel by

$$p = 1 + \frac{\pi}{2} + 2\theta_r - 2 \frac{1 + \frac{\Phi_{wc}}{\theta_\ell}}{1 - \frac{\Phi_{wc}}{\theta_\ell}} \theta \qquad [7.18]$$

where θ_ℓ (Figure 13a) is related to sinkage and shearing stress at A through Equation [6.34]

$$\theta_\ell = \theta_a + \Phi_{wc} = \theta_a + \frac{1}{2} \cos^{-1} \tau_w \qquad [7.19]$$

Summarizing, the stress distribution along the bow portion of the wheel is given by

$$\tau = \tau_w \qquad (AC,\ -\theta_a < \theta < 0) \qquad [7.20]$$

$$\sigma_w = -\,p - \sin 2\phi_{wc} = -\left(1 + \frac{\pi}{2} + 2\theta_r + \sin 2\phi_{wc}\right) + 2\,\frac{\theta_a + 2\phi_{wc}}{\theta_a}\,\theta \qquad (AC, -\theta_a < \theta < 0) \qquad [7.21]$$

Equations [7.20] and [7.21] give the stress distribution in terms of θ, θ_r, θ_a and τ_w.

The last point to be clarified is that of the rigid wedge at the bow, delimited by the free-surface and the slipline AB (Figure 13a).

The pressure at A is (from Equation [7.17] with $\theta = -\theta_a$)

$$p_A = 1 + \frac{\pi}{2} + 2\theta_r + 2\theta_a + 4\phi_{wc} \qquad [7.22]$$

This result is independent of the assumption of linearity of the line AC in the characteristic plane.

Hill (9) has shown that the rigid wedge at the bow is effectively in a rigid (elastic) state if

$$P_A \leq 1 + 3\pi - 2\theta_\ell \qquad [7.23]$$

the sign equal corresponding to a plastic state given by a centered fan at A.

Hence, from Equations [7.22] and [7.23] we find that

$$\theta_r \leq \frac{5\pi}{4} - 2\theta_a - 3\Phi_{wc} \qquad [7.24]$$

For θ_r larger than the limit of Equation [7.24] the soil at bow cannot sustain in a rigid state the stresses generated by the wheel. Then the plastic flow extends upstream causing probably bulldozing effects.

The application of condition [7.24] to the relationship between θ_r, θ_a and Φ_{wc} in Figure 20 shows that [7.24] is violated only for the largest sinkage ($\theta_a = 45^\circ$, $z \approx 0.3$) and at small shear stress between the wheel and the soil (low slippage). The corresponding region is shaded in Figure 20. The conclusion is that the picture of steady flow assumed in this work is probably not possible for driven wheels at sinkages larger than $z = 0.3$. We have not found in literature [5], [18], [22] examples of tests in which larger sinkage values have been realized.

8. FORCES ACTING ON THE WHEEL AND THE MINIMUM SLIPPAGE COEFFICIENT

Equations [7.5], [7.9], [7.20] and [7.21] gave the approximate stress distribution on the wheel. The distribution is represented in Figure 22 for the example discussed in Section 6 ($\theta_a = 30^o$, $z = 0.134$, $\Phi_{wc} = 35^o$, $\tau_w = 0.34$). From the diagram of Figure 20 it is found that the recovery angle is $\theta_r = 17.2^o$.

The normal stress is discontinuous at C, the jump due to the rigid core being $2 \sin 2\Phi_{wc}$. As the shearing stress on the wheel increases this jump diminishes. The normal stress σ_w has its maximum value at the bow and drops along the wheel. The isotropic pressure is continuous along the wheel. For the same sinkage, but a perfectly rough wheel ($\tau_w = 1$) the normal stress distribution is continuous and θ_r is larger, $\theta_r = 23^o$ (Figure 22). The shearing stress is, by assumption, constant along AC and drops to zero from C to R.

The forces acting on the wheel may be easily found by integrating the stresses, θ being the integration variable in the range $-\theta_a < \theta < \theta_r$.

A. The Vertical Force W (Flotation, Figure 22)

The vertical force acting on the wheel has four components

$$W = W_1 + W_2 + W_3 + W_4 \qquad [8.1]$$

where W_1 is the vertical projection of the normal stress σ_w acting on AC, W_2 results from σ_w on CR, W_3 from τ on AC and W_4 from τ on CR. All these components but W_4 are directed upward (positive).

Since $dx = \cos\theta\, d\theta$ and $dy = \sin\theta d\theta$, the expressions of the W components, according to Equations [7.5], [7.9], [7.20] and [7.21] are

$$W_1 = -\int_A^C \sigma_w dx = \int_{-\theta_a}^{o} \left[\left(1 + \frac{\pi}{2} + 2\theta_r + \sin 2\phi_{wc}\right) + 2\,\frac{\theta_\ell + \phi_{wc}}{\theta_\ell - \phi_{wc}}\,\theta\right] \cos\theta d\theta$$

$$= \left(1 + \frac{\pi}{2} + 2\theta_r + \sin 2\phi_{wc}\right) \sin\theta_a - 2\,\frac{\theta_\ell + \phi_{wc}}{\theta_\ell - \phi_{wc}}\,(1 - \theta_a \sin\theta_a - \cos\theta_a) \qquad [8.2]$$

$$W_2 = -\int_C^R \sigma_w dx = \int_o^{\theta_r} \left(1 + \frac{\pi}{2} + 2\theta_r - \sin 2\phi_{wc}\right)\left(1 - \frac{\theta}{\theta_r}\right) \cos\theta d\theta$$

$$= \left(1 + \frac{\pi}{2} + 2\theta_r - \sin 2\phi_{wc}\right) \frac{1 - \cos\theta_r}{\theta_r} \qquad [8.3]$$

$$W_3 = -\int_A^C \tau_w dy = -\tau_w \int_{-\theta_a}^{o} \sin\theta d\theta = \tau_w z = \underline{\cos 2\Phi_{wc}(1-\cos\theta_a)} \quad [8.4]$$

$$W_4 = -\int_A^R \tau dy = -\int_o^{\theta_r} \tau_w\left(1 - \frac{\theta}{\theta_r}\right) \sin\theta d\theta = \underline{\cos 2\Phi_{wc}\left(\frac{\sin\theta_r}{\theta_r} - 1\right)} \quad [8.5]$$

Hence, by summation, W is expressed in a closed form as a function of θ_a (sinkage), Φ_{wc} or τ_w (shearing stress on the wheel related to slippage), θ_r (recovery angle) and θ_ℓ. Since θ_r is itself a function of θ_a and τ_w (Figure 20) and the same is true for θ_ℓ ($\theta_\ell = \theta_a + \Phi_{wc}$) the flotation is in fact a function of θ_a and τ_w solely.

In Figure 23 the dependence of W on τ_w and z is represented graphically. The values have been obtained by using Figure 20 for finding θ_r and Equations [8.2]-[8.5] for W.

The computations show that the major part of W is, of course, given by W_1. As the shearing stress τ_w and the sinkage z increase, however, the other components of W may reach as much as 30 percent of its value. The neglection of the normal stresses on the rear portion as assumed by Bekker, theory, is not justified in this case.

As expected W increases sensibly with the sinkage. An interesting feature is the drop of W, for a given sinkage, with τ_w, i.e. with the slippage. A computation of an "average" stress obtained by dividing the flotation W to the contact length $\theta_a + \theta_r$, based on the results of Figures 20 and 23, shows that $W/(\theta_a + \theta_r)$ has an average value of 3.9 (for $15^o < \theta_a < 45^o, 10^o < \phi_{wc} < 40^o$) with deviations of maximum ± 13 percent.

B. Horizontal Force H (Resistance, Drawbar Pull, Figure 20)

The horizontal force, considered positive if it is resistive and negative, if it is propulsive, has again four components

$$H = R + H_2 + H_3 + H_4 \qquad [8.6]$$

where R results from σ_w on AC, H_2 from σ_w on CR, H_3 from τ on AC and H_4 from τ on CR (Figure 22).

The expressions of the different components of H are as follows

$$R = -\int_A^C \sigma_w dy = \int_o^{-\theta_a} \left[(1 + \pi/2 + 2\theta_r + \sin 2\phi_{wc}) + 2 \frac{\theta_\ell + \phi_{wc}}{\theta_\ell - \phi_{wc}} \theta \right] \sin \theta d\theta$$

$$= \underline{(1 + \pi/2 + 2\theta_r + \sin 2\phi_{wc})(1 - \cos \theta_a)}$$

$$\underline{- 2 \frac{\theta_\ell + \phi_{wc}}{\theta_\ell - \phi_{wc}} (\theta_a \cos \theta_a - \sin \theta_a)} \qquad [8.7]$$

$$H_2 = -\int_C^R \sigma_w dy = -\int_o^{\theta_r} (1 + \pi/2 + 2\theta_r - \sin 2\phi_{wc}) \left(1 - \frac{\theta}{\theta_r}\right) \cos\theta d\theta =$$

$$= \underline{(1 + \pi/2 + 2\theta_r - \sin 2\phi_{wc}) \left(\frac{\sin\theta_r}{\theta_r} - 1\right)} \qquad [8.8]$$

$$H_3 = -\int_A^C \tau_w dx = -\tau_w \int_{-\theta_a}^{o} \cos\theta d\theta = -\tau_w \sin\theta_a = \underline{-\cos 2\phi_{wc} \sin\theta_a} \qquad [8.9]$$

$$H_4 = -\int_C^R \tau dx = -\int_o^{\theta_r} \tau_w \left(1 - \frac{\theta}{\theta_r}\right) \cos\theta d\theta = \tau_w \frac{\cos\theta_r - 1}{\theta_r}$$

$$= \underline{\cos 2\phi_{wc} \frac{\cos\theta_r - 1}{\theta_r}} \qquad [8.10]$$

The force R is a resistive one, the other three forces are propulsive. Again, for a given sinkage and τ_w the values of H may be found through the relationships between θ_r and θ_a, τ_w. In Figure 24 the value of H as a function of τ_w (or ϕ_{wc}) for different sinkages is represented, as well as the value of R. In usual terminology R is the resistance, H is the minus draw-bar-pull and H-R is the traction.

As expected the resistance increases with the sinkage. For a given sinkage, both total forces and resistance drop as the shear stress increases, but the total force drops faster becoming negative (i.e. drawbar pull) at high values of τ_w and low values of z.

C. The Torque M

The torque acting on the wheel arises only from shearing stress. It is given, therefore, by

$$M = \int_A^R \tau d\theta = \tau_w \int_{-\theta_a}^{o} d\theta + \int_o^{\theta_r} \tau_w \left(1 + \frac{\theta}{\theta_r}\right) d\theta$$

$$= \tau_w \left(\theta_a + \frac{\theta_r}{2}\right) = \cos 2\Phi_{wc} \left(\theta_a + \frac{\theta_r}{2}\right) \quad [8.11]$$

D. The Minimum Slippage

The relationship between the assumed constant $\tau = \tau_w$ along the wheel (on AC) and the slippage has been discussed in Section 6d. Only a detailed analysis of the boundary layer between the wheel and the plastic zone may reveal the true nature of this relationship. At this moment one may use an empirical relationship between τ_w and S. At any rate, the analysis (Section 6d) has shown that a minimum slippage is necessary in order to maintain positive shear stress along the entire wheel. From Equation [6.39] S_m is given by

$$S_m = \frac{\text{Sin } \theta_a}{\text{Sin}\left|\phi_{wc}\right| + \sin \theta_a} \qquad [8.12]$$

i.e. S_m is depending on sinkage and on τ_w (or, otherwise stated τ_w depends on S_m and sinkage).

In Figure 23 the dependence of S_m on τ_w and z is represented graphically. For a given sinkage S_m increases with τ_w, the increase being very fast at high τ_w ($\tau_w > 0.8$)

The flow pattern suggested in this report for a driven wheel is possible only for $S \geq S_m$. At lower slippage coefficients the wheel starts to skid. For the small sinkages encountered in applications and moderate τ_w the required minimum slippage are of the order 0.35 - 0.40. At lower values the wheel is no more totally slipping and a different solution has to be contemplated.

For driven wheels without lateral spuds , a slippage coefficient of 0.35 - 0.40 is not high and it may be said that the present solution covers the whole practical range of slippages for driven wheels (18).

9. DISCUSSION OF RESULTS

A. Comparison With Experiments (General)

As stated in Section 2b, the existing experimental results are not adequate for a quantitative verification of the present work. Adequate experiments for this purpose have to fulfill the following requirements: (i) the soil behavior has to be controlled and known (homogeneity, stress-strain relationship, incompressibility). A soil behaving as close as possible to the plastic-rigid model has to be used. (ii) the wheel shape and motion has to be similar to those assumed here, i.e., two-dimensional, steady and with correct scaling of the inertial number H (iii) accurate measurements of velocity distribution in the soil body and stress distribution along the wheel have to be carried out.

Since no experimental data satisfying these requirements have been available, only a qualitative comparison between the trends shown by actual experiments and the theory is possible. Quantitative comparison is also made when possible.

B. The Recovery Angle

For the first time an approximate theoretical method of predicting the magnitude of the recovery angle θ_r has been presented. The values of θ_r seems high when compared with general accepted values of $\theta_r = 5^\circ - 6^\circ$. One has to keep in mind, however, that this latter value is based on experiments with wheels of finite width in which case a rut is created and part of the

soil is moved sidewise. Thus causes, obviously, a reduction of θ_r. Moreover, if the soil is compressible (as assumed in Bekker's theory) again smaller values of θ_r will be observed.

In the experiment of (18) (Figure 25) done with wide rollers in clay, values of θ_r of 16° have been observed; in (22) θ_r seems to be even higher, so that our results are by no means beyond the practical range, for the stipulated condition.

The increase of θ_r with τ_w, i.e. with slippage, (Figure 20) seems intuitively correct. One would expect that at stall θ_r will reach its maximum value $\theta_r = \theta_a$. In our results θ_r is below θ_a even for $S_m \rightarrow 1$. It must be, however, emphasized that the stall cannot be regarded as a limit case of flow and experiments tend to confirm it (see (21)).

C. The Normal Stress Distribution and the Flotation W

The maximum normal stress σ_w has been found at the bow A (Figure 22 is an example). The measurements of (18), (15) show that high values of σ_w exist at the bow, contradicting Bekker-Bernstein assumption (Figure 25). The maximum is close to the bow in (15), but near the bottom in (18). Experiments in sand also show that the maximum is between the bottom and the bow.

In discussing the work-hardening effect it will be shown that the maximum σ_w has in fact to be displaced from the bow, but it will be closer to it as the slippage increases.

No stress discontinuity has been observed in the measurements available to us, but a gradual drop of σ_w from the bottom to the rear has been measured in both (15) and (18) (Figure 25). The discontinuity is a crude approximation for this high drop.

The flotation W (Figure 23) has values of the order found in (5), being somehow higher. Since the experiments in (5) have been carried out with narrow wheels, the discrepancy is expectable. An effect observed in the same experiments (5) but ignored by Bekker's theory and empirically considered by Reece (13) in theory on wheels in sand is the drop of flotation with slippage. The present theory has predicted this effect (Figure 23). Moreover, its reason is quite transparent. As τ_w, i.e. the slippage, increases, the angle $\theta_\ell = \theta_a + \Phi_{wc}$ (Figure 13a) decreases and the slipline AC approaches the wheel. Since the magnitude of the pressure at the bow A depends on the bending of this slipline, the peak value of $\sigma_w = \sigma_{wA}$ decreases as the slipline approaches the wheel. The above effect may be expressed in a slightly different form by asserting that for a given W the sinkage will increase with slippage.

The normal stress vary along the wheel, which is different of Uffelmann's assumption of constant σ_w (18). The average normal stress $W/(\theta_a + \theta_r)$ is of order 39 in the present results compared with the value of order 5.7 assumed by Uffelmann (18). Our value is much closer to his measured value of 3.6 (Figure 25).

D. Resistance and Drawbar Pull

The high normal stress at rear is the main resistive factor. Drawbar-pull has been obtained only for small sinkages and high slippages (Figure 24). No experimental data for rims have been found, excepting (18).

Experiments with towed wheels tend to show that irrespective of the type of tested soil, the experimental data group satisfactory in a diagram in which R/W (resistance over flotation) are plotted as a function of sinkage. Firth (6) has found from different measurements for cylindrical wheels that a good fit for towed rigid wheels is

$$\frac{R}{W} = K \left(\frac{z'}{2R'} \right)^n \qquad [9.1]$$

with K = 0.75 and n = 0.45.

Based on the results of Figures 23 and 25 the values of R/W as a function of z for different τ_w have been plotted on a logarithmic paper (Figure 26). The dependence is well approximated by straight line which have approximately the same slope of n=0.5. The value of K differs with slippage, being lower at high slippages. For τ_w = 0.19, i.e. relatively low shear stress, K = 0.71. Hence, the present theory provides values quite close to those found for towed wheels.

E. Influence of Work-Hardening, Compressibility and Side Effects

It is a well established fact that clay shows a dependence of the yield stress on the strain which resembles work-hardening, i.e. an increase of the yield-stress with the strain.

The qualitative influence of the work-hardening has been considered in different sections. It is worthwhile to recall these effects and to discuss them briefly here.

A first effect is the diffusion of the discontinuity line AC which becomes a zone of transition rather than a line. At this stage it is difficult to estimate the thickness of the transition layer, but this may explain some upstream deformations not encountered in a rigid-plastic model.

Another effect is reflected in the normal stress distribution. Since the pressure increases with strain, it is expected that at the bow A the pressure will be lower than the value given by the rigid-plastic model and will increase rapidly along the wheel, reaching the rigid-plastic value in the region of high strain.

The compressibility of the soil will cause changes in the flow pattern. An apparent effect is the creation of a rut (i.e. the diminution of θ_r) and additional dissipation in compaction.

A narrow wheel creates a three-dimensional flow pattern. Experiments (21) show that the flow beneath the wheel exhibits the same features as in the case of a roller. A rut is now,

however, possible. For this reason and due to side effects the flotation will probably be lower than in the two-dimensional case.

Future theoretical work which will incorporate these effects is suggested in section 11.

F. Energy Considerations

The equation of energy is in the case of an incompressible material a simple transcription of the momentum equations and it is, therefore, not very helpful in the study of the mechanics of motion. It is useful for finding, for instance, the temperature changes in the material-which involves additional empirical data on thermal properties.

Since it is usual to express some results found from the momentum equations in terms of energy, it will be worthwhile to examine briefly the energy balance in the case of soil-wheel interaction. Considering the soil body (Figure 1), one can apply the equation of mechanical energy to a control volume delimited by: a vertical section 1-1 far upstream, a vertical section 2-2 far downstream (both from the free-surface to infinity downward), the free-surface and the soil-wheel interface. One of the basic assumptions underlying this work is that of uniform flow and unperturbed free-surface far from the wheel. In this case the energy flux through sections 1-1 and 2-2 is

$$\frac{dE_1}{dt} = U_o' \int (\sigma_{x1}' - \sigma_{x2}')dy' \qquad [9.2]$$

The free-surface is stress-free; there is no energy flow across it.

Work is done on the soil-wheel interface by shearing stress solely. The work rate is

$$\frac{dE_2}{dt} = V_w' \int \tau ds \qquad [9.3]$$

The energy equation states that

$$\frac{dE_1}{dt} + \frac{dE_2}{dt} = \frac{dEd}{dt} \qquad [9.4]$$

where

$\frac{dEd}{dt}$ is the rate of energy dissipation.

From the momentum equation

$$\int (\sigma_{x1}' - \sigma_{x2}')dy' = H' \qquad [9.5]$$

where H' is the total horizontal force acting on the wheel. By definition

$$\int \tau ds = - M' \qquad [9.6]$$

where M' is the torque acting on the wheel. Also $V'_w = \omega' r'$. Hence, Equation [9.4] becomes

$$H' U_o' - M' \omega' r' = \frac{dEd}{dt} \qquad [9.7]$$

Since in the case of a driven wheel the torque M' is applied to the wheel in clockwise direction, $M' < 0$. H' is positive if it is a resistance and negative if it is a drawbar pull.

Equation [9.7] states the simple result that the work done by the horizontal force and the torque are equal to the dissipation.

Dissipation occurs in the plastic-rigid model in the plastic zone solely. This zone has to be divided in three regions: the narrow transition layer between the rigid and plastic zone (considered a discontinuity layer), the bulk of the plastic zone and the boundary layer at the soil wheel interface.

The dissipation in the transition layer $\iint \tau' (\partial V/\partial n) dn ds$ where s and n are directions along and normal to the transition layer respectively and V' is the tangential velocity. For a perfect plastic material and no inertial effects $\tau' = k'$ and $\int (\partial V'/\partial n)\, dn = \delta V'$ (the velocity jump). The matter is more complex when work hardening and inertial effects are considered, but it will not be discussed here.

The dissipation in the plastic zone has been discussed in Section 3F.

In the boundary layer near the wheel the dissipation equals $\int \tau'(\omega' r' - V') \, ds$, where V' is the soil velocity.

In any computations based on energy considerations special attention has to be paid to the dissipation in the two thin layers which may account for a large part of the total dissipation.

G. Extension of the Method to Different Stress Conditions Along the Wheel

The solution of the plastic flow in the bow region (Section 6D) has been obtained by using the condition of constant shear stress $\tau = \tau_w$ along the wheel on AC.

There is no major difficulty in solving the problem with an arbitrary distribution of τ along the wheel, provided that the same picture of the slipline field is adopted.

In section 6d the τ boundary condition was used in order to locate the image of the line AC in the characteristic plane (Figure 14).

Assume that a relationship between τ and θ (position on the wheel $-\theta_a < \theta < 0$) is given

$$\tau = \tau(\theta) \qquad [9.8]$$

Equation [4.7] relates τ to Φ and θ. Hence, from Equations [4.7] and [9.8] we have

$$\tau(\theta) = \cos 2\ (\Phi-\theta) \qquad [9.9]$$

which permits to determine $\Phi-\theta$ along the wheel as a function of Φ. From the other hand Equations [4.8] which reflects the fact that the wheel is a streamline, gives

$$\frac{v_\beta}{v_\alpha} = -\ tg\ (\Phi-\theta) \qquad [9.10]$$

Since Φ is related to α, β by Equation [6.40], v_β/v_α on the wheel may be computed for a given $\tau(\theta)$. The same procedure as in the case of constant τ permits the location of the AC line in the characteristic plane (Figure 14).

This general procedure applies to frictional conditions, for instance, in which τ is proportional to σ_w. Since σ_w is a known function of α, β again, is relatively easy to find the points in the α,β plane which satisfy the assumed condition.

A dependence of τ along the wheel on the strain of the thin plastic layer adjacent to the wheel may also be treated in the same way. The strain is depending on the difference between the wheel velocity V_w and the plastic velocity, and the location θ. If τ is a known (say empirical) function of strain, again a relationship between v_α and v_β may be formed and the position of AC may be determined.

Concluding, as long as the stress condition along the wheel may be translated in a kinematic condition for v_α, v_β, Φ - it is relatively easy to solve the plastic flow problem in the bow region.

At the present stage, because of the lack of sufficient experimental or theoretical evidence, it seems unjustified to go beyond the assumption of constant τ.

10. SUMMARY AND CONCLUSIONS

A comprehensive theoretical solution of the soil-wheel interaction is for the first time presented. The soil flow is steady and two-dimensional, the wheel is cylindrical and rigid. Only the case of a driven slipping wheel is considered. The soil is assumed to be incompressible and to behavelike a rigid-plastic material, which may be approximately valid in the case of a soft saturated clay.

The flow of the soil in the region beneath the wheel is solved by integrating the equations of motion with appropriate boundary conditions. For the first time the influence of the inertial terms is discussed. Although the solution is obtained with the aid of the quasi-static equations, the flow field is built such that inertial influence is taken into account at discontinuity lines and points where the inertial effects are the most important.

In essence a plastic soil developes high normal stresses on the wheel, responsible for flotation and resistance, in the following way: The soil flowing beneath the wheel is undertaking large deformations which cause a plastic flow; in a plastic region the maximum shear stress is everywhere equal to the yield stress; the equilibrium of an element moving along curved streamlines requires pressure gradients in order to sustain the shear stress. These pressure gradients build up in high pressures beneath the wheel.

An approximate solution of the plastic flow problem is presented. The recovery angle, the vertical and horizontal forces acting on the wheel are found in an analytical form as functions of the sinkage and the magnitude of the shear stress on the wheel boundary. The latter is related to the minimum slippage coefficient, necessary to maintain positive shear stress on the wheel.

The solution permits for given wheel radius, vertical load and shear stress on the wheel (or minimum slippage) to determine the sinkage and the horizontal force. The procedures, using the analytical expressions or the graphs, is the following: for given vertical load (W') radius (r') yield stress (k') and shear stress along the wheel (τ'_w) (or minimum slippage S_m) the sinkage z=z'/r' is found from Figure 23. Figure 24 permits the determination of the resistance R' and the total horizontal force H! Figure 20 gives the recovery angle θ_r.

The results exhibit all the trends well known from experiments (like dependence of flotation on sinkage and slippage), without using the artificial empirical assumptions adopted in previous theories.

Although some quantitative agreement between the present theoretical results and measurements has been found, more and better experiments are necessary in order to validate the theory. For this reason the present work has to be regarded as a preliminary study.

The plastic-rigid theory has proved itself as an useful tool of analysis of soil-wheel interaction. The results so far obtained encourage the continuation of theoretical investigations which will further advance the understanding of the vehicle dynamics and provide sound foundations to a field of applied mechanics dominated by empiricism in the past.

11. SUGGESTIONS FOR FUTURE INVESTIGATIONS

The review of the literature and the theoretical analysis carried out in this report suggest some directions of special interest to be followed in future investigations of soil-wheel interaction in soft soil.

In a broad sense it seems that three directions are of major importance: (i) work toward a better quantitative characterization of different soils important in mobility research. A mechanical characterization means mainly constitutive equations relating the stress and strain tensors including strain-rate effects. The rigid-plastic equations represent one of the simplest types of models. (ii) thorough laboratory work with wheels moving in carefully prepared and controlled soil with accurate measurements of velocity field and stresses on the wheel. Experimental study of the boundary conditions at the soil-wheel interface. (iii) theoretical work in which the soil-wheel problem is attacked from basic principles, using existing knowledge. This type of work has to incorporate new results achieved in directions (i) and (ii).

The work presented here pertains to point (iii). In a narrow sense, the following theoretical aspects of soil-wheel interactions, direct continuations of the present work may be contemplated:

(1) Refinement of the solution in order to solve analytically the flow in the whole plastic region.

(2) Study of the inertial effects by solving the second order approximation in the perturbation scheme.

(3) Investigation of work-hardening effects.

(4) Extension of solution to towed wheels.

(5) Study of motion in sand soil.

(6) Study of three-dimensional effects for wheels of finite width.

(7) Study of non-steady effects by incorporating local accelerations and the time factor in the equations of flow.

Because of the complexity of the wheel problem we feel that the best way to estimate the above effects will be a study of a tracked vehicle, which is geometrically simpler. We strongly recommend, therefore, that future work should start with the solution of plastic-rigid flow beneath a track with consideration of inertial, work-hardening, three-dimensional and unsteady effects. The next immediate step should be the extension to the wheel problem.

REFERENCES

1. Alexander, T. M., "A Slipline Field for the Hot Rolling Process," Proc. Inst. Mech. Eng., Vol. 169, pp. 1021-1030, 1955.

2. Bekker, M. G., "The Theory of Land Locomotion," University of Michigan Press, Ann Arbor, 1956.

3. Bekker, M. G., "Off the Road Locomotion," University of Michigan Press, Ann Arbor, 1960.

4. Courant, R. and Hilbert, D., "Methods of Mathematical Physics," Interscience Publishers, N. Y. and London, Vol. II, 1962.

5. Cullen, R. M., Cullingford G. and Mayfield, B., "Rigid Wheels in Clay," Proc. 2nd Int. Conf. of the Int. Soc. for Terrain-Vehicle Systems, pp. 446-470, 1966.

6. Firth, B. W., "Wheel Shape-A Designer's Variable," Presented at the First International Conf. on Vehicle Mechanics, paper 3223, Detroit, 1968.

7. Harr, M. E., "Foundations of Theoretical Soil Mechanics," McGraw-Hill, N. Y., 1966.

8. Hill, R., "The Mathematical Theory of Plasticity." Oxford at the Clarendon Press, 1950.

9. Hill, R., "On the Limits Set by Plastic Yielding to the Intensity of Singularities of Stress," Journ. of the Mech. and Phys. of Solids, Vol. 2, pp. 278-285, 1954.

10. Prager, W. "An Introduction to Plasticity," Addison-Wesley Publishing Co., Reading, Mass., 1959.

11. Prager, W., "Finite Plastic Deformations in Rheology Theory and Applications," Edited by F. R. Firich, Vol. 1, Acedemic Press, N. Y., 1956.

12. Reece, A. R., "Principles of Soil-Vehicle Mechanics," Proc. Inst. Mech. Engrs., Vol. 180, pt. 2A, No. 2, pp. 45-66, 1966.

13. Reece, A. R., and Wong, T. Y., "Prediction of Rigid Wheel Performance Based on the Analysis of Soil-Wheel Stresses, Part I. Performance of Driven Rigid Wheels," Journ. of Terramechanics, Vol. 4, No. 1, pp. 81-98, 1967.

14. Scott, R. F., "Principles of Soil Mechanics," Addison-Webster, Reading, Mass., 1963.

15. Smith, M. E., "Tests with Rigid Wheels; Tests in Fat Clay," U. S. Army Engineer Waterways Exp Station, Vicksburg, Mississippi, Tech. Rep. No. 3-561 1, 35 p., 1958.

16. Spencer, A. M., "The Dynamic Plane Deformation of an Ideal Plastic - Rigid Solid," J. Mech. Phys. Solids, Vol. 8, pp. 262-279, 1960.

17. Thomas, T. Y., "Plastic Flow and Fracture in Solids," Academic Press, N. Y., 1956.

18. Uffelmann, F. L., "The Performance of Rigid Cylindrical Wheels on Clay Soil," Proc. 1st. Int. Conf. Mech. Soil-Vehicle Systems, pp. 111-130, 1961.

19. Wills, B.M.D., "The Load Sinkage Equation in Theory and Practice," Proc. of the 2nd Int. Conf. of the Int. Soc. for Terrain-Vehicle Systems, pp. 199-247, 1966.

20. Wills, B.M.D., Barrett, F. M. and Shaw, G. J., "An Investigation into Rolling Theories for Towed Rigid Wheels," J. Terramechanics Vol. 2, No. 1, pp. 24-53, 1965.

21. Wong, T. Y., and Reece, A. R., "Soil Failure Beneath Rigid Wheels," Proc. 2nd Int. Conf. of the Int. Soc. for Terrain-Vehicle Systems, pp. 425-446, 1966.

22. Wong, T. Y., "Behavior of Soil Beneath Rigid Wheels," J. Agric. Engr. Res., Vol. 12, No. 4, pp. 257-259, 1967.

APPENDIX 1

THE VELOCITY COMPONENTS AND ϕ IN THE FREE-SURFACE REGION (FIGURE 12) AS FUNCTION OF α, β

α (RAD.)	$2\beta - \frac{\pi}{4}$	v_α	v_β	V	ϕ (DEGREES)
0.805	0.785	0.693	-0.720	0.999	91.125
0.805	0.824	0.734	-0.734	1.039	93.375
0.824	0.785	0.678	-0.734	0.999	92.250
0.824	0.824	0.720	-0.748	1.038	94.500
0.824	0.863	0.762	-0.762	1.078	96.750
0.844	0.785	0.664	-0.747	0.999	93.375
0.844	0.824	0.705	-0.760	1.037	95.625
0.844	0.863	0.747	-0.775	1.076	97.875
0.844	0.903	0.790	-0.790	1.117	100.125
0.863	0.785	0.649	-0.760	0.999	94.500
0.863	0.824	0.690	-0.773	1.036	96.750
0.863	0.863	0.732	-0.787	1.075	99.000
0.863	0.903	0.774	-0.802	1.115	101.250
0.863	0.942	0.817	-0.817	1.156	103.500
0.883	0.785	0.634	-0.773	0.999	95.625
0.883	0.824	0.675	-0.785	1.036	97.875
0.883	0.863	0.716	-0.799	1.073	100.125
0.883	0.903	0.758	-0.814	1.112	102.375
0.883	0.942	0.801	-0.829	1.153	104.625
0.883	0.981	0.845	-0.845	1.195	106.875
0.903	0.785	0.619	-0.785	0.999	96.750
0.903	0.824	0.659	-0.797	1.035	99.000
0.903	0.863	0.700	-0.811	1.071	101.250
0.903	0.903	0.742	-0.825	1.110	103.500
0.903	0.942	0.785	-0.840	1.150	105.750
0.903	0.981	0.828	-0.856	1.191	108.000
0.903	1.021	0.872	-0.872	1.234	110.250
0.922	0.785	0.603	-0.797	0.999	97.875
0.922	0.824	0.643	-0.809	1.034	100.125
0.922	0.863	0.684	-0.822	1.070	102.375
0.922	0.903	0.726	-0.836	1.107	104.625
0.922	0.942	0.768	-0.851	1.146	106.875
0.922	0.981	0.811	-0.866	1.187	109.125
0.922	1.021	0.855	-0.883	1.229	111.375
0.922	1.060	0.900	-0.900	1.273	113.625

α (RAD.)	$2\beta - \frac{\pi}{4}$	v_α	v_β	V	ϕ (DEGREES)
0.942	0.785	0.587	-0.809	0.999	99.000
0.942	0.824	0.627	-0.820	1.033	101.250
0.942	0.863	0.668	-0.833	1.068	103.500
0.942	0.903	0.709	-0.847	1.105	105.750
0.942	0.942	0.751	-0.861	1.143	108.000
0.942	0.981	0.794	-0.876	1.183	110.250
0.942	1.021	0.838	-0.892	1.224	112.500
0.942	1.060	0.882	-0.909	1.267	114.750
0.942	1.099	0.927	-0.927	1.311	116.999
0.962	0.785	0.571	-0.820	0.999	100.125
0.962	0.824	0.611	-0.832	1.032	102.375
0.962	0.863	0.652	-0.844	1.066	104.625
0.962	0.903	0.693	-0.857	1.102	106.875
0.962	0.942	0.734	-0.871	1.140	109.125
0.962	0.981	0.777	-0.886	1.179	111.375
0.962	1.021	0.820	-0.902	1.219	113.625
0.962	1.060	0.864	-0.918	1.261	115.874
0.962	1.099	0.909	-0.936	1.304	118.125
0.962	1.138	0.954	-0.954	1.349	120.375
0.981	0.785	0.555	-0.831	0.999	101.250
0.981	0.824	0.595	-0.842	1.031	103.500
0.981	0.863	0.635	-0.854	1.065	105.750
0.981	0.903	0.676	-0.867	1.100	108.000
0.981	0.942	0.717	-0.881	1.136	110.250
0.981	0.981	0.759	-0.895	1.174	112.500
0.981	1.021	0.802	-0.911	1.214	114.750
0.981	1.060	0.846	-0.927	1.255	116.999
0.981	1.099	0.890	-0.944	1.298	119.250
0.981	1.138	0.935	-0.962	1.342	121.500
0.981	1.178	0.981	-0.981	1.387	123.749
1.001	0.785	0.539	-0.842	0.999	102.375
1.001	0.824	0.578	-0.853	1.030	104.625
1.001	0.863	0.618	-0.864	1.063	106.875
1.001	0.903	0.659	-0.877	1.097	109.125
1.001	0.942	0.700	-0.890	1.133	111.375
1.001	0.981	0.742	-0.904	1.170	113.625
1.001	1.021	0.784	-0.919	1.209	115.874
1.001	1.060	0.828	-0.935	1.249	118.125
1.001	1.099	0.872	-0.952	1.291	120.375
1.001	1.138	0.916	-0.970	1.334	122.625
1.001	1.178	0.961	-0.988	1.379	124.875
1.001	1.217	1.007	-1.007	1.425	127.125
1.021	0.785	0.522	-0.852	0.999	103.500

α (RAD.)	$2\theta - \frac{\pi}{4}$	v_α	v_β	V	ϕ (DEGREES)
1.021	0.824	0.56_	-0.863	1.029	105.750
1.021	0.863	0.601	-0.874	1.061	108.000
1.021	0.903	0.641	-0.886	1.094	110.250
1.021	0.942	0.682	-0.899	1.129	112.500
1.021	0.981	0.724	-0.913	1.166	114.750
1.021	1.021	0.766	-0.928	1.204	116.999
1.021	1.060	0.809	-0.943	1.243	119.250
1.021	1.099	0.853	-0.960	1.284	121.500
1.021	1.138	0.897	-0.977	1.326	123.749
1.021	1.178	0.942	-0.995	1.370	126.000
1.021	1.217	0.987	-1.014	1.415	128.250
1.021	1.256	1.034	-1.034	1.462	130.499
1.040	0.785	0.505	-0.862	0.999	104.625
1.040	0.824	0.54_	-0.873	1.028	106.875
1.040	0.863	0.584	-0.884	1.059	109.125
1.040	0.903	0.624	-0.895	1.091	111.375
1.040	0.942	0.664	-0.908	1.125	113.625
1.040	0.981	0.706	-0.922	1.161	115.874
1.040	1.021	0.748	-0.936	1.198	118.125
1.040	1.060	0.791	-0.951	1.237	120.375
1.040	1.099	0.834	-0.967	1.277	122.625
1.040	1.138	0.878	-0.984	1.319	124.875
1.040	1.178	0.922	-1.001	1.362	127.125
1.040	1.217	0.968	-1.020	1.406	129.375
1.040	1.256	1.013	-1.039	1.452	131.625
1.040	1.295	1.060	-1.060	1.499	133.875
1.060	0.785	0.488	-0.872	0.999	105.750
1.060	0.824	0.527	-0.882	1.028	108.000
1.060	0.863	0.566	-0.893	1.057	110.250
1.060	0.903	0.606	-0.904	1.089	112.500
1.060	0.942	0.647	-0.917	1.122	114.750
1.060	0.981	0.688	-0.930	1.157	116.999
1.060	1.021	0.729	-0.944	1.193	119.250
1.060	1.060	0.772	-0.958	1.231	121.500
1.060	1.099	0.815	-0.974	1.270	123.749
1.060	1.138	0.858	-0.990	1.311	126.000
1.060	1.178	0.903	-1.008	1.353	128.250
1.060	1.217	0.947	-1.026	1.397	130.499
1.060	1.256	0.993	-1.045	1.442	132.750
1.060	1.295	1.039	-1.065	1.488	135.000
1.060	1.335	1.086	-1.086	1.536	137.249
1.079	0.785	0.471	-0.881	0.999	106.875
1.079	0.824	0.509	-0.891	1.027	109.125
1.079	0.863	0.549	-0.901	1.055	111.375
1.079	0.903	0.588	-0.913	1.086	113.625
1.079	0.942	0.628	-0.925	1.118	115.874

α (RAD.)	$2\theta - \frac{\pi}{4}$	v_α	v_β	V	ϕ (DEGREES)
1.079	0.981	0.669	-0.937	1.152	118.125
1.079	1.021	0.711	-0.951	1.187	120.375
1.079	1.060	0.753	-0.965	1.224	122.624
1.079	1.099	0.796	-0.980	1.263	124.875
1.079	1.138	0.839	-0.997	1.303	127.125
1.079	1.178	0.883	-1.013	1.344	129.375
1.079	1.217	0.927	-1.031	1.387	131.625
1.079	1.256	0.972	-1.050	1.431	133.875
1.079	1.295	1.018	-1.069	1.477	136.125
1.079	1.335	1.064	-1.090	1.524	138.375
1.079	1.374	1.111	-1.111	1.572	140.625
1.099	0.785	0.453	-0.891	0.999	108.000
1.099	0.824	0.492	-0.900	1.026	110.250
1.099	0.863	0.531	-0.910	1.054	112.500
1.099	0.903	0.570	-0.921	1.083	114.750
1.099	0.942	0.610	-0.932	1.114	116.999
1.099	0.981	0.651	-0.945	1.147	119.250
1.099	1.021	0.692	-0.958	1.182	121.500
1.099	1.060	0.734	-0.972	1.218	123.749
1.099	1.099	0.776	-0.987	1.256	126.000
1.099	1.138	0.819	-1.002	1.295	128.250
1.099	1.178	0.863	-1.019	1.335	130.500
1.099	1.217	0.907	-1.036	1.377	132.750
1.099	1.256	0.952	-1.055	1.421	135.000
1.099	1.295	0.997	-1.074	1.465	137.250
1.099	1.335	1.043	-1.094	1.511	139.500
1.099	1.374	1.089	-1.115	1.559	141.750
1.099	1.413	1.136	-1.136	1.607	144.000
1.119	0.785	0.436	-0.899	0.999	109.125
1.119	0.824	0.474	-0.908	1.025	111.375
1.119	0.863	0.513	-0.918	1.052	113.625
1.119	0.903	0.552	-0.928	1.080	115.875
1.119	0.942	0.592	-0.940	1.111	118.125
1.119	0.981	0.632	-0.952	1.143	120.375
1.119	1.021	0.673	-0.964	1.176	122.625
1.119	1.060	0.715	-0.978	1.212	124.875
1.119	1.099	0.757	-0.993	1.248	127.125
1.119	1.138	0.799	-1.008	1.287	129.375
1.119	1.178	0.843	-1.024	1.326	131.625
1.119	1.217	0.886	-1.041	1.367	133.875
1.119	1.256	0.931	-1.059	1.410	136.125
1.119	1.295	0.976	-1.078	1.454	138.375
1.119	1.335	1.021	-1.097	1.499	140.625
1.119	1.374	1.067	-1.118	1.546	142.875
1.119	1.413	1.114	-1.139	1.594	145.125
1.119	1.452	1.161	-1.161	1.643	147.375

α (RAD.)	$2\beta - \frac{\pi}{4}$	v_α	v_β	V	ϕ (DEGREES)
1.138	0.785	0.418	-0.908	0.999	110.250
1.138	0.824	0.456	-0.916	1.024	112.500
1.138	0.863	0.495	-0.926	1.050	114.750
1.138	0.903	0.534	-0.936	1.077	116.999
1.138	0.942	0.573	-0.947	1.107	119.250
1.138	0.981	0.613	-0.958	1.138	121.500
1.138	1.021	0.654	-0.971	1.171	123.749
1.138	1.060	0.695	-0.984	1.205	126.000
1.138	1.099	0.737	-0.998	1.241	128.250
1.138	1.138	0.780	-1.013	1.278	130.500
1.138	1.178	0.823	-1.029	1.317	132.750
1.138	1.217	0.866	-1.045	1.358	135.000
1.138	1.256	0.910	-1.063	1.399	137.250
1.138	1.295	0.955	-1.081	1.442	139.500
1.138	1.335	1.000	-1.100	1.487	141.750
1.138	1.374	1.045	-1.120	1.533	144.000
1.138	1.413	1.092	-1.141	1.580	146.250
1.138	1.452	1.139	-1.163	1.628	148.500
1.138	1.492	1.186	-1.186	1.677	150.750
1.158	0.785	0.400	-0.916	0.999	111.375
1.158	0.824	0.438	-0.924	1.023	113.625
1.158	0.863	0.476	-0.933	1.048	115.875
1.158	0.903	0.515	-0.943	1.074	118.125
1.158	0.942	0.555	-0.953	1.103	120.375
1.158	0.981	0.595	-0.964	1.133	122.625
1.158	1.021	0.635	-0.977	1.165	124.875
1.158	1.060	0.676	-0.989	1.199	127.125
1.158	1.099	0.718	-1.003	1.234	129.375
1.158	1.138	0.760	-1.018	1.270	131.625
1.158	1.178	0.802	-1.033	1.308	133.875
1.158	1.217	0.845	-1.049	1.348	136.125
1.158	1.256	0.889	-1.066	1.388	138.375
1.158	1.295	0.933	-1.084	1.431	140.625
1.158	1.335	0.978	-1.103	1.474	142.875
1.158	1.374	1.023	-1.123	1.519	145.125
1.158	1.413	1.069	-1.143	1.565	147.375
1.158	1.452	1.116	-1.165	1.613	149.625
1.158	1.492	1.163	-1.187	1.662	151.875
1.158	1.531	1.210	-1.210	1.712	154.125
1.178	0.785	0.382	-0.923	0.999	112.500
1.178	0.824	0.420	-0.931	1.022	114.750
1.178	0.863	0.458	-0.940	1.046	116.999
1.178	0.903	0.497	-0.949	1.072	119.250
1.178	0.942	0.536	-0.959	1.099	121.500
1.178	0.981	0.576	-0.970	1.128	123.749
1.178	1.021	0.616	-0.982	1.159	126.000
1.178	1.060	0.657	-0.995	1.192	128.250
1.178	1.099	0.698	-1.008	1.226	130.500
1.178	1.138	0.740	-1.022	1.262	132.750
1.178	1.178	0.782	-1.037	1.299	135.000
1.178	1.217	0.825	-1.053	1.338	137.250
1.178	1.256	0.868	-1.069	1.378	139.500
1.178	1.295	0.912	-1.087	1.419	141.750
1.178	1.335	0.956	-1.105	1.462	144.000
1.178	1.374	1.001	-1.124	1.506	146.250
1.178	1.413	1.047	-1.145	1.551	148.500
1.178	1.452	1.093	-1.166	1.598	150.750
1.178	1.492	1.139	-1.187	1.646	153.000
1.178	1.531	1.186	-1.210	1.695	155.250
1.178	1.570	1.234	-1.234	1.745	157.500

APPENDIX 2

THE VELOCITY COMPONENTS AND ϕ IN THE BOW PLASTIC REGION (FIGURE 12)

α (RAD.)	β (RAD.)	v_α	v_β	v_β / v_α	V	φ (DEGREES)	α (RAD.)	β (RAD.)	v_α	v_β	v_β / v_α	V	φ (DEGREES)
0.000	0.000	1.871	0.000	0.000	1.871	0.000	-0.226	0.000	1.846	0.224	0.121	1.859	-13.000
0.000	-0.061	1.868	0.114	0.061	1.871	-3.500	-0.226	-0.061	1.816	0.336	0.185	1.847	-16.500
0.000	-0.122	1.857	0.228	0.122	1.871	-7.000	-0.226	-0.122	1.780	0.446	0.250	1.836	-20.000
0.000	-0.183	1.840	0.341	0.185	1.871	-10.500	-0.226	-0.183	1.738	0.554	0.318	1.824	-23.500
0.000	-0.244	1.816	0.452	0.249	1.871	-14.000	-0.226	-0.244	1.689	0.659	0.390	1.813	-27.000
0.000	-0.305	1.785	0.562	0.315	1.871	-17.499	-0.226	-0.305	1.634	0.760	0.465	1.802	-30.500
0.000	-0.366	1.747	0.670	0.383	1.871	-21.000	-0.226	-0.366	1.573	0.858	0.545	1.792	-34.000
0.000	-0.427	1.703	0.776	0.455	1.871	-24.500	-0.226	-0.427	1.506	0.952	0.632	1.782	-37.500
0.000	-0.488	1.652	0.878	0.531	1.871	-28.000	-0.226	-0.488	1.434	1.042	0.726	1.773	-41.000
0.000	-0.549	1.595	0.977	0.612	1.871	-31.500	-0.226	-0.549	1.356	1.127	0.831	1.764	-44.500
0.000	-0.610	1.533	1.073	0.700	1.871	-34.999	-0.226	-0.610	1.273	1.208	0.948	1.755	-48.000
-0.056	0.000	1.870	0.056	0.030	1.870	-3.250	-0.283	0.000	1.831	0.279	0.152	1.853	-16.250
-0.056	-0.061	1.860	0.170	0.091	1.867	-6.750	-0.283	-0.061	1.796	0.390	0.217	1.838	-19.749
-0.056	-0.122	1.843	0.283	0.153	1.864	-10.250	-0.283	-0.122	1.754	0.499	0.284	1.823	-23.250
-0.056	-0.183	1.819	0.395	0.217	1.862	-13.750	-0.283	-0.183	1.705	0.604	0.354	1.809	-26.750
-0.056	-0.244	1.788	0.505	0.282	1.859	-17.250	-0.283	-0.244	1.650	0.707	0.428	1.796	-30.250
-0.056	-0.305	1.751	0.614	0.350	1.856	-20.749	-0.283	-0.305	1.590	0.806	0.507	1.782	-33.750
-0.056	-0.366	1.707	0.719	0.421	1.853	-24.250	-0.283	-0.366	1.523	0.901	0.591	1.770	-37.250
-0.056	-0.427	1.657	0.822	0.496	1.850	-27.750	-0.283	-0.427	1.451	0.992	0.683	1.758	-40.750
-0.056	-0.488	1.601	0.922	0.575	1.848	-31.250	-0.283	-0.488	1.373	1.078	0.785	1.746	-44.250
-0.056	-0.549	1.539	1.018	0.661	1.845	-34.749	-0.283	-0.549	1.291	1.160	0.898	1.736	-47.750
-0.056	-0.610	1.471	1.110	0.754	1.843	-38.249	-0.283	-0.610	1.204	1.236	1.026	1.726	-51.249
-0.113	0.000	1.865	0.113	0.060	1.866	-6.500	-0.340	0.000	1.814	0.333	0.183	1.844	-19.500
-0.113	-0.061	1.848	0.226	0.122	1.862	-10.000	-0.340	-0.061	1.772	0.443	0.250	1.827	-23.000
-0.113	-0.122	1.825	0.338	0.185	1.856	-13.500	-0.340	-0.122	1.724	0.550	0.319	1.810	-26.500
-0.113	-0.183	1.795	0.449	0.250	1.850	-17.000	-0.340	-0.183	1.669	0.653	0.391	1.793	-30.000
-0.113	-0.244	1.758	0.558	0.317	1.845	-20.500	-0.340	-0.244	1.609	0.754	0.468	1.777	-33.500
-0.113	-0.305	1.715	0.664	0.387	1.839	-24.000	-0.340	-0.305	1.543	0.850	0.551	1.761	-36.999
-0.113	-0.366	1.665	0.767	0.460	1.834	-27.500	-0.340	-0.366	1.471	0.942	0.640	1.747	-40.499
-0.113	-0.427	1.609	0.867	0.538	1.828	-31.000	-0.340	-0.427	1.394	1.030	0.738	1.733	-44.000
-0.113	-0.488	1.548	0.964	0.622	1.823	-34.500	-0.340	-0.488	1.311	1.112	0.848	1.720	-47.500
-0.113	-0.549	1.480	1.056	0.713	1.818	-38.000	-0.340	-0.549	1.224	1.190	0.971	1.707	-51.000
-0.113	-0.610	1.407	1.144	0.813	1.814	-41.499	-0.340	-0.610	1.133	1.262	1.113	1.696	-54.500
-0.170	0.000	1.857	0.169	0.091	1.864	-9.750	-0.397	0.000	1.793	0.366	0.215	1.835	-22.750
-0.170	-0.061	1.834	0.282	0.153	1.856	-13.250	-0.397	-0.061	1.745	0.494	0.283	1.814	-26.250
-0.170	-0.122	1.804	0.393	0.217	1.847	-16.750	-0.397	-0.122	1.691	0.599	0.354	1.794	-29.750
-0.170	-0.183	1.768	0.502	0.284	1.838	-20.249	-0.397	-0.183	1.631	0.701	0.429	1.775	-33.250
-0.170	-0.244	1.725	0.609	0.353	1.830	-23.750	-0.397	-0.244	1.565	0.799	0.510	1.757	-36.750
-0.170	-0.305	1.676	0.713	0.425	1.821	-27.250	-0.397	-0.305	1.493	0.892	0.597	1.740	-40.250
-0.170	-0.366	1.620	0.813	0.502	1.813	-30.750	-0.397	-0.366	1.416	0.981	0.692	1.723	-43.750
-0.170	-0.427	1.559	0.911	0.584	1.806	-34.250	-0.397	-0.427	1.334	1.065	0.798	1.707	-47.250
-0.170	-0.488	1.492	1.004	0.673	1.798	-37.750	-0.397	-0.488	1.247	1.144	0.917	1.693	-50.750
-0.170	-0.549	1.419	1.093	0.770	1.791	-41.250	-0.397	-0.549	1.156	1.217	1.053	1.679	-54.250
-0.170	-0.610	1.341	1.177	0.877	1.785	-44.750	-0.397	-0.610	1.061	1.285	1.211	1.667	-57.749

α (RAD.)	β (RAD.)	v_α	v_β	v_β / v_α	V	φ (DEGREES)	α (RAD.)	β (RAD.)	v_α	v_β	v_β / v_α	V	φ (DEGREES)
-0.453	0.000	1.770	0.438	0.247	1.823	-26.000	-0.680	0.000	1.648	0.629	0.381	1.764	-39.000
-0.453	-0.061	1.716	0.544	0.317	1.800	-29.500	-0.680	-0.061	1.571	0.727	0.463	1.731	-42.500
-0.453	-0.122	1.656	0.647	0.391	1.778	-33.000	-0.680	-0.122	1.4[illegible]	0.821	0.551	1.700	-46.000
-0.453	-0.183	1.590	0.747	0.469	1.757	-36.500	-0.680	-0.183	1.401	0.909	0.648	1.670	-49.500
-0.453	-0.244	1.518	0.842	0.554	1.736	-40.000	-0.680	-0.244	1.309	0.992	0.757	1.643	-53.000
-0.453	-0.305	1.441	0.932	0.646	1.717	-43.500	-0.680	-0.305	1.214	1.069	0.880	1.617	-56.500
-0.453	-0.366	1.359	1.018	0.748	1.698	-47.000	-0.680	-0.366	1.114	1.140	1.023	1.594	-60.000
-0.453	-0.427	1.273	1.098	0.862	1.681	-50.500	-0.680	-0.427	1.010	1.205	1.192	1.573	-63.499
-0.453	-0.488	1.182	1.173	0.992	1.665	-54.000	-0.680	-0.488	0.904	1.264	1.397	1.554	-67.000
-0.453	-0.549	1.086	1.242	1.143	1.651	-57.500	-0.680	-0.549	0.795	1.316	1.654	1.537	-70.500
-0.453	-0.610	0.987	1.306	1.322	1.637	-61.000	-0.680	-0.610	0.684	1.361	1.989	1.523	-73.999
-0.510	0.000	1.744	0.488	0.280	1.811	-29.249	-0.737	0.000	1.611	0.672	0.417	1.746	-42.250
-0.510	-0.061	1.684	0.593	0.352	1.785	-32.750	-0.737	-0.061	1.529	0.768	0.502	1.711	-45.750
-0.510	-0.122	1.618	0.694	0.429	1.760	-36.250	-0.737	-0.122	1.441	0.859	0.596	1.677	-49.250
-0.510	-0.183	1.546	0.790	0.511	1.737	-39.750	-0.737	-0.183	1.349	0.944	0.699	1.646	-52.750
-0.510	-0.244	1.469	0.883	0.600	1.714	-43.250	-0.737	-0.244	1.252	1.023	0.817	1.617	-56.250
-0.510	-0.305	1.387	0.970	0.699	1.693	-46.750	-0.737	-0.305	1.152	1.097	0.952	1.591	-59.750
-0.510	-0.366	1.301	1.052	0.808	1.673	-50.250	-0.737	-0.366	1.048	1.164	1.110	1.567	-63.250
-0.510	-0.427	1.209	1.129	0.933	1.655	-53.749	-0.737	-0.427	0.942	1.225	1.300	1.545	-66.750
-0.510	-0.488	1.114	1.200	1.076	1.638	-57.249	-0.737	-0.488	0.832	1.279	1.537	1.526	-70.250
-0.510	-0.549	1.015	1.265	1.245	1.622	-60.750	-0.737	-0.549	0.720	1.327	1.841	1.510	-73.750
-0.510	-0.610	0.913	1.324	1.450	1.608	-64.250	-0.737	-0.610	0.606	1.367	2.253	1.496	-77.250
-0.567	0.000	1.715	0.537	0.313	1.797	-32.500	-0.794	0.000	1.572	0.713	0.453	1.726	-45.500
-0.567	-0.061	1.649	0.640	0.388	1.769	-35.999	-0.794	-0.061	1.484	0.806	0.543	1.689	-49.000
-0.567	-0.122	1.577	0.738	0.468	1.741	-39.499	-0.794	-0.122	1.391	0.894	0.642	1.654	-52.500
-0.567	-0.183	1.500	0.832	0.554	1.716	-43.000	-0.794	-0.183	1.294	0.976	0.754	1.621	-56.000
-0.567	-0.244	1.418	0.921	0.649	1.691	-46.500	-0.794	-0.244	1.193	1.052	0.881	1.591	-59.500
-0.567	-0.305	1.331	1.005	0.755	1.669	-50.000	-0.794	-0.305	1.089	1.122	1.030	1.564	-63.000
-0.567	-0.366	1.240	1.084	0.874	1.647	-53.500	-0.794	-0.366	0.982	1.185	1.207	1.539	-66.500
-0.567	-0.427	1.145	1.157	1.010	1.628	-57.000	-0.794	-0.427	0.872	1.242	1.424	1.517	-70.000
-0.567	-0.488	1.045	1.224	1.170	1.610	-60.500	-0.794	-0.488	0.759	1.292	1.701	1.498	-73.500
-0.567	-0.549	0.943	1.285	1.362	1.594	-64.000	-0.794	-0.549	0.645	1.335	2.069	1.482	-77.000
-0.567	-0.610	0.837	1.339	1.599	1.579	-67.500	-0.794	-0.610	0.529	1.370	2.590	1.469	-80.500
-0.623	0.000	1.683	0.584	0.347	1.781	-35.750	-0.850	0.000	1.531	0.751	0.491	1.705	-48.750
-0.623	-0.061	1.611	0.684	0.424	1.751	-39.250	-0.850	-0.061	1.437	0.842	0.586	1.666	-52.250
-0.623	-0.122	1.534	0.781	0.508	1.721	-42.750	-0.850	-0.122	1.339	0.927	0.692	1.629	-55.750
-0.623	-0.183	1.452	0.872	0.600	1.694	-46.250	-0.850	-0.183	1.238	1.006	0.812	1.595	-59.250
-0.623	-0.244	1.365	0.958	0.701	1.668	-49.750	-0.850	-0.244	1.133	1.078	0.951	1.564	-62.750
-0.623	-0.305	1.273	1.039	0.815	1.643	-53.250	-0.850	-0.305	1.025	1.144	1.116	1.536	-66.250
-0.623	-0.366	1.178	1.113	0.945	1.621	-56.750	-0.850	-0.366	0.914	1.203	1.316	1.511	-69.750
-0.623	-0.427	1.078	1.182	1.096	1.600	-60.249	-0.850	-0.427	0.801	1.256	1.568	1.489	-73.250
-0.623	-0.488	0.975	1.245	1.276	1.582	-63.750	-0.850	-0.488	0.685	1.301	1.897	1.471	-76.750
-0.623	-0.549	0.869	1.302	1.496	1.565	-67.250	-0.850	-0.549	0.569	1.340	2.354	1.455	-80.250
-0.623	-0.610	0.761	1.351	1.775	1.551	-70.750	-0.850	-0.610	0.451	1.371	3.037	1.443	-83.750

α (RAD.)	β (RAD.)	v_α	v_β	v_β / v_α	V	φ (DEGREES)
-0.907	0.000	1.487	0.788	0.529	1.683	-52.000
-0.907	-0.061	1.388	0.875	0.630	1.641	-55.500
-0.907	-0.122	1.286	0.957	0.744	1.603	-59.000
-0.907	-0.183	1.180	1.032	0.874	1.568	-62.500
-0.907	-0.244	1.071	1.101	1.028	1.536	-66.000
-0.907	-0.305	0.959	1.163	1.212	1.508	-69.500
-0.907	-0.366	0.845	1.219	1.441	1.483	-73.000
-0.907	-0.427	0.729	1.267	1.736	1.462	-76.500
-0.907	-0.488	0.611	1.308	2.137	1.444	-80.000
-0.907	-0.549	0.493	1.341	2.721	1.429	-83.500
-0.907	-0.610	0.373	1.368	3.662	1.418	-87.000
-0.964	0.000	1.441	0.821	0.569	1.659	-55.250
-0.964	-0.061	1.338	0.906	0.677	1.616	-58.750
-0.964	-0.122	1.231	0.985	0.799	1.576	-62.249
-0.964	-0.183	1.121	1.056	0.942	1.540	-65.750
-0.964	-0.244	1.008	1.122	1.112	1.508	-69.250
-0.964	-0.305	0.893	1.180	1.321	1.480	-72.750
-0.964	-0.366	0.776	1.231	1.586	1.455	-76.250
-0.964	-0.427	0.657	1.274	1.939	1.434	-79.749
-0.964	-0.488	0.537	1.311	2.439	1.417	-83.250
-0.964	-0.549	0.417	1.340	3.214	1.403	-86.750
-0.964	-0.610	0.296	1.362	4.599	1.394	-90.250
-1.021	0.000	1.394	0.852	0.611	1.634	-58.499
-1.021	-0.061	1.286	0.934	0.726	1.589	-62.000
-1.021	-0.122	1.174	1.009	0.859	1.549	-65.500
-1.021	-0.183	1.060	1.077	1.016	1.512	-69.000
-1.021	-0.244	0.944	1.139	1.206	1.479	-72.500
-1.021	-0.305	0.825	1.193	1.444	1.451	-76.000
-1.021	-0.366	0.706	1.240	1.756	1.427	-79.500
-1.021	-0.427	0.584	1.279	2.187	1.406	-83.000
-1.021	-0.488	0.463	1.311	2.831	1.390	-86.500
-1.021	-0.549	0.341	1.336	3.917	1.378	-90.000
-1.021	-0.610	0.219	1.353	6.175	1.370	-93.500
-1.077	0.000	1.345	0.880	0.654	1.607	-61.750
-1.077	-0.061	1.232	0.959	0.778	1.561	-65.249
-1.077	-0.122	1.116	1.031	0.923	1.520	-68.750
-1.077	-0.183	0.999	1.096	1.097	1.483	-72.250
-1.077	-0.244	0.879	1.153	1.311	1.450	-75.750
-1.077	-0.305	0.757	1.203	1.587	1.422	-79.250
-1.077	-0.366	0.635	1.245	1.960	1.398	-82.750
-1.077	-0.427	0.512	1.281	2.500	1.379	-86.250
-1.077	-0.488	0.388	1.308	3.365	1.365	-89.750
-1.077	-0.549	0.265	1.328	5.003	1.354	-93.250
-1.077	-0.610	0.142	1.341	9.396	1.348	-96.750

α (RAD.)	β (RAD.)	v_α	v_β	v_β / v_α	V	φ (DEGREES)
-1.134	0.000	1.294	0.906	0.700	1.580	-65.000
-1.134	-0.061	1.177	0.981	0.833	1.532	-68.500
-1.134	-0.122	1.057	1.050	0.992	1.490	-71.999
-1.134	-0.183	0.936	1.111	1.186	1.453	-75.500
-1.134	-0.244	0.813	1.164	1.431	1.420	-78.999
-1.134	-0.305	0.689	1.210	1.755	1.392	-82.500
-1.134	-0.366	0.564	1.248	2.211	1.370	-86.000
-1.134	-0.427	0.439	1.279	2.909	1.352	-89.500
-1.134	-0.488	0.314	1.302	4.137	1.339	-93.000
-1.134	-0.549	0.190	1.317	6.919	1.331	-96.500
-1.134	-0.610	0.067	1.325	19.766	1.327	-100.000

APPENDIX 3

THE MAPPING OF THE BOW PLASTIC ZONE (FIGURE 12) FROM THE CHARACTERISTIC PLANE ON THE PHYSICAL PLANE

α (RAD.)	β (RAD.)	x	y
-0.1135E 01	0.0000E 00	-0.5004E 00	-0.8657E 00
-0.1100E 01	-0.1500E-01	-0.4830E 00	-0.8755E 00
-0.1100E 01	0.0000E 00	-0.4932E 00	-0.8806E 00
-0.1050E 01	-0.3500E-01	-0.4565E 00	-0.8896E 00
-0.1050E 01	-0.1500E-01	-0.4714E 00	-0.8977E 00
-0.1050E 01	0.0000E 00	-0.4810E 00	-0.9031E 00
-0.1000E 01	-0.5500E-01	-0.4296E 00	-0.9029E 00
-0.1000E 01	-0.3500E-01	-0.4443E 00	-0.9114E 00
-0.1000E 01	-0.1500E-01	-0.4584E 00	-0.9200E 00
-0.1000E 01	0.0000E 00	-0.4673E 00	-0.9256E 00
-0.9500E 00	-0.7500E-01	-0.4023E 00	-0.9154E 00
-0.9500E 00	-0.5500E-01	-0.4168E 00	-0.9244E 00
-0.9500E 00	-0.3500E-01	-0.4305E 00	-0.9333E 00
-0.9500E 00	-0.1500E-01	-0.4437E 00	-0.9423E 00
-0.9500E 00	0.0000E 00	-0.4520E 00	-0.9481E 00
-0.9000E 00	-0.1000E 00	-0.3793E 00	-0.9252E 00
-0.9000E 00	-0.7500E-01	-0.3911E 00	-0.9329E 00
-0.9000E 00	-0.5500E-01	-0.4047E 00	-0.9424E 00
-0.9000E 00	-0.3500E-01	-0.4176E 00	-0.9517E 00
-0.9000E 00	-0.1500E-01	-0.4300E 00	-0.9610E 00
-0.9000E 00	0.0000E 00	-0.4377E 00	-0.9671E 00
-0.8500E 00	-0.1220E 00	-0.3533E 00	-0.9354E 00
-0.8500E 00	-0.1000E 00	-0.3662E 00	-0.9445E 00
-0.8500E 00	-0.7500E-01	-0.3771E 00	-0.9525E 00
-0.8500E 00	-0.5500E-01	-0.3898E 00	-0.9623E 00
-0.8500E 00	-0.3500E-01	-0.4019E 00	-0.9720E 00
-0.8500E 00	-0.1500E-01	-0.4134E 00	-0.9815E 00
-0.8500E 00	0.0000E 00	-0.4205E 00	-0.9877E 00
-0.8000E 00	-0.1450E 00	-0.3279E 00	-0.9446E 00
-0.8000E 00	-0.1220E 00	-0.3401E 00	-0.9537E 00
-0.8000E 00	-0.1000E 00	-0.3522E 00	-0.9631E 00
-0.8000E 00	-0.7500E-01	-0.3622E 00	-0.9712E 00
-0.8000E 00	-0.5500E-01	-0.3741E 00	-0.9813E 00
-0.8000E 00	-0.3500E-01	-0.3853E 00	-0.9913E 00
-0.8000E 00	-0.1500E-01	-0.3959E 00	-0.1001E 01

α (RAD.)	β (RAD.)	x	y
-0.8000E 00	0.0000E 00	-0.4024E 00	-0.1007E 01
-0.7500E 00	-0.1730E 00	-0.3070E 00	-0.9516E 00
-0.7500E 00	-0.1450E 00	-0.3168E 00	-0.9592E 00
-0.7500E 00	-0.1220E 00	-0.3282E 00	-0.9686E 00
-0.7500E 00	-0.1000E 00	-0.3395E 00	-0.9783E 00
-0.7500E 00	-0.7500E-01	-0.3487E 00	-0.9866E 00
-0.7500E 00	-0.5500E-01	-0.3597E 00	-0.9970E 00
-0.7500E 00	-0.3500E-01	-0.3701E 00	-0.1007E 01
-0.7500E 00	-0.1500E-01	-0.3799E 00	-0.1017E 01
-0.7500E 00	0.0000E 00	-0.3859E 00	-0.1023E 01
-0.7000E 00	-0.1980E 00	-0.2832E 00	-0.9590E 00
-0.7000E 00	-0.1730E 00	-0.2941E 00	-0.9679E 00
-0.7000E 00	-0.1450E 00	-0.3030E 00	-0.9756E 00
-0.7000E 00	-0.1220E 00	-0.3135E 00	-0.9852E 00
-0.7000E 00	-0.1000E 00	-0.3240E 00	-0.9951E 00
-0.7000E 00	-0.7500E-01	-0.3323E 00	-0.1003E 01
-0.7000E 00	-0.5500E-01	-0.3425E 00	-0.1014E 01
-0.7000E 00	-0.3500E-01	-0.3520E 00	-0.1024E 01
-0.7000E 00	-0.1500E-01	-0.3610E 00	-0.1034E 01
-0.7000E 00	0.0000E 00	-0.3664E 00	-0.1040E 01
-0.6500E 00	-0.2250E 00	-0.2610E 00	-0.9653E 00
-0.6500E 00	-0.1980E 00	-0.2708E 00	-0.9737E 00
-0.6500E 00	-0.1730E 00	-0.2809E 00	-0.9828E 00
-0.6500E 00	-0.1450E 00	-0.2890E 00	-0.9905E 00
-0.6500E 00	-0.1220E 00	-0.2988E 00	-0.1000E 01
-0.6500E 00	-0.1000E 00	-0.3084E 00	-0.1010E 01
-0.6500E 00	-0.7500E-01	-0.3159E 00	-0.1018E 01
-0.6500E 00	-0.5500E-01	-0.3252E 00	-0.1029E 01
-0.6500E 00	-0.3500E-01	-0.3340E 00	-0.1039E 01
-0.6500E 00	-0.1500E-01	-0.3421E 00	-0.1050E 01
-0.6500E 00	0.0000E 00	-0.3469E 00	-0.1056E 01
-0.6000E 00	-0.2550E 00	-0.2417E 00	-0.9703E 00
-0.6000E 00	-0.2250E 00	-0.2500E 00	-0.9778E 00
-0.6000E 00	-0.1980E 00	-0.2591E 00	-0.9866E 00
-0.6000E 00	-0.1730E 00	-0.2684E 00	-0.9957E 00
-0.6000E 00	-0.1450E 00	-0.2757E 00	-0.1003E 01
-0.6000E 00	-0.1220E 00	-0.2847E 00	-0.1013E 01
-0.6000E 00	-0.1000E 00	-0.2935E 00	-0.1023E 01
-0.6000E 00	-0.7500E-01	-0.3003E 00	-0.1031E 01
-0.6000E 00	-0.5500E-01	-0.3088E 00	-0.1042E 01
-0.6000E 00	-0.3500E-01	-0.3167E 00	-0.1053E 01
-0.6000E 00	-0.1500E-01	-0.3241E 00	-0.1063E 01
-0.6000E 00	0.0000E 00	-0.3284E 00	-0.1069E 01

α (RAD.)	β (RAD.)	x	y
-0.5500E 00	-0.2830E 00	-0.2203E 00	-0.9754E 00
-0.5500E 00	-0.2550E 00	-0.2293E 00	-0.9838E 00
-0.5500E 00	-0.2250E 00	-0.2369E 00	-0.9913E 00
-0.5500E 00	-0.1980E 00	-0.2451E 00	-0.1000E 01
-0.5500E 00	-0.1730E 00	-0.2536E 00	-0.1009E 01
-0.5500E 00	-0.1450E 00	-0.2602E 00	-0.1017E 01
-0.5500E 00	-0.1220E 00	-0.2683E 00	-0.1027E 01
-0.5500E 00	-0.1000E 00	-0.2763E 00	-0.1037E 01
-0.5500E 00	-0.7500E-01	-0.2824E 00	-0.1045E 01
-0.5500E 00	-0.5500E-01	-0.2901E 00	-0.1056E 01
-0.5500E 00	-0.3500E-01	-0.2972E 00	-0.1066E 01
-0.5500E 00	-0.1500E-01	-0.3038E 00	-0.1077E 01
-0.5500E 00	0.0000E 00	-0.3076E 00	-0.1083E 01
-0.5000E 00	-0.3130E 00	-0.2007E 00	-0.9796E 00
-0.5000E 00	-0.2830E 00	-0.2087E 00	-0.9874E 00
-0.5000E 00	-0.2550E 00	-0.2170E 00	-0.9960E 00
-0.5000E 00	-0.2250E 00	-0.2238E 00	-0.1003E 01
-0.5000E 00	-0.1980E 00	-0.2313E 00	-0.1012E 01
-0.5000E 00	-0.1730E 00	-0.2390E 00	-0.1021E 01
-0.5000E 00	-0.1450E 00	-0.2449E 00	-0.1029E 01
-0.5000E 00	-0.1220E 00	-0.2523E 00	-0.1039E 01
-0.5000E 00	-0.1000E 00	-0.2595E 00	-0.1049E 01
-0.5000E 00	-0.7500E-01	-0.2648E 00	-0.1057E 01
-0.5000E 00	-0.5500E-01	-0.2717E 00	-0.1069E 01
-0.5000E 00	-0.3500E-01	-0.2781E 00	-0.1078E 01
-0.5000E 00	-0.1500E-01	-0.2839E 00	-0.1088E 01
-0.5000E 00	0.0000E 00	-0.2872E 00	-0.1094E 01
-0.4500E 00	-0.3430E 00	-0.1811E 00	-0.9834E 00
-0.4500E 00	-0.3130E 00	-0.1890E 00	-0.9914E 00
-0.4500E 00	-0.2830E 00	-0.1962E 00	-0.9993E 00
-0.4500E 00	-0.2550E 00	-0.2037E 00	-0.1007E 01
-0.4500E 00	-0.2250E 00	-0.2098E 00	-0.1015E 01
-0.4500E 00	-0.1980E 00	-0.2166E 00	-0.1023E 01
-0.4500E 00	-0.1730E 00	-0.2235E 00	-0.1033E 01
-0.4500E 00	-0.1450E 00	-0.2287E 00	-0.1040E 01
-0.4500E 00	-0.1220E 00	-0.2353E 00	-0.1050E 01
-0.4500E 00	-0.1000E 00	-0.2417E 00	-0.1061E 01
-0.4500E 00	-0.7500E-01	-0.2464E 00	-0.1068E 01
-0.4500E 00	-0.5500E-01	-0.2525E 00	-0.1079E 01
-0.4500E 00	-0.3500E-01	-0.2582E 00	-0.1090E 01
-0.4500E 00	-0.1500E-01	-0.2633E 00	-0.1100E 01
-0.4500E 00	0.0000E 00	-0.2661E 00	-0.1105E 01
-0.4000E 00	-0.3700E 00	-0.1584E 00	-0.9873E 00
-0.4000E 00	-0.3430E 00	-0.1673E 00	-0.9967E 00
-0.4000E 00	-0.3130E 00	-0.1744E 00	-0.1004E 01
-0.4000E 00	-0.2830E 00	-0.1809E 00	-0.1012E 01
-0.4000E 00	-0.2550E 00	-0.1876E 00	-0.1020E 01
-0.4000E 00	-0.2250E 00	-0.1929E 00	-0.1028E 01
-0.4000E 00	-0.1980E 00	-0.1989E 00	-0.1036E 01
-0.4000E 00	-0.1730E 00	-0.2050E 00	-0.1045E 01
-0.4000E 00	-0.1450E 00	-0.2095E 00	-0.1053E 01
-0.4000E 00	-0.1220E 00	-0.2153E 00	-0.1062E 01
-0.4000E 00	-0.1000E 00	-0.2210E 00	-0.1073E 01
-0.4000E 00	-0.7500E-01	-0.2250E 00	-0.1080E 01
-0.4000E 00	-0.5500E-01	-0.2303E 00	-0.1091E 01
-0.4000E 00	-0.3500E-01	-0.2352E 00	-0.1101E 01
-0.4000E 00	-0.1500E-01	-0.2396E 00	-0.1111E 01
-0.4000E 00	0.0000E 00	-0.2420E 00	-0.1116E 01
-0.3500E 00	-0.4000E 00	-0.1386E 00	-0.9903E 00
-0.3500E 00	-0.3700E 00	-0.1462E 00	-0.9986E 00
-0.3500E 00	-0.3430E 00	-0.1543E 00	-0.1008E 01
-0.3500E 00	-0.3130E 00	-0.1606E 00	-0.1016E 01
-0.3500E 00	-0.2830E 00	-0.1664E 00	-0.1023E 01
-0.3500E 00	-0.2550E 00	-0.1723E 00	-0.1032E 01
-0.3500E 00	-0.2250E 00	-0.1770E 00	-0.1039E 01
-0.3500E 00	-0.1980E 00	-0.1823E 00	-0.1047E 01
-0.3500E 00	-0.1730E 00	-0.1877E 00	-0.1056E 01
-0.3500E 00	-0.1450E 00	-0.1915E 00	-0.1063E 01
-0.3500E 00	-0.1220E 00	-0.1966E 00	-0.1073E 01
-0.3500E 00	-0.1000E 00	-0.2015E 00	-0.1083E 01
-0.3500E 00	-0.7500E-01	-0.2049E 00	-0.1090E 01
-0.3500E 00	-0.5500E-01	-0.2096E 00	-0.1100E 01
-0.3500E 00	-0.3500E-01	-0.2137E 00	-0.1110E 01
-0.3500E 00	-0.1500E-01	-0.2175E 00	-0.1120E 01
-0.3500E 00	0.0000E 00	-0.2195E 00	-0.1125E 01
-0.3000E 00	-0.4300E 00	-0.1186E 00	-0.9929E 00
-0.3000E 00	-0.4000E 00	-0.1262E 00	-0.1001E 01
-0.3000E 00	-0.3700E 00	-0.1329E 00	-0.1009E 01
-0.3000E 00	-0.3430E 00	-0.1403E 00	-0.1019E 01
-0.3000E 00	-0.3130E 00	-0.1459E 00	-0.1026E 01
-0.3000E 00	-0.2830E 00	-0.1504E 00	-0.1034E 01
-0.3000E 00	-0.2550E 00	-0.1562E 00	-0.1042E 01
-0.3000E 00	-0.2250E 00	-0.1602E 00	-0.1049E 01
-0.3000E 00	-0.1980E 00	-0.1648E 00	-0.1057E 01
-0.3000E 00	-0.1730E 00	-0.1695E 00	-0.1065E 01
-0.3000E 00	-0.1450E 00	-0.1727E 00	-0.1072E 01
-0.3000E 00	-0.1220E 00	-0.1771E 00	-0.1082E 01
-0.3000E 00	-0.1000E 00	-0.1814E 00	-0.1092E 01
-0.3000E 00	-0.7500E-01	-0.1842E 00	-0.1099E 01
-0.3000E 00	-0.5500E-01	-0.1881E 00	-0.1109E 01
-0.3000E 00	-0.3500E-01	-0.1916E 00	-0.1119E 01
-0.3000E 00	-0.1500E-01	-0.1947E 00	-0.1128E 01
-0.3000E 00	0.0000E 00	-0.1963E 00	-0.1133E 01
-0.2500E 00	-0.4600E 00	-0.9897E-01	-0.9950E 00

α (RAD.)	β (RAD.)	x	y
-0.2500E 00	-0.4300E 00	-0.1061E 00	-0.1003E 01
-0.2500E 00	-0.4000E 00	-0.1127E 00	-0.1012E 01
-0.2500E 00	-0.3700E 00	-0.1188E 00	-0.1020E 01
-0.2500E 00	-0.3430E 00	-0.1253E 00	-0.1029E 01
-0.2500E 00	-0.3130E 00	-0.1302E 00	-0.1037E 01
-0.2500E 00	-0.2830E 00	-0.1346E 00	-0.1044E 01
-0.2500E 00	-0.2550E 00	-0.1392E 00	-0.1052E 01
-0.2500E 00	-0.2250E 00	-0.1426E 00	-0.1058E 01
-0.2500E 00	-0.1980E 00	-0.1465E 00	-0.1066E 01
-0.2500E 00	-0.1730E 00	-0.1506E 00	-0.1075E 01
-0.2500E 00	-0.1450E 00	-0.1532E 00	-0.1081E 01
-0.2500E 00	-0.1220E 00	-0.1569E 00	-0.1090E 01
-0.2500E 00	-0.1000E 00	-0.1605E 00	-0.1100E 01
-0.2500E 00	-0.7500E-01	-0.1628E 00	-0.1106E 01
-0.2500E 00	-0.5500E-01	-0.1661E 00	-0.1116E 01
-0.2500E 00	-0.3500E-01	-0.1689E 00	-0.1126E 01
-0.2500E 00	-0.1500E-01	-0.1714E 00	-0.1135E 01
-0.2500E 00	0.0000E 00	-0.1727E 00	-0.1140E 01
-0.2000E 00	-0.4900E 00	-0.7305E-01	-0.9968E 00
-0.2000E 00	-0.4600E 00	-0.8606E-01	-0.1005E 01
-0.2000E 00	-0.4300E 00	-0.9249E-01	-0.1014E 01
-0.2000E 00	-0.4000E 00	-0.9837E-01	-0.1022E 01
-0.2000E 00	-0.3700E 00	-0.1037E 00	-0.1030E 01
-0.2000E 00	-0.3430E 00	-0.1095E 00	-0.1039E 01
-0.2000E 00	-0.3130E 00	-0.1137E 00	-0.1047E 01
-0.2000E 00	-0.2830E 00	-0.1175E 00	-0.1054E 01
-0.2000E 00	-0.2550E 00	-0.1214E 00	-0.1061E 01
-0.2000E 00	-0.2250E 00	-0.1242E 00	-0.1067E 01
-0.2000E 00	-0.1980E 00	-0.1275E 00	-0.1075E 01
-0.2000E 00	-0.1730E 00	-0.1309E 00	-0.1083E 01
-0.2000E 00	-0.1450E 00	-0.1330E 00	-0.1089E 01
-0.2000E 00	-0.1220E 00	-0.1361E 00	-0.1098E 01
-0.2000E 00	-0.1000E 00	-0.1391E 00	-0.1107E 01
-0.2000E 00	-0.7500E-01	-0.1409E 00	-0.1113E 01
-0.2000E 00	-0.5500E-01	-0.1435E 00	-0.1123E 01
-0.2000E 00	-0.3500E-01	-0.1458E 00	-0.1132E 01
-0.2000E 00	-0.1500E-01	-0.1477E 00	-0.1141E 01
-0.2000E 00	0.0000E 00	-0.1487E 00	-0.1145E 01
-0.1500E 00	-0.5200E 00	-0.5910E-01	-0.9982E 00
-0.1500E 00	-0.4900E 00	-0.6593E-01	-0.1007E 01
-0.1500E 00	-0.4600E 00	-0.7219E-01	-0.1015E 01
-0.1500E 00	-0.4300E 00	-0.7790E-01	-0.1024E 01
-0.1500E 00	-0.4000E 00	-0.8307E-01	-0.1032E 01
-0.1500E 00	-0.3700E 00	-0.8770E-01	-0.1040E 01
-0.1500E 00	-0.3430E 00	-0.9279E-01	-0.1049E 01
-0.1500E 00	-0.3130E 00	-0.9641E-01	-0.1056E 01
-0.1500E 00	-0.2830E 00	-0.9955E-01	-0.1062E 01
-0.1500E 00	-0.2550E 00	-0.1028E 00	-0.1070E 01
-0.1500E 00	-0.2250E 00	-0.1051E 00	-0.1075E 01
-0.1500E 00	-0.1980E 00	-0.1078E 00	-0.1083E 01

α (RAD.)	β (RAD.)	x	y
-0.1500E 00	-0.1730E 00	-0.1106E 00	-0.1091E 01
-0.1500E 00	-0.1450E 00	-0.1122E 00	-0.1096E 01
-0.1500E 00	-0.1220E 00	-0.1148E 00	-0.1104E 01
-0.1500E 00	-0.1000E 00	-0.1171E 00	-0.1113E 01
-0.1500E 00	-0.7500E-01	-0.1185E 00	-0.1119E 01
-0.1500E 00	-0.5500E-01	-0.1205E 00	-0.1128E 01
-0.1500E 00	-0.3500E-01	-0.1223E 00	-0.1137E 01
-0.1500E 00	-0.1500E-01	-0.1237E 00	-0.1145E 01
-0.1500E 00	0.0000E 00	-0.1244E 00	-0.1149E 01
-0.1000E 00	-0.5500E 00	-0.3912E-01	-0.9992E 00
-0.1000E 00	-0.5200E 00	-0.4577E-01	-0.1008E 01
-0.1000E 00	-0.4900E 00	-0.5186E-01	-0.1017E 01
-0.1000E 00	-0.4600E 00	-0.5740E-01	-0.1025E 01
-0.1000E 00	-0.4300E 00	-0.6240E-01	-0.1033E 01
-0.1000E 00	-0.4000E 00	-0.6688E-01	-0.1041E 01
-0.1000E 00	-0.3700E 00	-0.7085E-01	-0.1049E 01
-0.1000E 00	-0.3430E 00	-0.7525E-01	-0.1058E 01
-0.1000E 00	-0.3130E 00	-0.7826E-01	-0.1064E 01
-0.1000E 00	-0.2830E 00	-0.8084E-01	-0.1071E 01
-0.1000E 00	-0.2550E 00	-0.8355E-01	-0.1078E 01
-0.1000E 00	-0.2250E 00	-0.8534E-01	-0.1083E 01
-0.1000E 00	-0.1980E 00	-0.8750E-01	-0.1089E 01
-0.1000E 00	-0.1730E 00	-0.8976E-01	-0.1097E 01
-0.1000E 00	-0.1450E 00	-0.9100E-01	-0.1102E 01
-0.1000E 00	-0.1220E 00	-0.9295E-01	-0.1110E 01
-0.1000E 00	-0.1000E 00	-0.9476E-01	-0.1116E 01
-0.1000E 00	-0.7500E-01	-0.9572E-01	-0.1123E 01
-0.1000E 00	-0.5500E-01	-0.9723E-01	-0.1133E 01
-0.1000E 00	-0.3500E-01	-0.9845E-01	-0.1141E 01
-0.1000E 00	-0.1500E-01	-0.9941E-01	-0.1149E 01
-0.1000E 00	0.0000E 00	-0.9983E-01	-0.1152E 01
-0.5000E-01	-0.5800E 00	-0.1913E-01	-0.9998E 00
-0.5000E-01	-0.5500E 00	-0.2560E-01	-0.1008E 01
-0.5000E-01	-0.5200E 00	-0.3151E-01	-0.1017E 01
-0.5000E-01	-0.4900E 00	-0.3686E-01	-0.1026E 01
-0.5000E-01	-0.4600E 00	-0.4171E-01	-0.1034E 01
-0.5000E-01	-0.4300E 00	-0.4603E-01	-0.1042E 01
-0.5000E-01	-0.4000E 00	-0.4985E-01	-0.1050E 01
-0.5000E-01	-0.3700E 00	-0.5320E-01	-0.1057E 01
-0.5000E-01	-0.3430E 00	-0.5693E-01	-0.1066E 01
-0.5000E-01	-0.3130E 00	-0.5939E-01	-0.1072E 01
-0.5000E-01	-0.2830E 00	-0.6144E-01	-0.1078E 01
-0.5000E-01	-0.2550E 00	-0.6362E-01	-0.1084E 01
-0.5000E-01	-0.2250E 00	-0.6497E-01	-0.1089E 01
-0.5000E-01	-0.1980E 00	-0.6665E-01	-0.1095E 01
-0.5000E-01	-0.1730E 00	-0.6839E-01	-0.1102E 01
-0.5000E-01	-0.1450E 00	-0.6926E-01	-0.1107E 01
-0.5000E-01	-0.1220E 00	-0.7071E-01	-0.1114E 01
-0.5000E-01	-0.1000E 00	-0.7201E-01	-0.1122E 01
-0.5000E-01	-0.7500E-01	-0.7263E-01	-0.1127E 01

α (RAD.)	β (RAD.)	x	y
-0.5000E-01	-0.5500E-01	-0.7363E-01	-0.1136E 01
-0.5000E-01	-0.3500E-01	-0.7439E-01	-0.1144E 01
-0.5000E-01	-0.1500E-01	-0.7493E-01	-0.1151E 01
-0.5000E-01	0.0000E 00	-0.7514E-01	-0.1154E 01
0.0000E 00	-0.6100E 00	0.6652E-03	-0.9999E 00
0.0000E 00	-0.5800E 00	-0.5421E-02	-0.1009E 01
0.0000E 00	-0.5500E 00	-0.1115E-01	-0.1018E 01
0.0000E 00	-0.5200E 00	-0.1634E-01	-0.1027E 01
0.0000E 00	-0.4900E 00	-0.2101E-01	-0.1035E 01
0.0000E 00	-0.4600E 00	-0.2516E-01	-0.1043E 01
0.0000E 00	-0.4300E 00	-0.2883E-01	-0.1051E 01
0.0000E 00	-0.4000E 00	-0.3203E-01	-0.1058E 01
0.0000E 00	-0.3700E 00	-0.3479E-01	-0.1065E 01
0.0000E 00	-0.3430E 00	-0.3790E-01	-0.1073E 01
0.0000E 00	-0.3130E 00	-0.3984E-01	-0.1079E 01
0.0000E 00	-0.2830E 00	-0.4143E-01	-0.1084E 01
0.0000E 00	-0.2550E 00	-0.4312E-01	-0.1090E 01
0.0000E 00	-0.2250E 00	-0.4408E-01	-0.1094E 01
0.0000E 00	-0.1980E 00	-0.4532E-01	-0.1100E 01
0.0000E 00	-0.1730E 00	-0.4660E-01	-0.1107E 01
0.0000E 00	-0.1450E 00	-0.4716E-01	-0.1110E 01
0.0000E 00	-0.1220E 00	-0.4815E-01	-0.1118E 01
0.0000E 00	-0.1000E 00	-0.4899E-01	-0.1125E 01
0.0000E 00	-0.7500E-01	-0.4934E-01	-0.1129E 01
0.0000E 00	-0.5500E-01	-0.4987E-01	-0.1137E 01
0.0000E 00	-0.3500E-01	-0.5021E-01	-0.1145E 01
0.0000E 00	-0.1500E-01	-0.5038E-01	-0.1152E 01
0.0000E 00	0.0000E 00	-0.5040E-01	-0.1155E 01

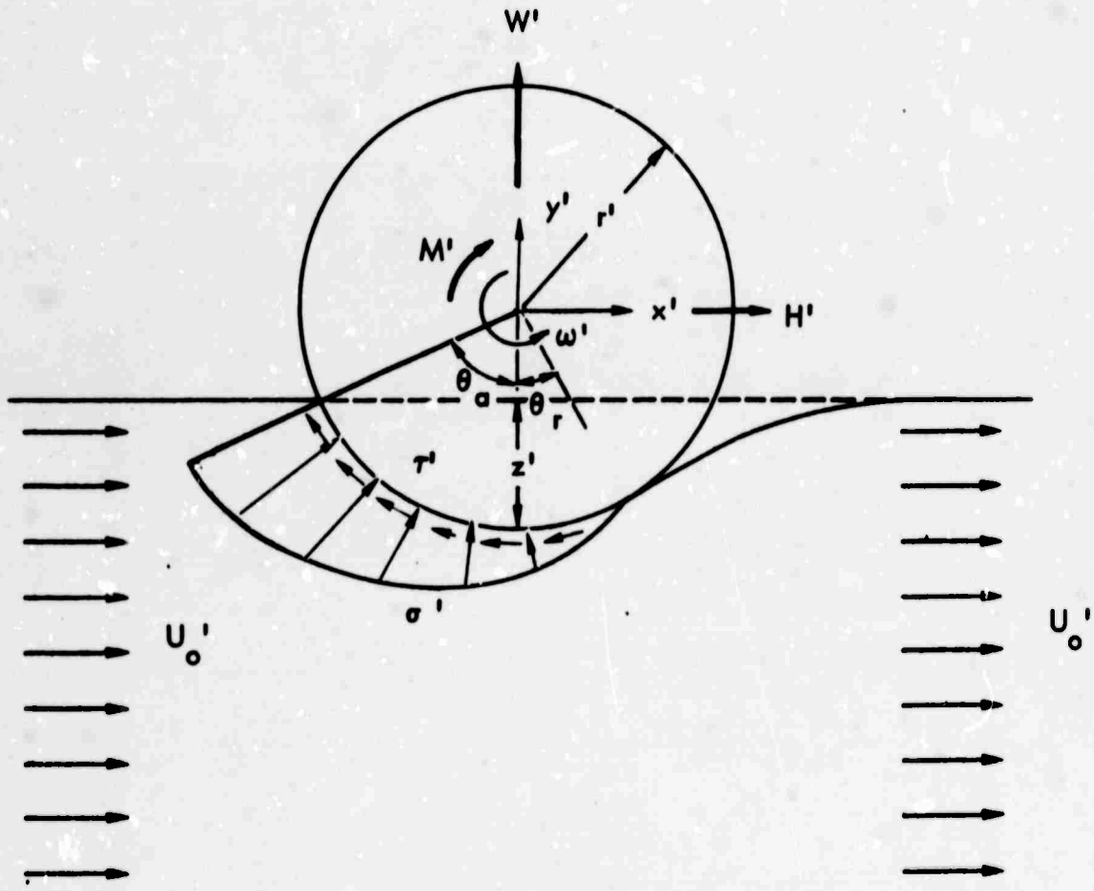

FIGURE 1 - A DRIVEN TWO-DIMENSIONAL WHEEL OVER A SEMI-INFINITE SOIL BODY

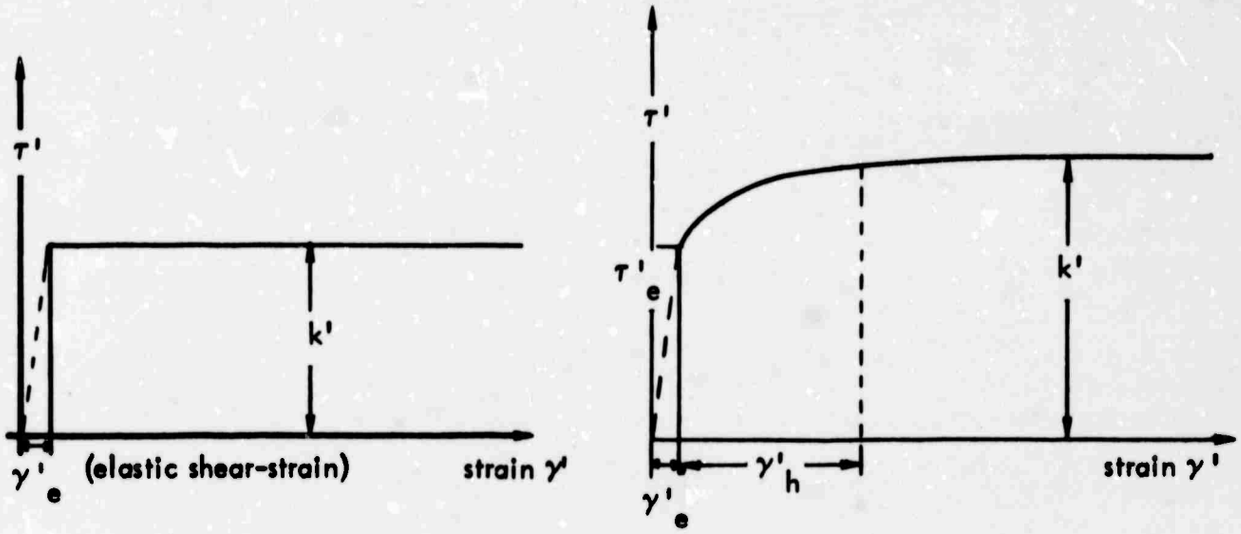

a. IDEAL ELASTIC-PLASTIC MATERIAL
(FOR RIGID-PLASTIC $\gamma'_e = 0$)

b. WORK-HARDENING MATERIAL.
(FOR RIGID WORK-HARDENING $\gamma'_e = 0$,
FOR RIGID-PLASTIC $\gamma'_e = 0$, $\gamma'_h = 0$)

FIGURE 2 - THE DEPENDENCE OF THE MAXIMUM SHEAR STRESS ON STRAIN

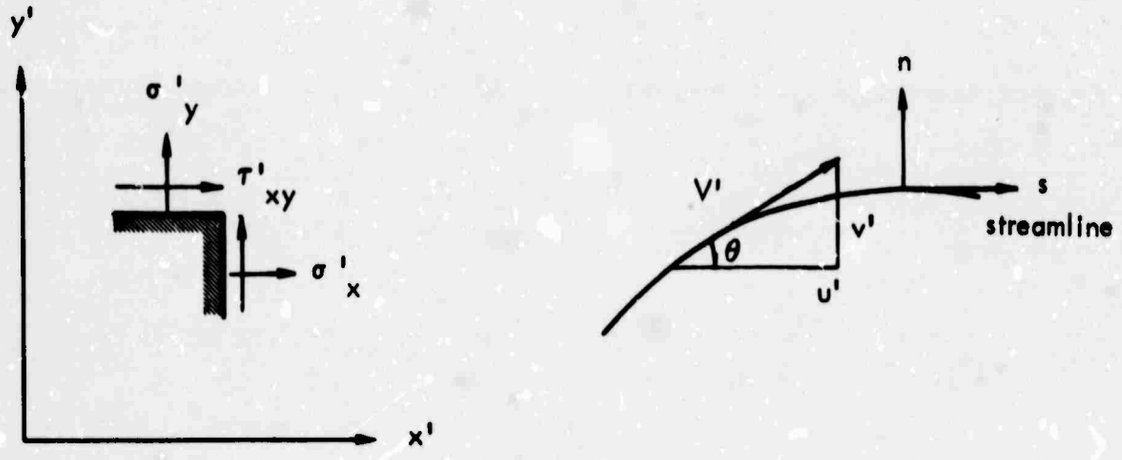

FIGURE 3 - STRESS AND VELOCITY COMPONENTS IN CARTESIAN COORDINATES

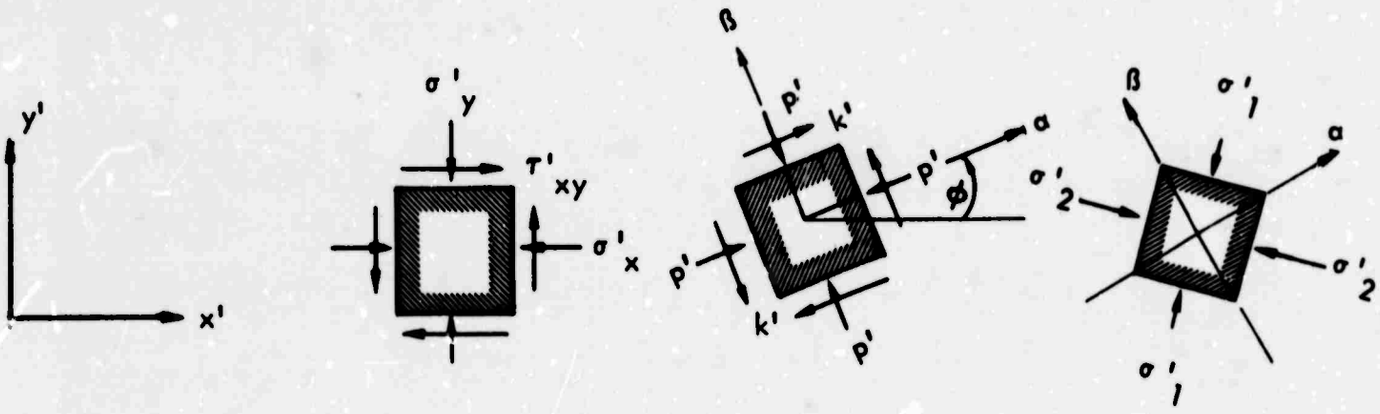

a. CARTESIAN COORDINATES

b. MAXIMUM-SHEAR STRESS DIRECTIONS

c. PRINCIPAL DIRECTIONS

FIGURE 4 - STRESSES AT A POINT REFERRED TO DIFFERENT DIRECTIONS

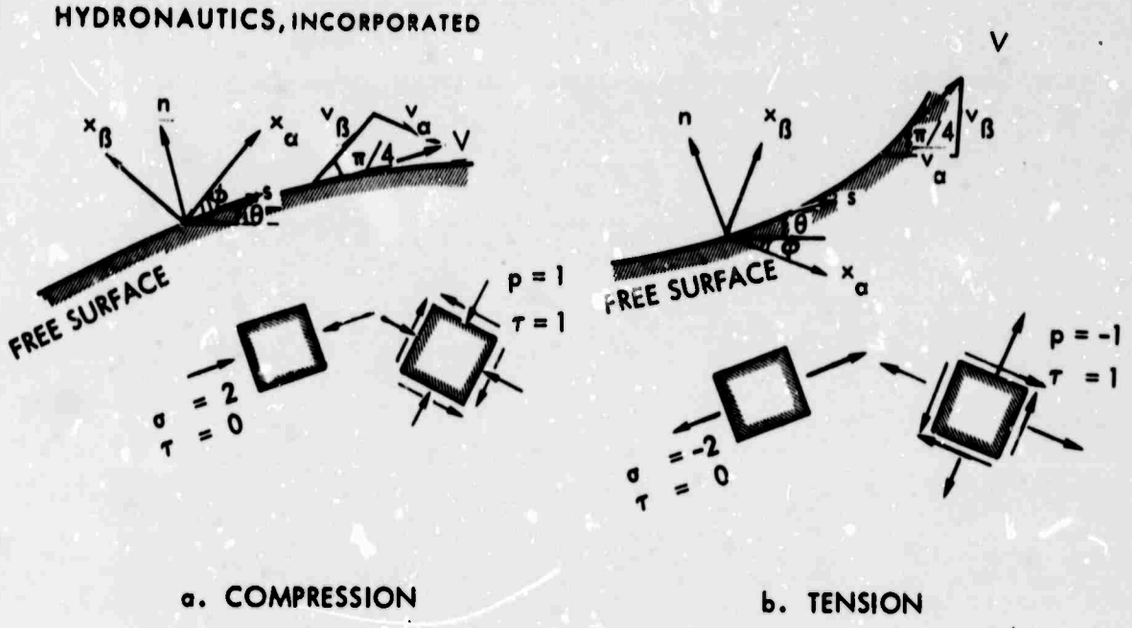

a. COMPRESSION

b. TENSION

FIGURE 5 - PLASTIC FLOW ALONG A FREE SURFACE

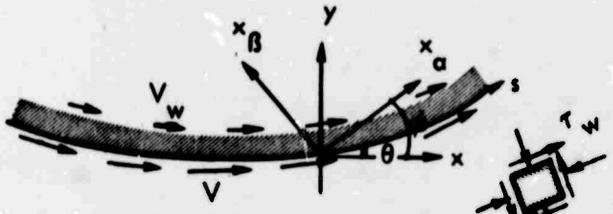

a. SLIPPING BOUNDARY ($V > V_w$), RETARDED FLOW ($\frac{\partial V}{\partial s} < 0$), $\pi/4 > \phi - \theta > 0$

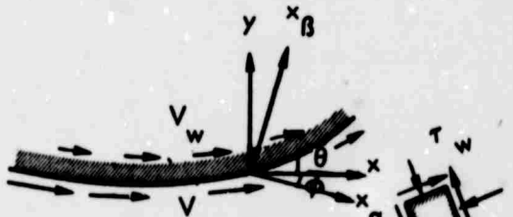

b. SLIPPING BOUNDARY ($V > V_w$), ACCELERATED FLOW ($\frac{\partial V}{\partial s} > 0$), $0 > \phi - \theta > -\frac{\pi}{4}$

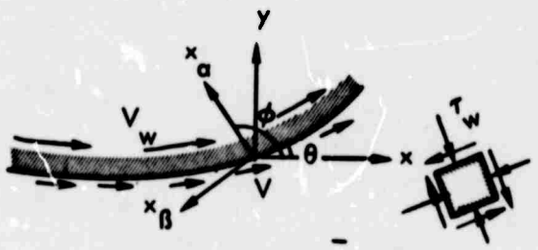

c. SKIDDING BOUNDARY ($V < V_w$)

$$\left| \phi - \theta \right| > \frac{\pi}{4}$$

FIGURE 6 - PLASTIC FLOW ALONG A RIGID BODY

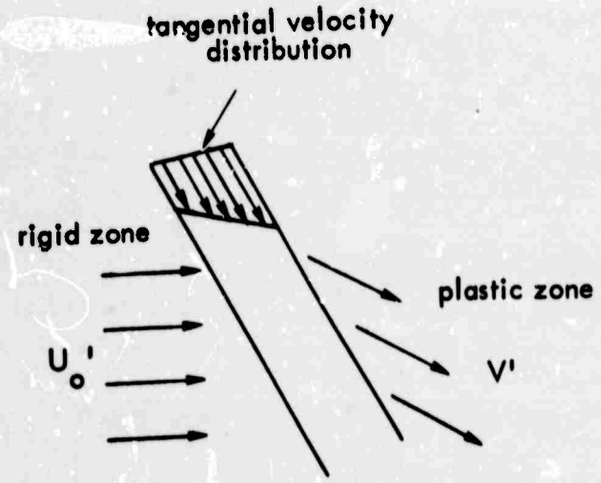

a. THIN PLASTIC LAYER

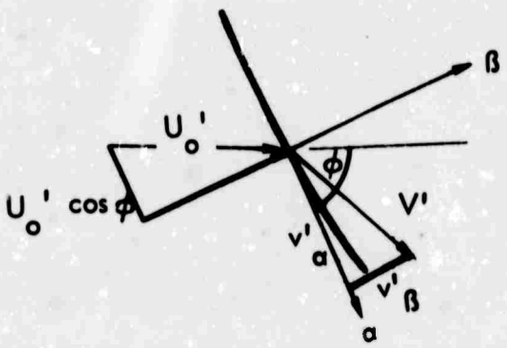

$$\delta V' = v'_a - U_o' \cos\phi$$

b. KINEMATICS OF DISCONTINUITY

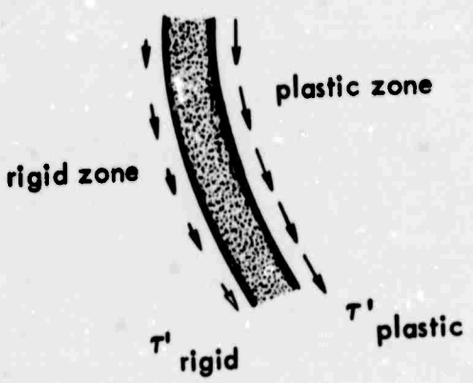

$$\delta \tau' = \rho' (U_o' \cos \phi)\ \delta V'$$

c. SHEAR STRESS

FIGURE 7 - A LINE OF VELOCITY DISCONTINUITY AT THE BOUNDARY BETWEEN A RIGID AND A PLASTIC REGION

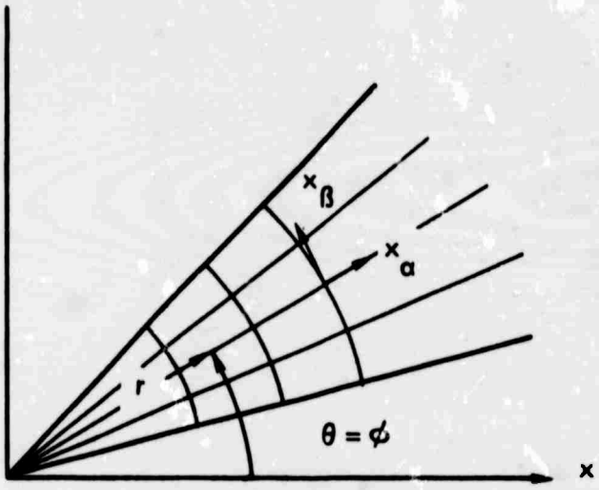

a. A CENTERED FAN

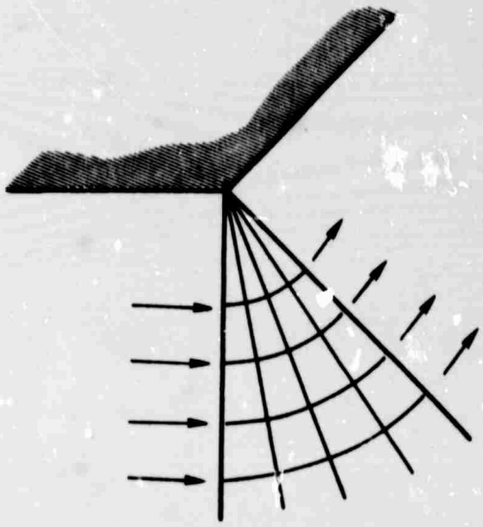

b. A CENTERED FAN AT A CONCAVE CORNER

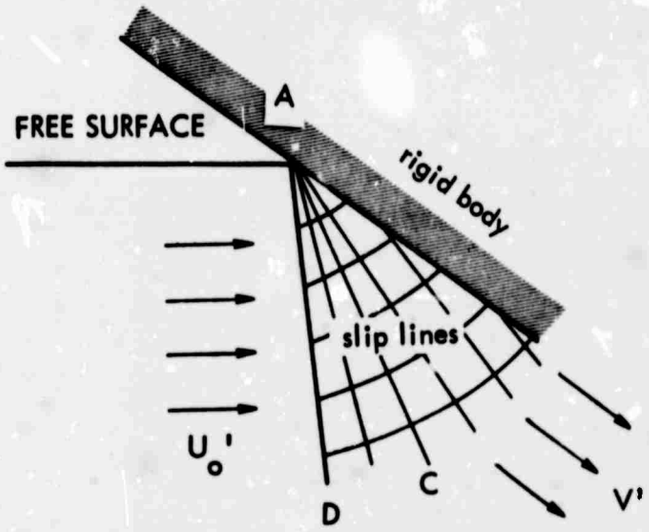

c. FLOW DETAIL IN SHEET-DRAWING (FROM [8 p. 173]). AD- DISCONTINUITY LINE, DAC - CENTERED FAN

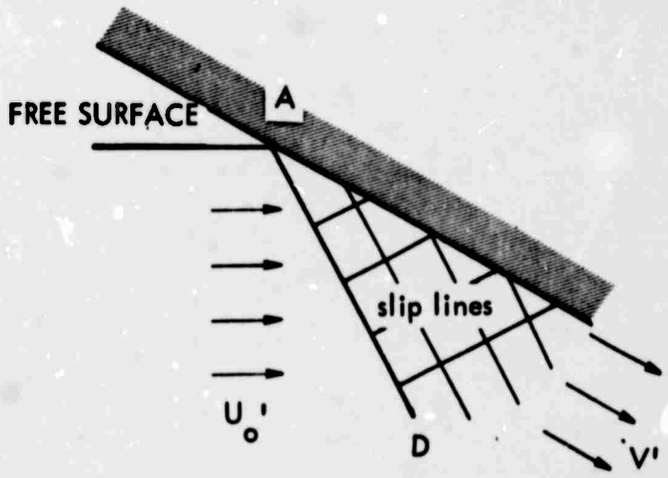

d. FLOW AS IN c., WITH INERTIAL TERMS CONSIDERED. (AD - DISCONTINUITY LINE)

FIGURE 8 - FLOW IN A CENTERED FAN AND AT THE INTERSECTION BETWEEN THE FREE-SURFACE AND A RIGID BODY

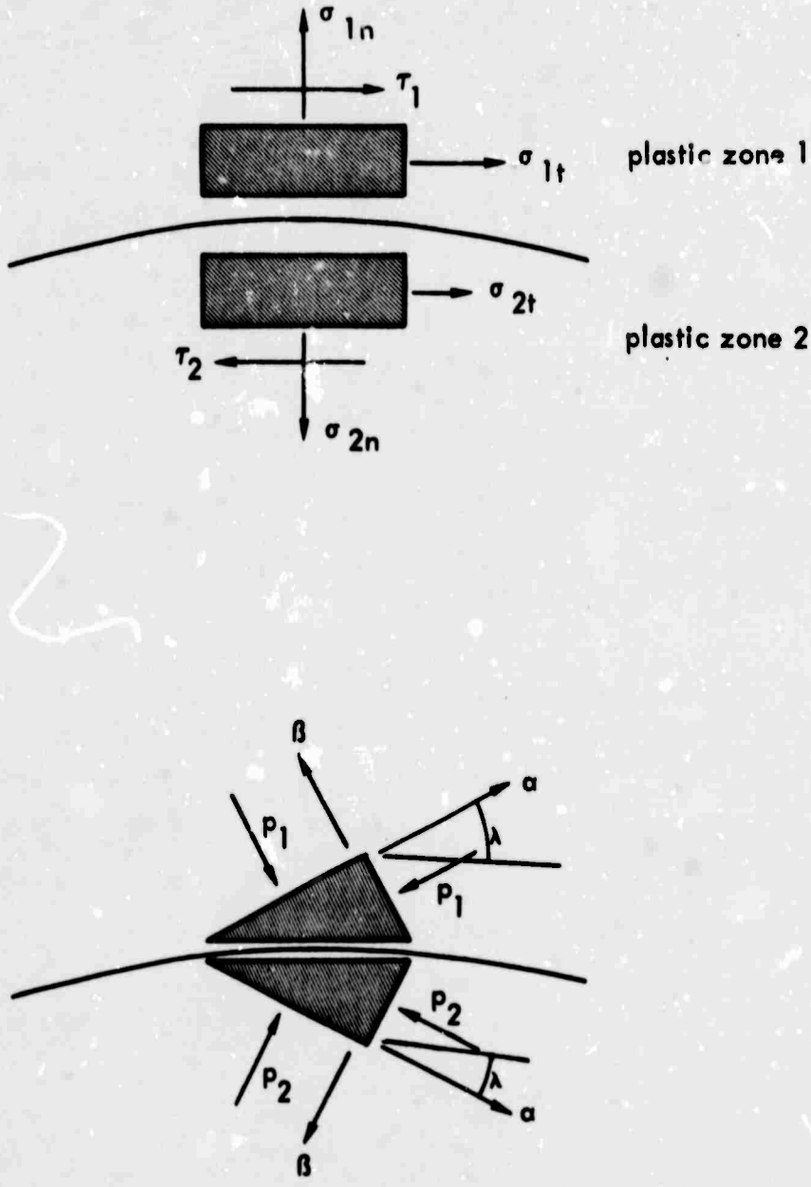

FIGURE 9 - A LINE OF STRESS DISCONTINUITY

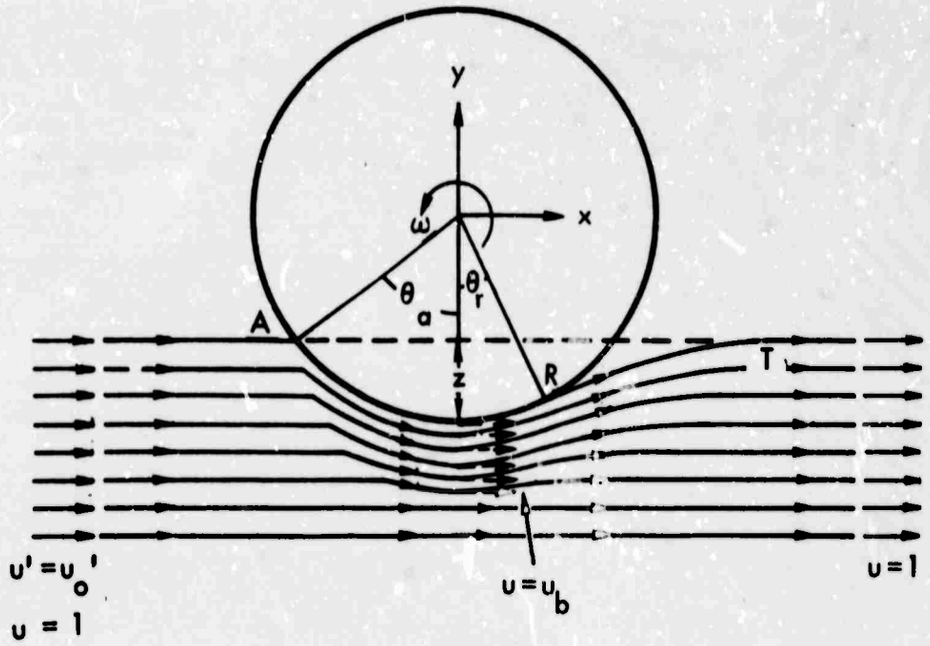

a. FREE - SURFACE AND STREAMLINES

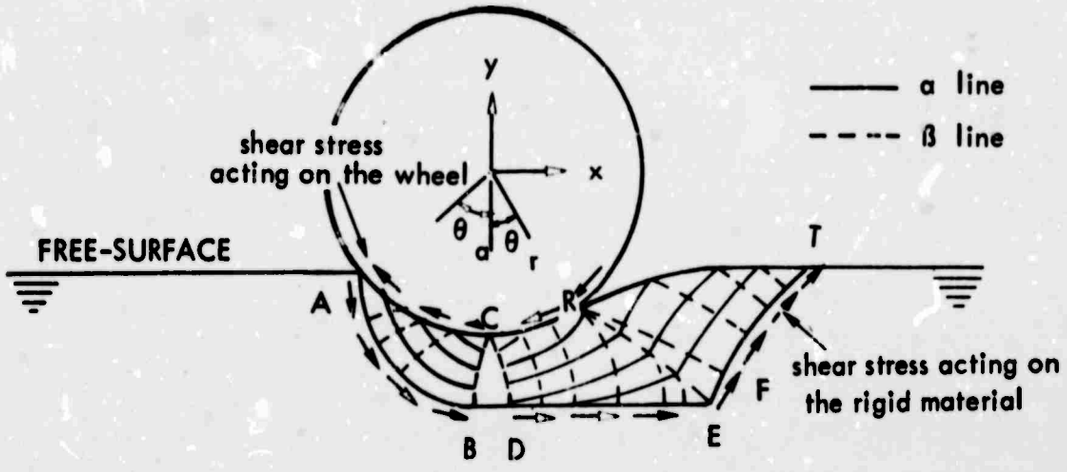

b. SLIP-LINE FIELD

FIGURE 10 - QUALITATIVE REPRESENTATION OF THE PLASTIC FLOW PATTERN

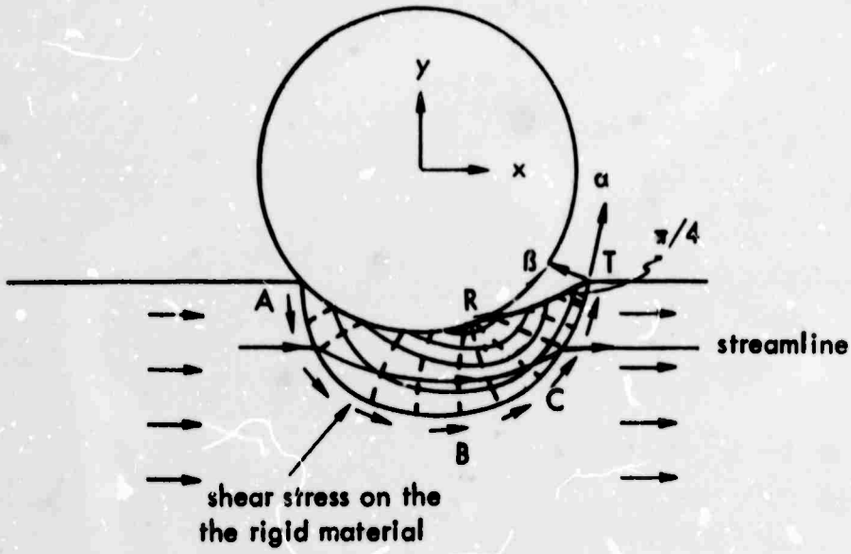

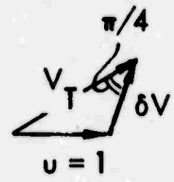

velocity triangle at T

FIGURE 11 - AN INCORRECT SLIP-LINE FIELD

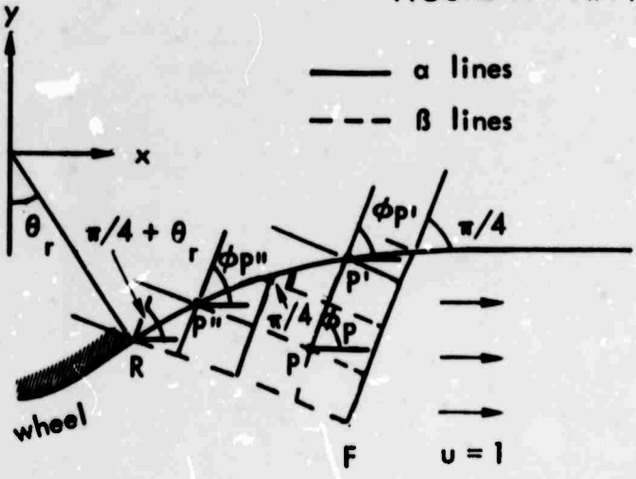

a. THE PHYSICAL PLANE x,y

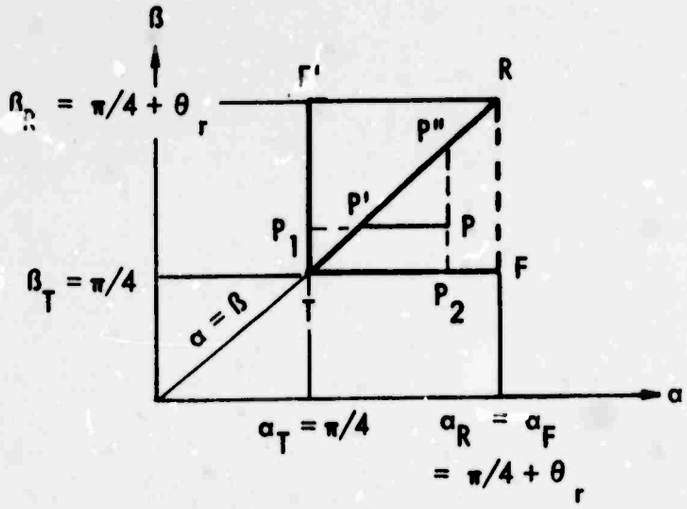

b. THE CHARACTERISTIC PLANE α,ß

FIGURE 12 - THE FREE-SURFACE REGION

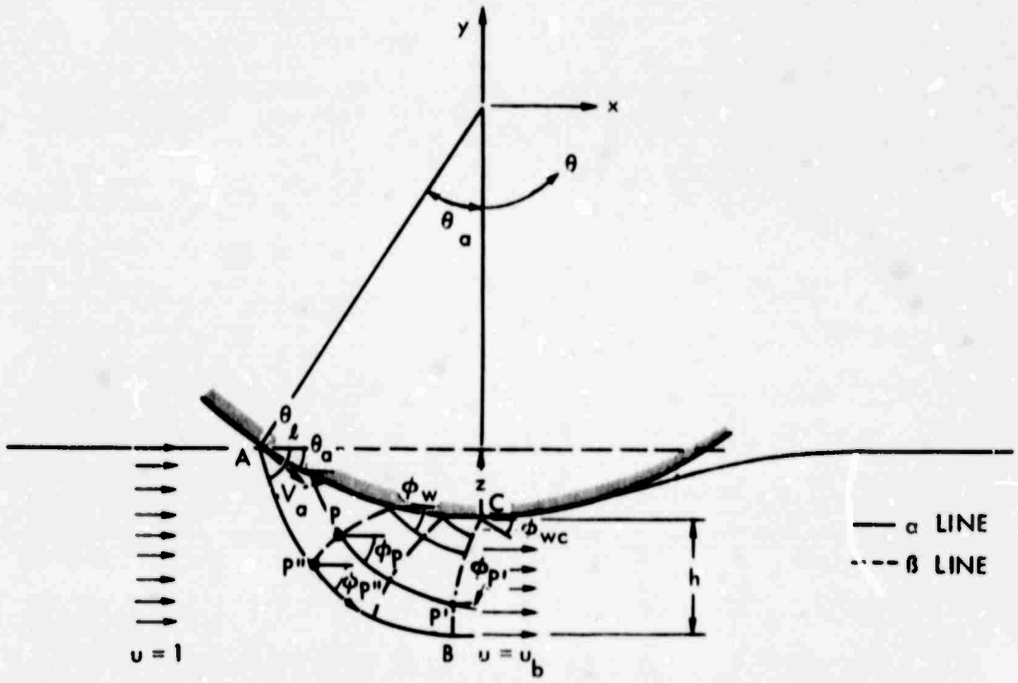

a. THE PHYSICAL PLANE x, y

b. THE VELOCITY TRIANGLE AT A

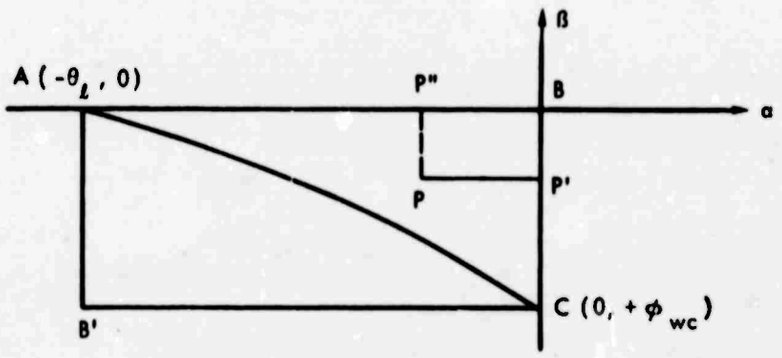

c. THE CHARACTERISTIC PLANE α, ß

FIGURE 13 - PLASTIC FLOW IN THE BOW REGION

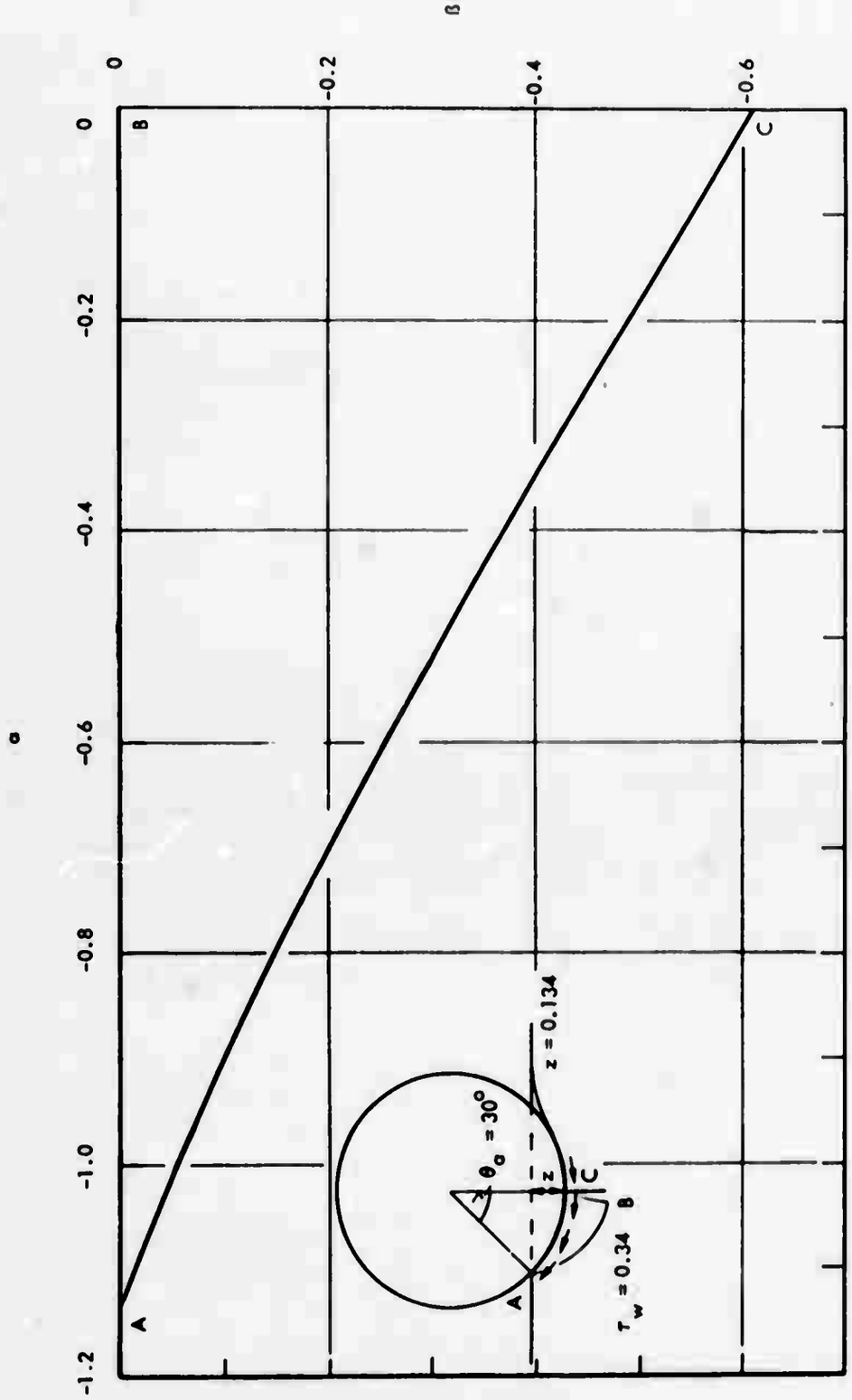

FIGURE 14 - THE CHARACTERISTIC PLANE (EXAMPLE OF EQUATION 6.53)

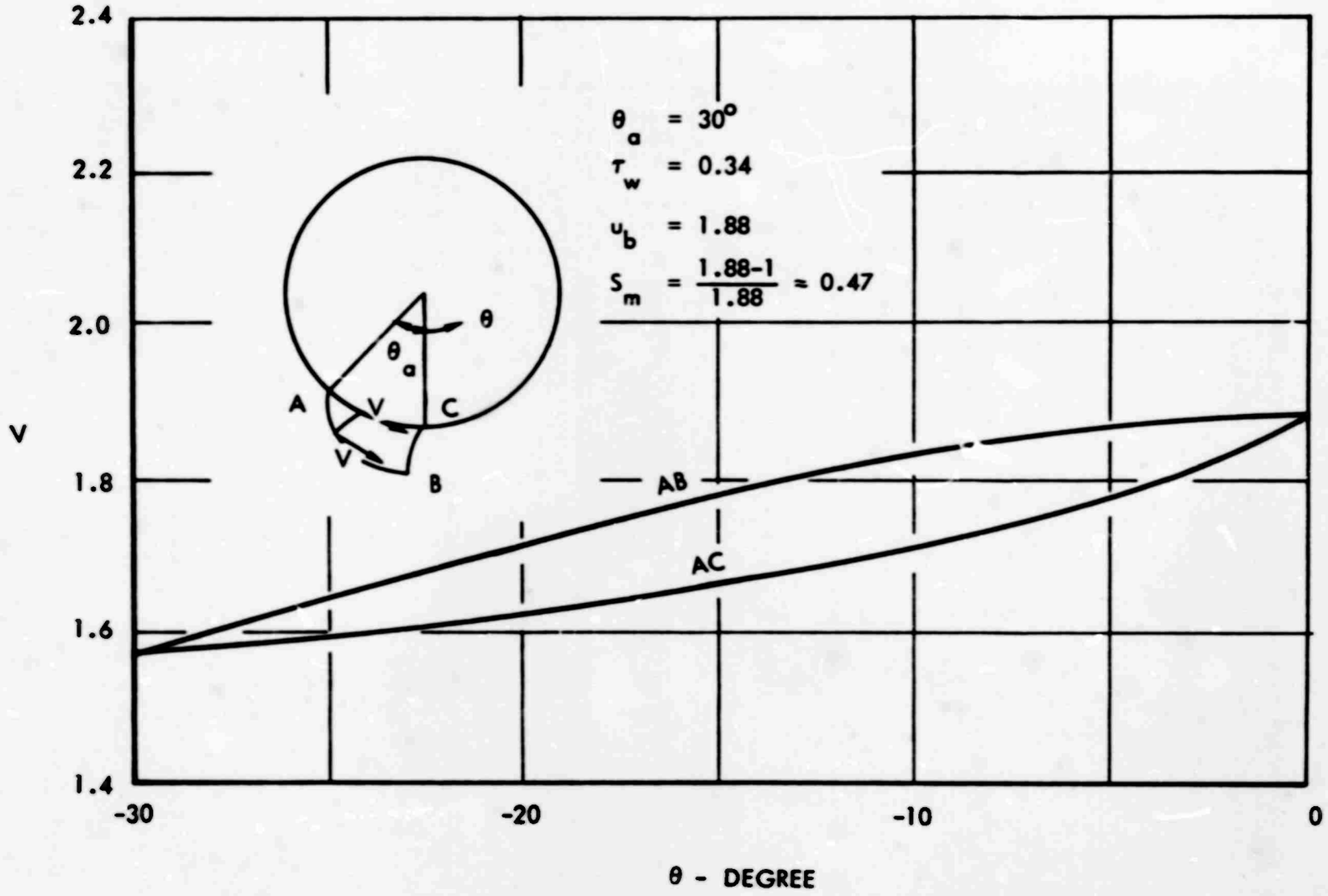

FIGURE 15 - THE VELOCITY DISTRIBUTION ALONG AC (SOIL-WHEEL INTERFACE) AND AB (MARGINAL CHARACTERISTICS)

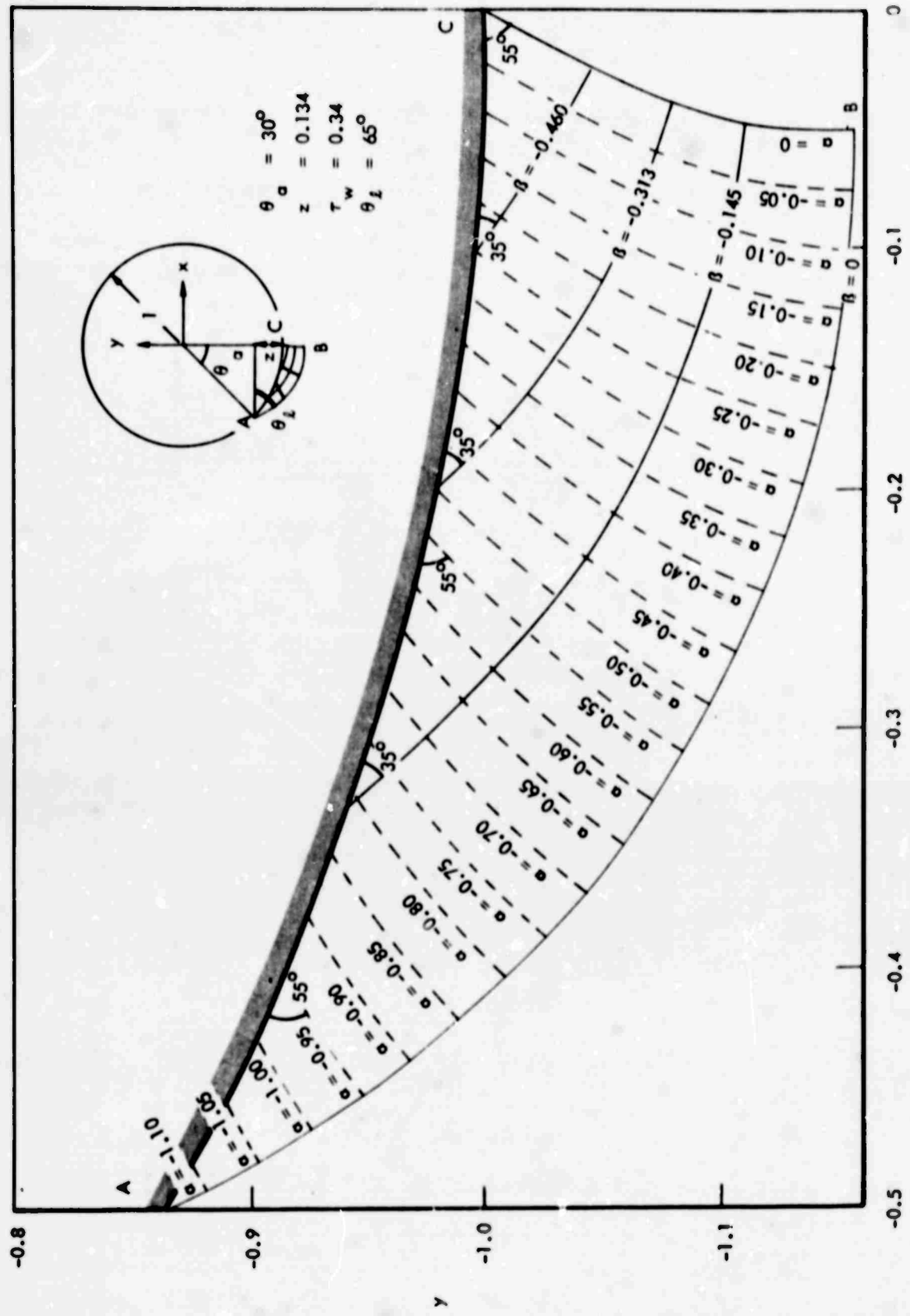

FIGURE 16 – THE SLIP-LINE FIELD IN THE BOW REGION (EXAMPLE OF EQUATION 6.53)

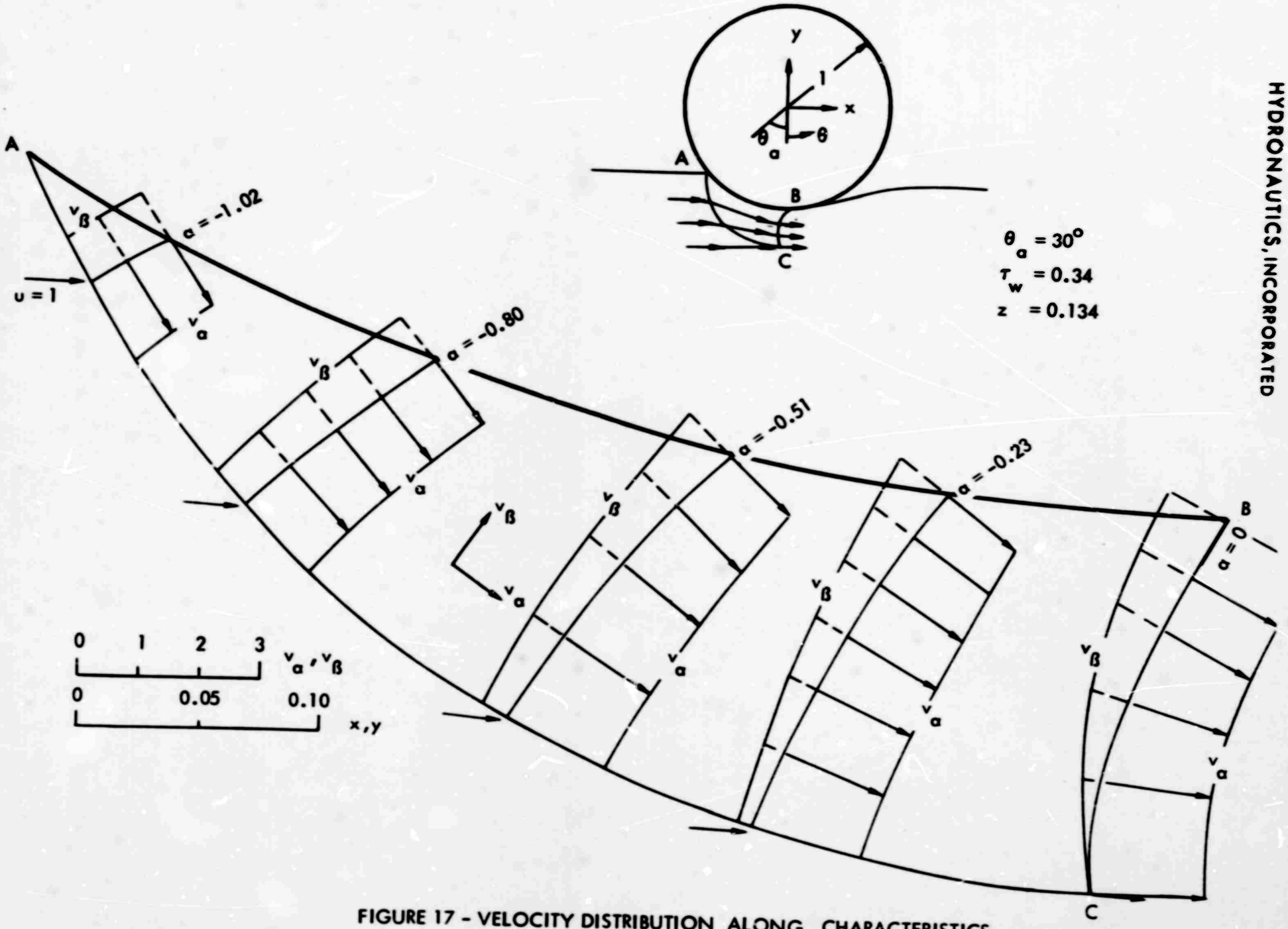

FIGURE 17 - VELOCITY DISTRIBUTION ALONG CHARACTERISTICS

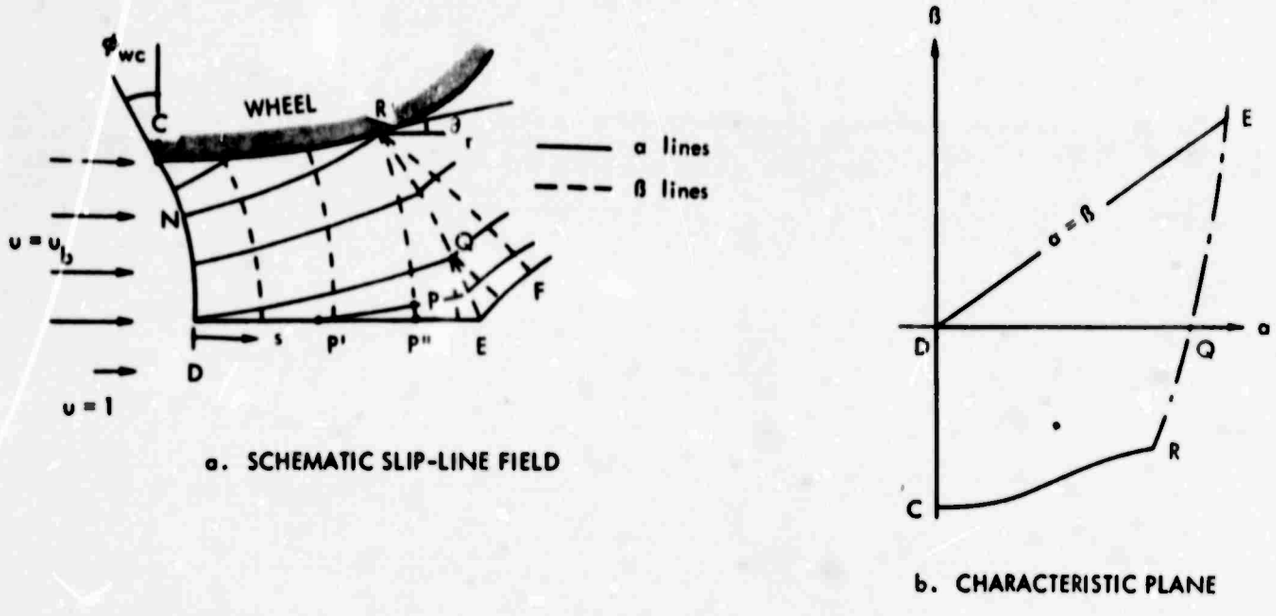

a. SCHEMATIC SLIP-LINE FIELD

b. CHARACTERISTIC PLANE

FIGURE 18 - THE PLASTIC FLOW IN THE INTERMEDIATE REGION CDERC

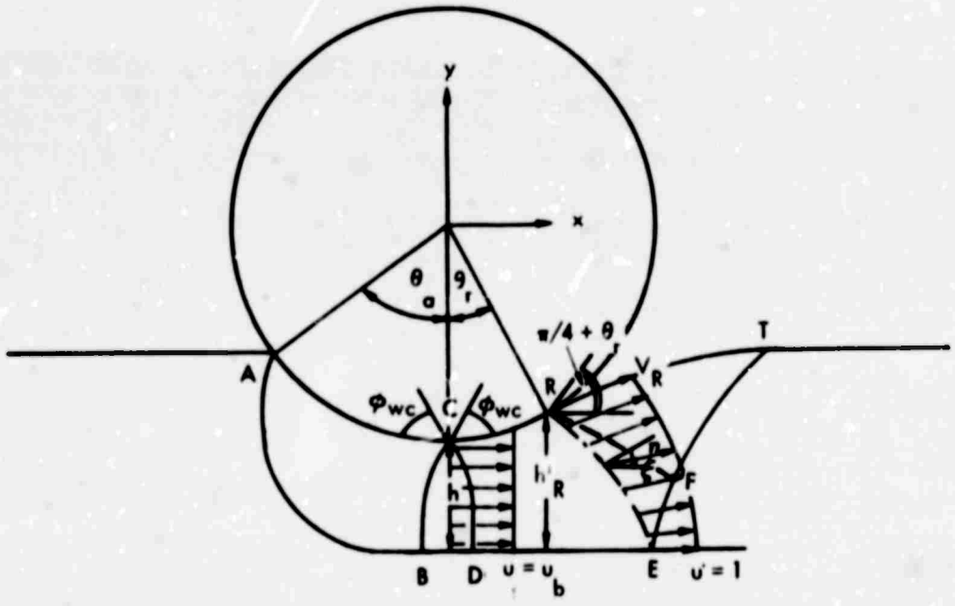

FIGURE 19 - CONTINUITY OF FLOW IN REGION CDERC

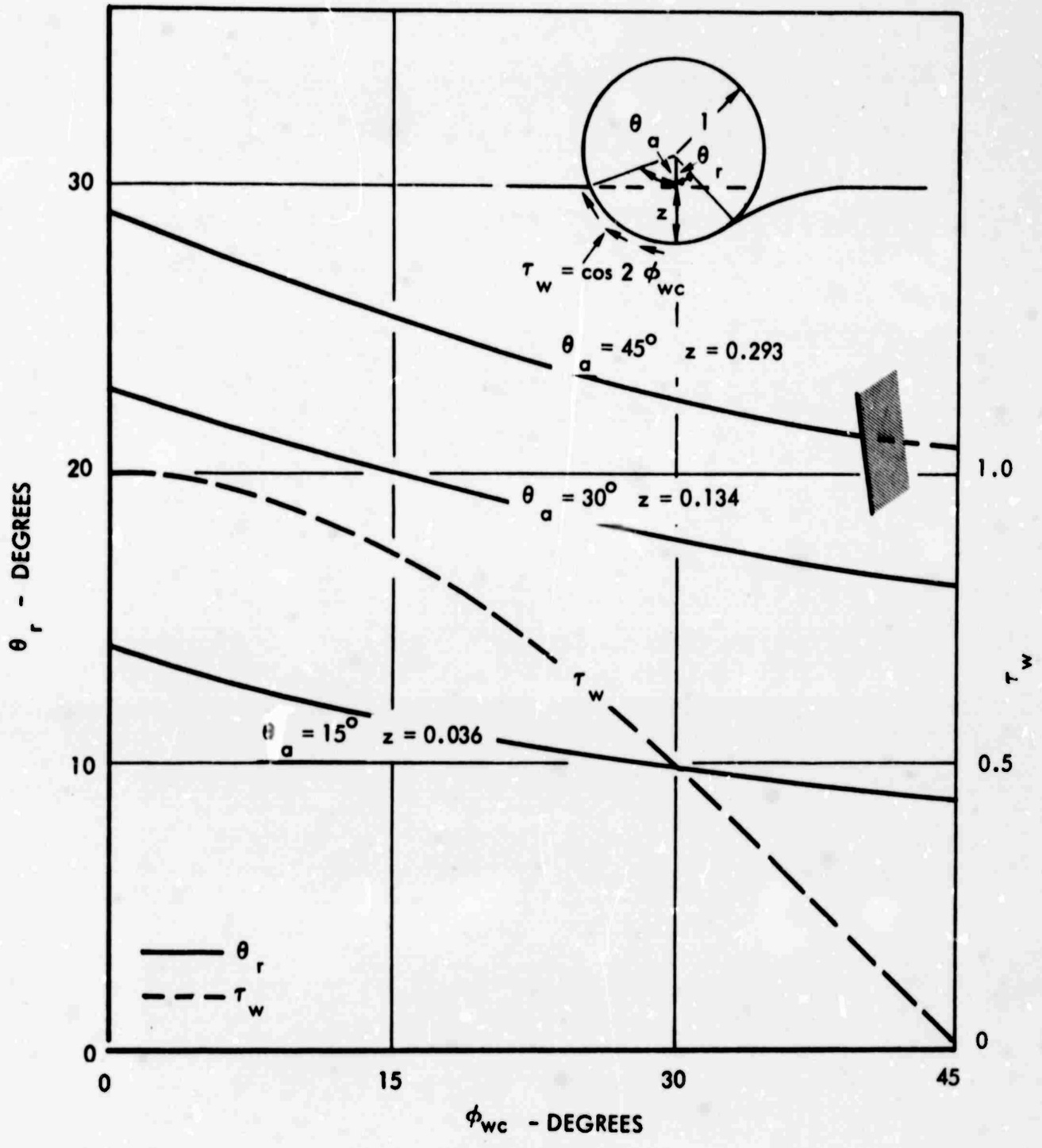

FIGURE 20 - THE DETACHMENT ANGLE θ_r AS FUNCTION OF SINKAGE AND SHEAR STRESS ON THE WHEEL

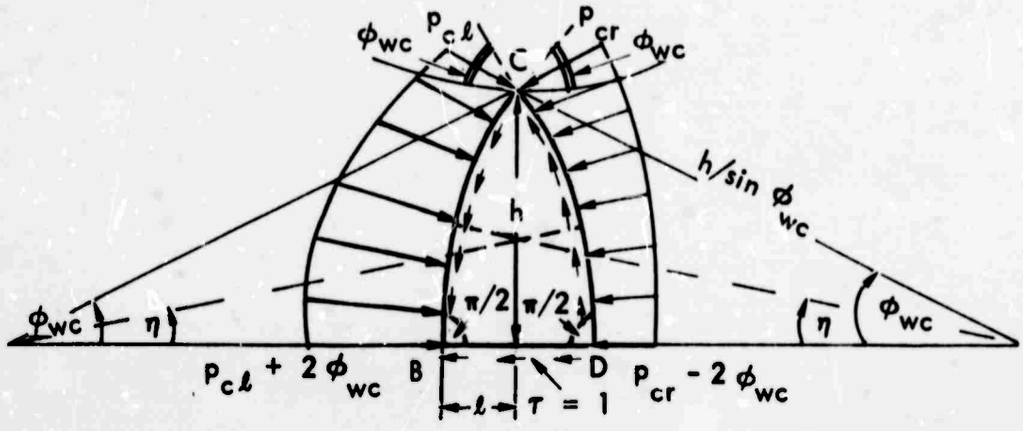

FIGURE 21 - THE EQUILIBRIUM OF THE RIGID CORE CBDC

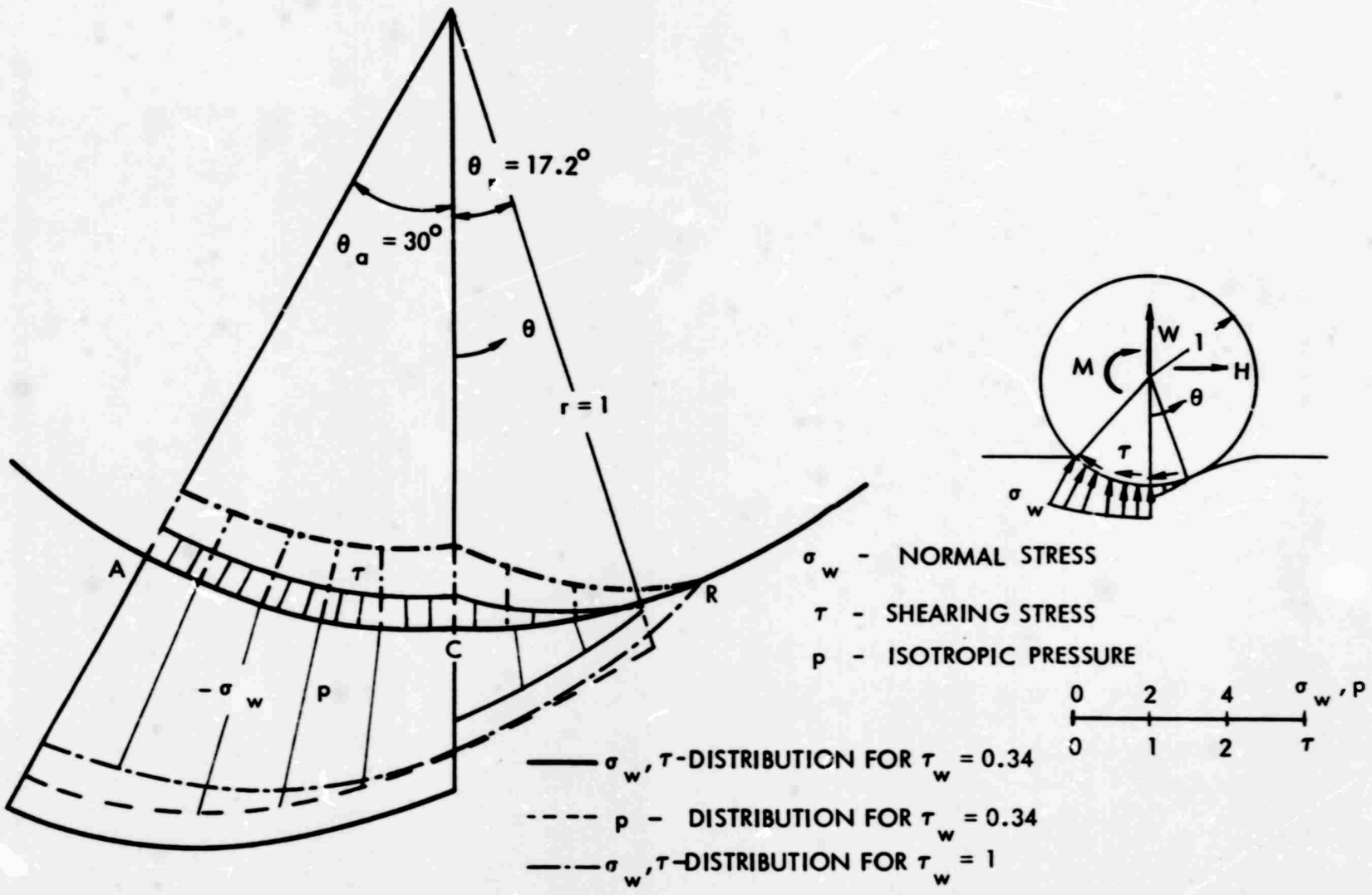

FIGURE 22 - THE APPROXIMATE DISTRIBUTION OF STRESS ALONG THE WHEEL (EXAMPLE OF EQUATION 6.53)

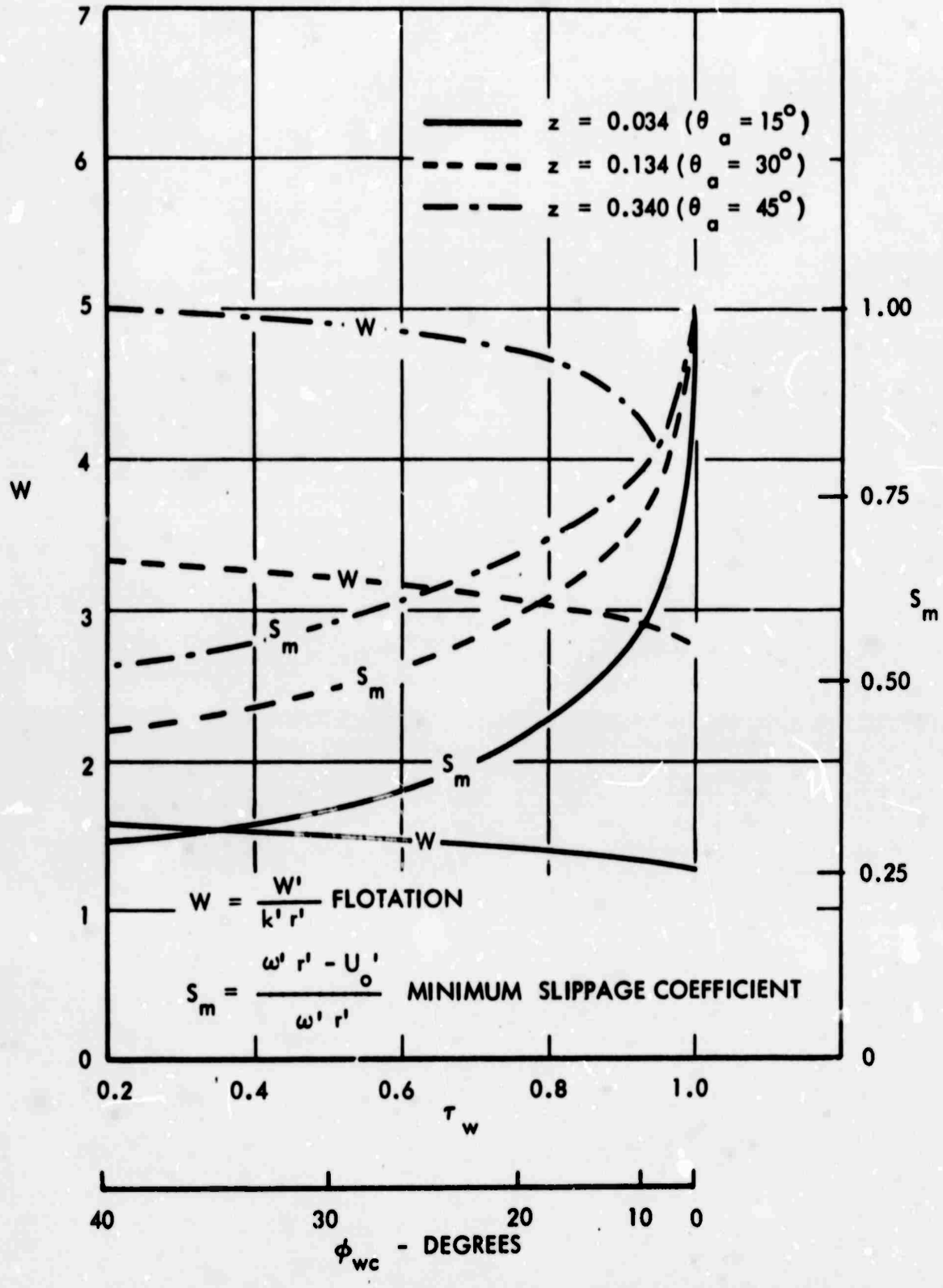

FIGURE 23 - FLOTATION AND MINIMUM SLIPPAGE COEFFICIENT AS FUNCTION OF SINKAGE AND SHEAR STRESS

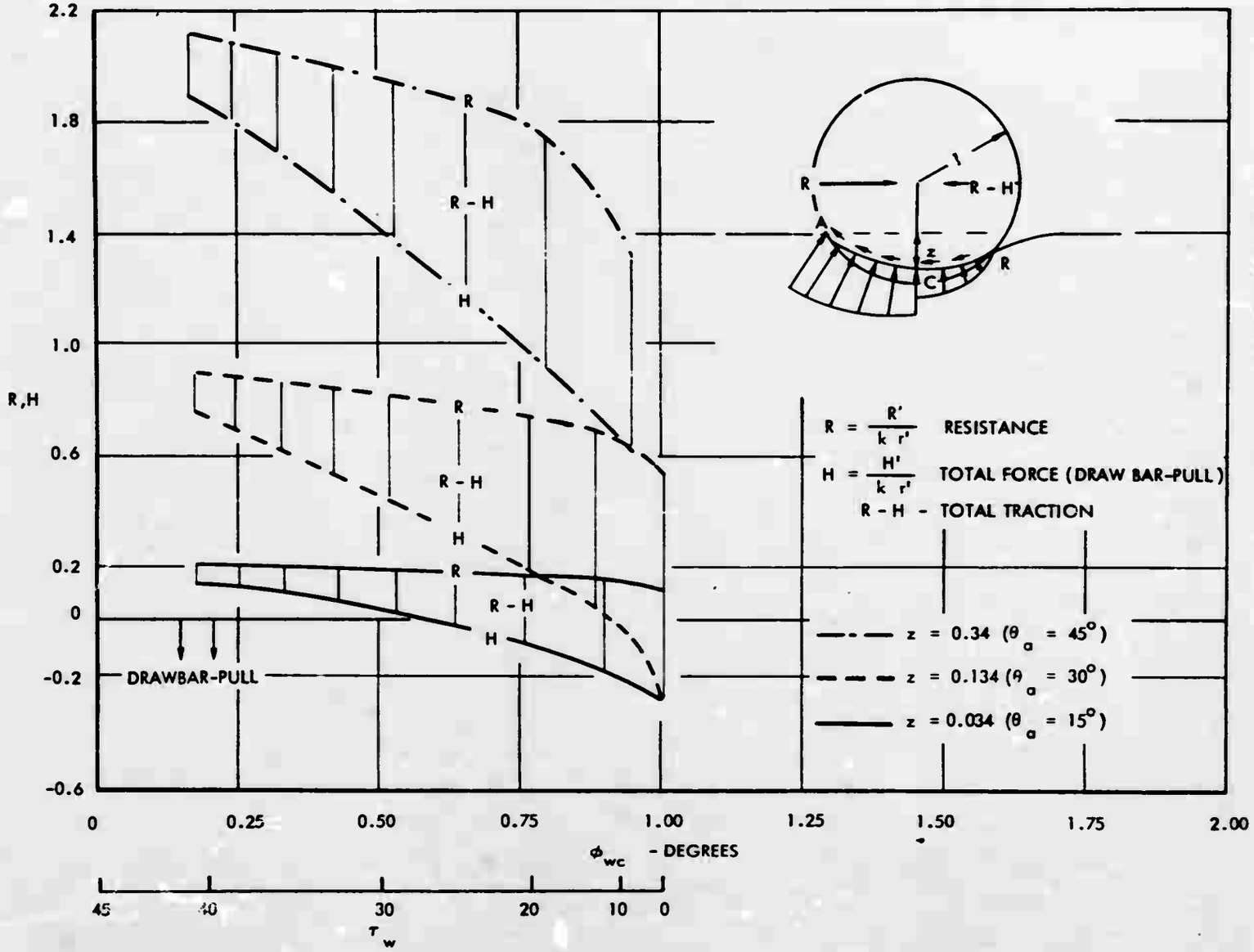

FIGURE 24 - RESISTANCE AND TOTAL HORIZONTAL FORCE AS FUNCTIONS OF SHEAR STRESS AND SINKAGE

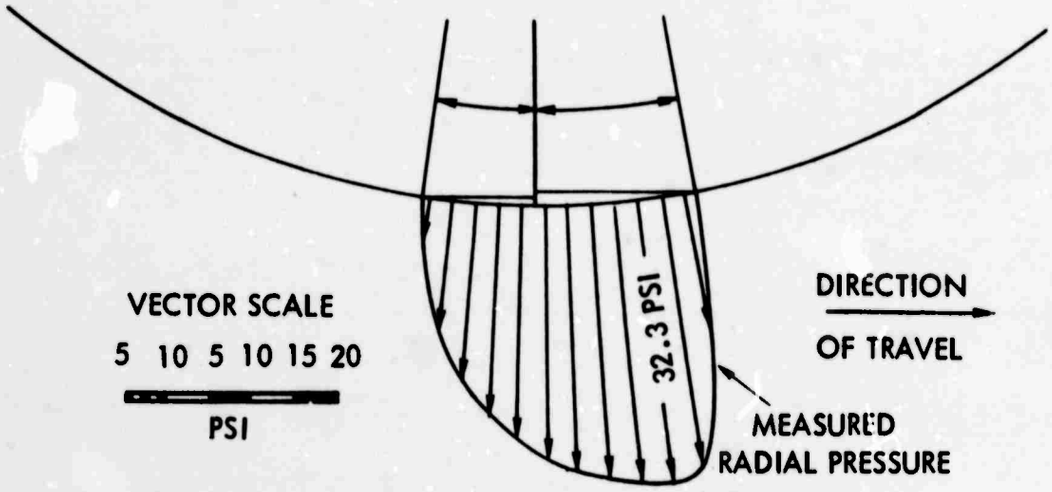

(a)

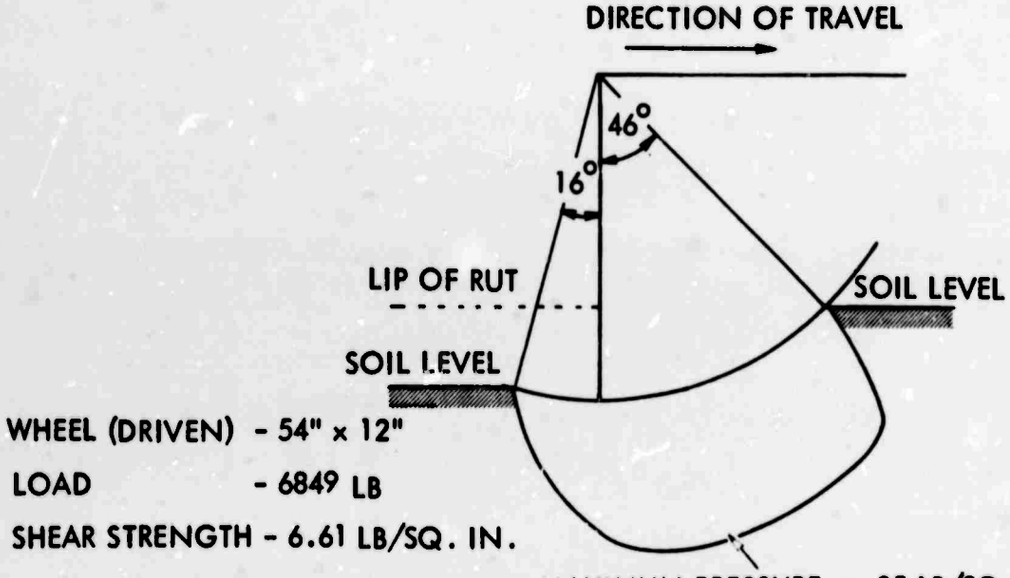

WHEEL (DRIVEN) - 54" x 12"

LOAD - 6849 LB

SHEAR STRENGTH - 6.61 LB/SQ. IN.

SLIP - 30%

MAXIMUM PRESSURE = 35 LB/SQ. IN.

AVERAGE PRESSURE = 20 LB/SQ. IN.

$$\frac{W'}{k' r' (\theta_a + \theta_r)} = \frac{6849 \times 180}{6.61 \times 27 \times 12 \times 61 \times 3.14} = 3.6$$

(b)

FIGURE 25 - MEASURED NORMAL STRESS DISTRIBUTION
(a) REF. (15), p. 27 (b) REF. (18), p. 120

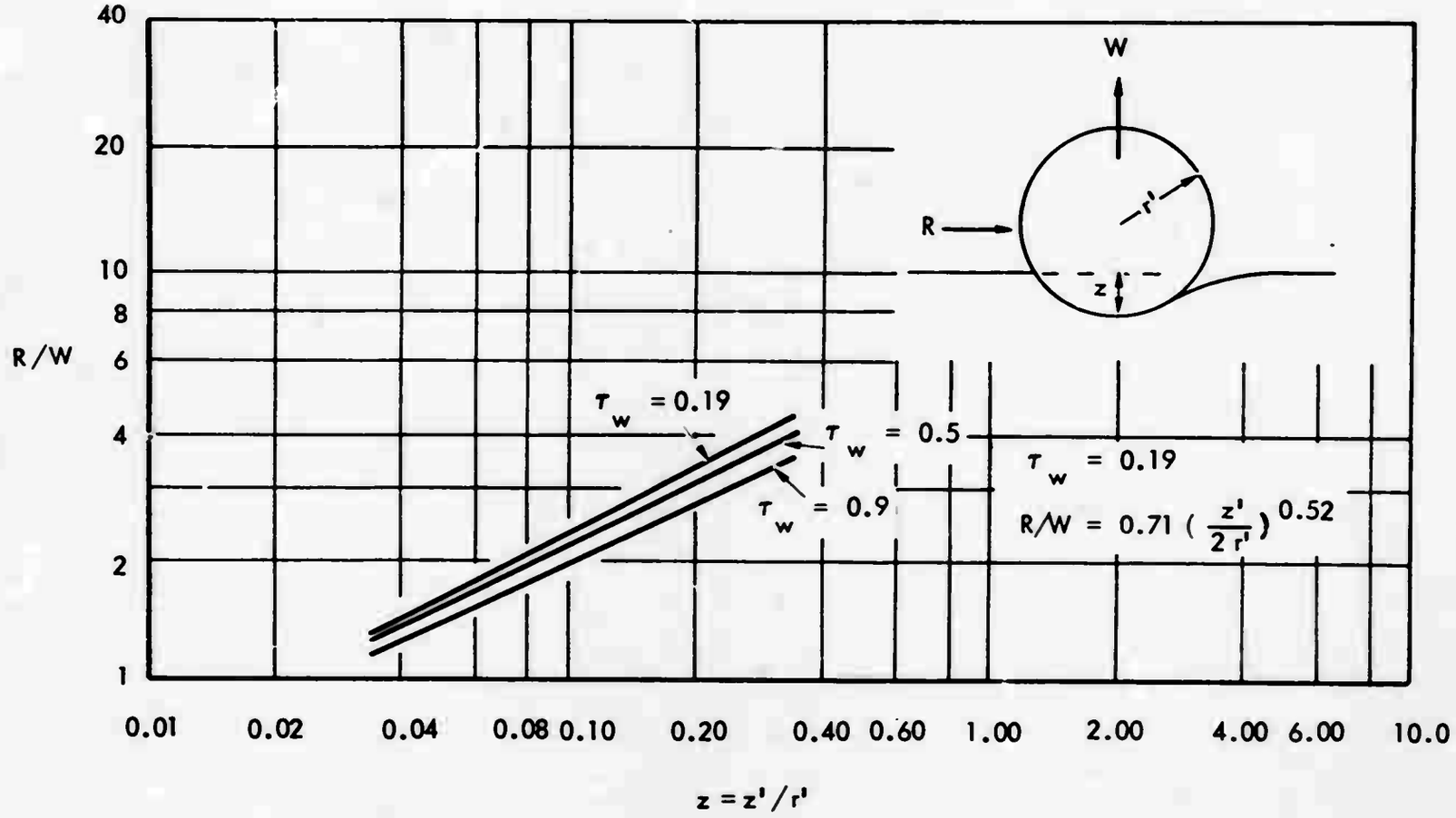

FIGURE 26 - RESISTANCE OVER FLOTATION AS FUNCTION OF SINKAGE

UNCLASSIFIED

Security Classification

DOCUMENT CONTROL DATA · R&D

(Security classification of title, body of abstract and indexing annotation must be entered when the overall report is classified)

1. ORIGINATING ACTIVITY (Corporate author) HYDRONAUTICS, Incorporated, Pindell School Road, Howard County, Laurel, Maryland	2a. REPORT SECURITY CLASSIFICATION UNCLASSIFIED 2b. GROUP

3. REPORT TITLE

A STUDY OF THE STEADY FLOW OF A RIGID-PLASTIC CLAY BENEATH A DRIVEN RIGID WHEEL

4. DESCRIPTIVE NOTES (Type of report and inclusive dates)

Technical Report

5. AUTHOR(S) (Last name, first name, initial)

Dagan, G. and Tulin, M. P.

6. REPORT DATE	7a. TOTAL NO. OF PAGES	7b. NO. OF REFS
August 1968	151	22

8a. CONTRACT OR GRANT NO. DAHC 04-67-C-0005 b. PROJECT NO. ARPA Order No. 841 c. d.	9a. ORIGINATOR'S REPORT NUMBER(S) TECHNICAL REPORT 823-1 9b. OTHER REPORT NO(S) (Any other numbers that may be assigned this report)

10. AVAILABILITY/LIMITATION NOTICES

Distribution of this document is unlimited

11. SUPPLEMENTARY NOTES	12. SPONSORING MILITARY ACTIVITY Advanced Research Projects Agency Project AGILE Department of Defense

13. ABSTRACT

The steady two-dimensional flow beneath a driven rigid cylindrical wheel moving in a soft saturated clay is solved by assuming that the soil behaves like a rigid-plastic material. The general equations of plastic flow are discussed, with emphasis on the inertial effects which generally are not negligible. A plastic flow pattern is suggested and the quasi-static equations of flow are integrated in two regions of the plastic zone. An approximate solution provides the magnitude of the recovery angle, the vertical and horizontal forces and the torque acting on the wheel as function of wheel radius, sinkage and shear stress along the wheel (assumed constant on the bow portion). A minimum slippage necessary to maintain the shear stress on the wheel is found. The theoretical results are compared with some existing measurements and the agreement is generally satisfactory.

DD FORM 1 JAN 68 1473

UNCLASSIFIED

Security Classification

UNCLASSIFIED

Security Classification

14 KEY WORDS	LINK A		LINK B		LINK C	
	ROLE	WT	ROLE	WT	ROLE	WT
Plastic flow pattern Soil behavior Vehicle soil interaction						

INSTRUCTIONS

1. ORIGINATING ACTIVITY: Enter the name and address of the contractor, subcontractor, grantee, Department of Defense activity or other organization *(corporate author)* issuing the report.

2a. REPORT SECURITY CLASSIFICATION: Enter the overall security classification of the report. Indicate whether "Restricted Data" is included. Marking is to be in accordance with appropriate security regulations.

2b. GROUP: Automatic downgrading is specified in DoD Directive 5200.10 and Armed Forces Industrial Manual. Enter the group number. Also, when applicable, show that optional markings have been used for Group 3 and Group 4 as authorized.

3. REPORT TITLE: Enter the complete report title in all capital letters. Titles in all cases should be unclassified. If a meaningful title cannot be selected without classification, show title classification in all capitals in parenthesis immediately following the title.

4. DESCRIPTIVE NOTES: If appropriate, enter the type of report, e.g., interim, progress, summary, annual, or final. Give the inclusive dates when a specific reporting period is covered.

5. AUTHOR(S): Enter the name(s) of author(s) as shown on or in the report. Enter last name, first name, middle initial. If military, show rank and branch of service. The name of the principal author is an absolute minimum requirement.

6. REPORT DATE: Enter the date of the report as day, month, year, or month, year. If more than one date appears on the report, use date of publication.

7a. TOTAL NUMBER OF PAGES: The total page count should follow normal pagination procedures, i.e., enter the number of pages containing information.

7b. NUMBER OF REFERENCES: Enter the total number of references cited in the report.

8a. CONTRACT OR GRANT NUMBER: If appropriate, enter the applicable number of the contract or grant under which the report was written.

8b, 8c, & 8d. PROJECT NUMBER: Enter the appropriate military department identification, such as project number, subproject number, system numbers, task number, etc.

9a. ORIGINATOR'S REPORT NUMBER(S): Enter the official report number by which the document will be identified and controlled by the originating activity. This number must be unique to this report.

9b. OTHER REPORT NUMBER(S): If the report has been assigned any other report numbers *(either by the originator or by the sponsor)*, also enter this number(s).

10. AVAILABILITY/LIMITATION NOTICES: Enter any limitations on further dissemination of the report, other than those imposed by security classification, using standard statements such as:

(1) "Qualified requesters may obtain copies of this report from DDC."

(2) "Foreign announcement and dissemination of this report by DDC is not authorized."

(3) "U. S. Government agencies may obtain copies of this report directly from DDC. Other qualified DDC users shall request through _____."

(4) "U. S. military agencies may obtain copies of this report directly from DDC. Other qualified users shall request through _____."

(5) "All distribution of this report is controlled. Qualified DDC users shall request through _____."

If the report has been furnished to the Office of Technical Services, Department of Commerce, for sale to the public, indicate this fact and enter the price, if known.

11. SUPPLEMENTARY NOTES: Use for additional explanatory notes.

12. SPONSORING MILITARY ACTIVITY: Enter the name of the departmental project office or laboratory sponsoring *(paying for)* the research and development. Include address.

13. ABSTRACT: Enter an abstract giving a brief and factual summary of the document indicative of the report, even though it may also appear elsewhere in the body of the technical report. If additional space is required, a continuation sheet shall be attached.

It is highly desirable that the abstract of classified reports be unclassified. Each paragraph of the abstract shall end with an indication of the military security classification of the information in the paragraph, represented as *(TS)*, *(S)*, *(C)*, or *(U)*.

There is no limitation on the length of the abstract. However, the suggested length is from 150 to 225 words.

14. KEY WORDS: Key words are technically meaningful terms or short phrases that characterize a report and may be used as index entries for cataloging the report. Key words must be selected so that no security classification is required. Identifiers, such as equipment model designation, trade name, military project code name, geographic location, may be used as key words but will be followed by an indication of technical context. The assignment of links, roles, and weights is optional.

DD FORM 1 JAN 64 1473 (BACK)

023551

UNCLASSIFIED

Security Classification